الجمهورية الجزائية الدمقراطية الشعبية
République Algérienne Démocratique et Populaire
وزارة التعليم العالي والبحث العلمي
Ministère de l'enseignement supérieur et de la recherche scientifique

Université Ziane Achour - Djelfa
Faculté des Sciences et de la Technologie

جامعة زيان عاشور - الجلفة -
كلية العلوم والتكنلوجيا

Département de Génie Mécanique

THÈSE

Spécialité : Génie Mécanique
Option : Modélisation en Mécanique

Présentée par :

NAAS Toufik Tayeb

Intitulée

Comportement hydrodynamique et thermique d'un fluide non Newtonien Pseudoplastique dans une géométrie complexe

Soutenu publiquement le : 08.03.2017 devant le jury composé de :

	NOM et Prénom	Grade	Etablissement de rattachement	Désignation
Mr.	HACHI Brahim El khalil	Professeur	Université de Djelfa	Président
Mr.	BENZAOUI Ahmed	Professeur	Université de Bab Ezzouar USTHB	Directeur de thèse
Mr.	LASBET Yahia	MCB	Université de Djelfa	Co-directeur de thèse
Mr.	BEN MOUSSA Hocine	Professeur	Université de Batna 2	Examinateur
Mme.	AMOURA Meriem	MCA	Université de Bab Ezzouar USTHB	Examinateur
Mr.	MESSELMI Farid	MCA	Université de Djelfa	Examinateur

ANNEE 2017

Contents

.

Acknowledgements

First and foremost, praises and thanks to ALLAH almighty who has been giving me everything to accomplish this study.

There is not enough space, here, to mention all the people who have helped me, with scientific discussions, or with their friendship and encouragement, during this thesis work. I would like to thank all of them.

I would like to thank my advisors,Pr. Benzaoui Ahmed from USTHB university and Dr. Lasbet Yahia from Ziane Achour university of Djelfa, for their guidance, and constant support throughout my graduate research.I sincerely appreciate their teaching, encouragement, and being always available to help.

I would also like to thank thepresident of committee; Pr. Hachi Ibrahim El Khalil from Ziane Achour university of Djelfa, and the committee members, Pr. Ben Moussa Hocine from the university of Batna 2, Dr. AmouraMeriem from USTHB university and Dr. MesselmiFarid from ZianeAchour university of Djelfa, for reading the thesis and offering constructive comments.

I would like to thank some of the professors;Dr. Boukhalkhal Ahmed Lamine, Dr. Kouadri Amar, Dr. Kezran cheikh and Dr. Aidaoui Lakhdar in Mechanical engineering department, with whom I have taken courses and learnt new concepts, and gained a lot of knowledge. I would also like to acknowledge the help of my colleagues in the laboratory of development in mechanics and materials LDMM, University of Djelfa.

Last but not least, I would like to thank my parents, my big and small families, for always being supportive, also for their comprehension, patience and prayers.

Dedicate to
My dear parents,
My family ...To my daughter

Nomenclature

Lettre

Ac	cross-section surface area, (m^2)
a*	geometric constant in generalized Reynolds number, equation (2.7)
b*	geometric constant in generalized Reynolds number, equation (2.7)
Be	Bejan number
c	mass specific heat, (j/Kg.K)
D	deformation rate, (s^{-1})
D_h	hydraulic diameter, (m)
H	heat transfer coefficient,(W /K.m^2)
h_{mean}	mean heat transfer coefficient,(W /K.m^2)
H	Helicity
H	horizontal
k	power-law consistency index, (Pa/s)
L	total length of the geometry, (m)
M_d	Mixing degree
n	Power-law index
Ns	non-dimensional entropy generation
Nu_{local}	local Nusselt number
Nu_{mean}	mean Nusselt number
P	pressure, (Pa)
Pe	Peclet number
Po	Poiseuille number
Po_{local}	local Poiseuille number
Po_{mean}	mean Poiseuille number
$q"$	wall heat flux, (W/m^2)
$\dot{Q}$	heat transfer rate, (W)
R	normalized ration
R_0	ratio (T_{min}/T_{max}) at the entry section
Re	Reynolds number for Newtonian fluid
Re_g	generalized Reynolds number for non-Newtonian fluid
s	curvilinear coordinate, m
S	strain rate, (s^{-1})
S'''_{gen}	global entropy generation, (W/ K. m^3)
S'''_T	entropy generation due to heat transfer, (W/ K.m^3)
S'''_P	entropy generation due to friction factor, (W/ K.m^3)
S_{mean}	mean Strain rate, (s^{-1})
T	fluid temperature, (K)
T_b	

T_w	mean bulk temperature fluid
T_i	perimeter average wall temperature, (K)
$\overline{T}$	temperature at the node i, (K)
T_{min}	mean temperature at the cross section, (K)
T_{max}	minimum temperature, (K)
T_s	maximum temperature, (K)
U_i	static temperature, (K)
V	mean velocity at the inlet section, (m/s)
V_z	velocity vector
X, Y, Z	axial velocity, (m/s)
	coordinates in Cartesian coordinate system, (m).

Grec Symbol

Δ	laplacian
α^*	geometric constant forgeneralized Reynolds number, Table 2.3
β_i	constant in equation (2.6) of velocity profiles
λ	thermal conductivity, (W/K.m)
$\dot{\gamma}$	shear rate, (s^{-1})
τ	shear stress, (Pa)
μ	constant viscosity for Newtonian fluid, (N s /m^2)
μ_{app}	apparent viscosity for non-Newtonian fluid, (N s /m^2)
ρ	fluid density (kg m^{-3})
σ_0	standard deviation at the entry section
$\mho$	total volume of the fluid
Ω	mean Deformation rate, (s^{-1})
Ω_{mean}	mean vortex intensity, (s^{-1})
ω_{mean}	mean vortex intensity at the cross section.

List of figures

List of tables

General Introduction

There are many methods to enhance the thermal and hydrodynamic performances of the system included in many industrial applications. One of these ways, the chaotic flow has received considerable attention for many years. The chaotic advection regime presents a sub-laminar flow where the particle trajectories are almightily erratic and chaotic. This regime is comparable to turbulent regime in terms of performances. Thanks to Assan Aref [1] who invented this type of flows. In his work, Aref outlined the chaotic kinematic of fluid particle trajectories in the two-dimensional periodic flows using Poincaré section as one of the important tools for the analysis of dynamic systems.

One of the potential chaotic channels which can present a good way to improve the performances of the heat transfer rates and the energetic efficiency of the systems is the C-shaped geometry which the flow is steady and open three dimensional. Among the authors who have used this geometry in their research, we can cite [2-8].

Robin et al [2] presented different configurations of implementing chaotic advection to passively enhance fluid mixing. Their experimental results showed that the mixing capability of the C-shaped geometry increases with increasing Reynolds number, and mixing rates in the serpentine channel are consistent with the occurrence of chaotic advection.

Beebe et al [3] investigated a general framework for improving mixing in micro fluidic applications. The mixer design was fabricated using a compression micro-molding process to create chaotic flow channels. Experimental analyses demonstrated the effectiveness of the resulting design ingenerating chaos in the flow and hence improving mixing.

A numerical study of the mixing of two fluids in micro-channels has performed by Liu et al [4]. The mixing phenomena were tested for three micro-mixers: a square-wave mixer, a three-dimensional serpentine mixer (C-shaped channel) and a staggered herringbone mixer. Their results shows that the C-shaped mixer and staggered herringbone mixer mix the fluids to a greater extent than does the square wave mixer.

Lasbet et al [5] characterized the C-shaped channel as a new design for the PEM fuel cell cooling system where the fluid is Newtonian (water). Their heat performance is considerably improved compared to that when the flow is regular (straight channel).Their showed that the convective heat transfer coefficient of the C-shaped channel is about six times that of the straight channel. This high performance is examined because of chaotic regions in the flow. Another numerical analyze has undertaken by Lasbet et al [6] in which various channel geometries (straight channel, zigzag, square-wave mixer geometry, and C-shaped, V-shaped, and B-shaped geometry) have proposed in order to generate chaotic flows. Using CFD, such geometry was characterized in terms of both their thermal mixing performances and their hydrodynamic performances. The square-wave mixer geometry leads to a convective heat transfer coefficient about four times that in the straight channel, an improvement classically attributed to the presence of the right-angle bends that create recirculation zones and secondary flow. In the C-shaped geometry, the chaotic

trajectory produces the greatest heat transfer intensification while the V-shaped geometry, which was designed to reduce the pressure loss compared to the C-shaped geometry, presents the best compromise between large convective heat transfer and reasonable pressure losses. For the B-shaped geometry, designed to reduce machining cost, the thermal and hydraulic performances are almost equivalent to those of the V-shaped geometry.

Recently, an experimental study of the heat transfer and pressure of drop Newtonian fluid for different chaotic geometries was conducted by Cathy Castelain et al [7]. Heat exchanges were carefully analyzed to obtain the convective heat transfer coefficient for each channel. The results showed a comparison of the average Nusselt number, the average Poiseuille number, and the ratio Po/Nu for all geometries considered. Thus, lowest value of the Po/Nu ratio is obtained with the V-shaped geometry. The B-shaped, zigzag channel and U-shaped geometries also present an interesting compromise, slightly better than the C-shaped geometry. The highest exergy efficiency is obtained with the C-shape, closely followed by the B-shape, zigzag channel, V-shape and U-shape geometries.

More recently, Lasbet et al [8] studied the influence of the geometry scale on the kinematic behavior of the fluid flow for C-shaped channel. The fluid flow behavior was characterized in terms of the deformation rate, rotation rate, dimensionless Helicity contours and the pressure losses.

The most working fluid in these researches is a Newtonian fluid where the viscosity does not affected by the deformation rate. So, our contribution in this thesis is to outline and analyze the thermal and hydrodynamic behavior of power-law non-Newtonian fluid in C-shaped geometry in comparison to thestraight channel. The energetic efficient of this geometry in terms of heat transfer (Nusselt number), fluid flow (Poiseuille number) and entropy generation were calculated as function of generalized Reynolds number Re_g and power-law index n.

CHAPTER 1

Literature Review

1.1 Introduction

In this chapter, a comprehensivesurvey is presented for the hydrodynamic, the thermal mixing and heat transfer flow in straight and complex geometries.Analytical, Experimental and numerical works for hydrodynamic flow are first stated. After that, the enhancement of thermal mixing and heat transfer are reviewed for laminar flow. Then, previous studiesare presented for entropy generation.

1.2 Rheological fluid behavior

Fluids treated in the traditional hypothesis of fluid mechanics are the Newtonian fluid. The former is completely frictionless, so that shear stress has a linear relationship between shear stress and shear rate. On the other hand, the behavior of many real fluids used in the mechanical industries is not sufficiently described by these models. Most real fluids exhibit non-Newtonian behavior, which means that the apparent viscosity (shear stress divided by shear rate) is not constant at a given temperature and pressure but is dependent on flow conditions such as flow geometry, shear rate,… etc.
Metzner [100] grouped fluids into three general classes:

- Purely viscous fluids: Generalized Newtonian fluids: The rate of shear at any point of the fluid is dependent only by the current value of the shear stress. These are also called: "Generalized Newtonian fluids", "time independent" or "inelastic fluids".
- Viscoelastic fluids: more complex materials for which the shear stress and rate of shear depends on the time for which the shear is applied. They are called: "time-dependent fluids".
- Time-dependent fluids: Materials exhibiting properties of both viscous fluids and elastic solids, and showing partial elastic recovery to the original state when a deformation or stress is applied. These materials are called "Viscoelastic fluids"

Qualitative flow curves on linear scales for these three types of fluid behavior are shown in Figure 1.1.

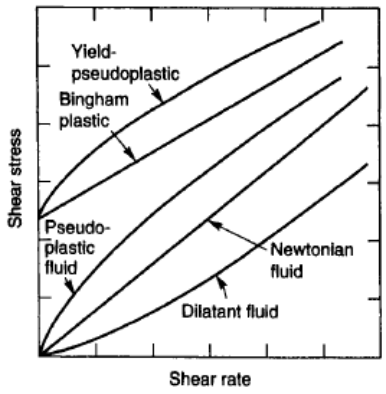

Figure 1.1: Types of time-independent flow behavior

There are also fluids which have characteristics that are a combination of the three properties mentioned below. There are also materials that are either elastic solids or viscous fluids depending on the current conditions.

1.2.1 Time-independent fluid behavior

This fluid can be further subdivided into three types: Shear-thinning (pseudoplastic) fluids, viscoplastic fluids and shear-thickening (Dilatant) fluids:

1.2.1.a Shear-thinning or Pseudoplastic fluids

In Shear-thinning or pseudoplastic fluids, the viscosity decreases with increasing shear rate. Both at very low and at very high shear rates, most pseudoplastic fluid solutions exhibitNewtonian behavior, shear stress-shear rate plots become straight lines, as shown in Figure 1.2.

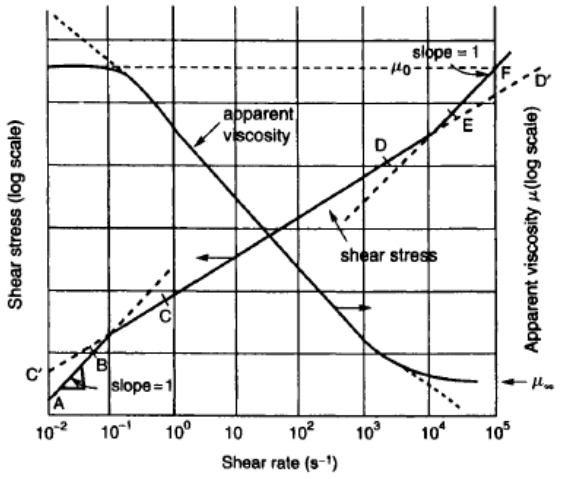

Figure 1.2: Schematic representation of shear-thinning behavior

- **The power-law or Ostwald de Waele model**

The relationship between shear stress and shear for a shear-thinning fluid can be given by the following expression: $\mu_{app} = \mathrm{k}\,\dot{\gamma}^{\mathrm{n}-1}$ (1.1)

Where k(Pa/s) is power-law consistency index and n is the flow behavior index of the fluid.

For n< 1 the fluid exhibits pseudoplastic characteristics.

n = 1 the fluid exhibits Newtonian characteristics.

n> 1 the fluid exhibits dilatant characteristics.

1.2.1.bViscoplastic fluid

These types of fluids behavior resist any deformation initially and deform only when the applied stress exceeds a critical value which is sometimes referred to as yield stress (tau_0). on the contrary, such a material will deform elastically when the externally applied stress is smaller than the yield stress.

Various models like the Bingham plastic model, Casson and Herschel-Bulkley Model are available for modeling such viscoplastic flows.

- **The Herschel-Bulkley model**

Herschel-Bulkley model is generated from the equation of the Power law model, and it is written as:

$$\tau_{yx} = \tau_0 + m\left(\dot{\gamma}_{yx}\right)^n \text{for} \left|\tau_{yx}\right| > |\tau_0| \quad (1.2)$$

$$\dot{\gamma}_{yx} = 0 \text{for } \left|\tau_{yx}\right| < |\tau_0| \quad (1.3)$$

Note that for n =1 the model becomes Bingham model

1.2.2Time-dependent fluid behavior

The flow behavior of many important materials cannot be described by asimple rheological equation like (1.1) or (1.2). Hence, apparent viscosities maydepend not only on the rate of shear but also on the time for which the fluid has beensubjected to shearing. Theirapparent viscosities gradually become less as the 'internal' structure of the material isprogressively broken down. Time-dependent fluid behavior may be further sub-divided into two categories: thixotropyand rheopexy or negative thixotropy.

1.3Hydrodynamic behavior in ducts

1.3.1 Straight ducts

The predictions of pressure drops forfluids flowing in ducts of various cross sections is importantin engineering systems. Therefore, wideanalytical, experimental and numerical studies have been carried outon such flowapplications. For laminar non-Newtonianfluids,Wheeler et al [9] measured the Friction factor and the Poiseuille number for sodium Carboxy-Methyl-Cellulose fluid (CMC) flowing through a rectangular duct. Gervang and Larsen[10] studied the elastic effects of non-Newtonian fluid in straight ducts of rectangular cross section.

Parket al [11] investigated numerical solution of fully developed flow for a modified power law fluid in a rectangular duct. Their solutions was applicable to pseudoplastic fluids over a wide shear rate range from non-Newtonian behavior at low shear rates, through a transition region, to power law behavior at higher shear rates.

Capobianchi [12] reported the pressure drop ofhydrodynamic fully developed flows of non-Newtonian fluids in rectangular ducts. He analyzed the Poiseuille number for both pseudoplastic and dilatant regions as function of fluid behavior index.

Tazraei and Riasi [13] analyzed the laminar flow of a Carreau fluid inside rectangular channel. They observed that the effect of various physical parameters on velocity distribution with different dimensional aspects.

Recently, Numerical investigation of non-Newtonian Carreau Model presented by Riasi et al[14].They discussed that the effect of time constant magnitude on the behavior of unsteady velocity and shear stress profiles, and pressure responses in laminar shear thinning flows.

More recently, Devakar et al [15] numerically investigatedthe fully developed flow of non-Newtonian fluids in a straight square channel through the porous medium.They considered the Jeffrey fluid model as working fluid. Their numerical results observed that, the velocity andvolume flow rate decrease with an increase in couple stress parameter, whilethe velocity and volume flow rate increase with an increase in pressuregradient, as shown in figure 1. 1.

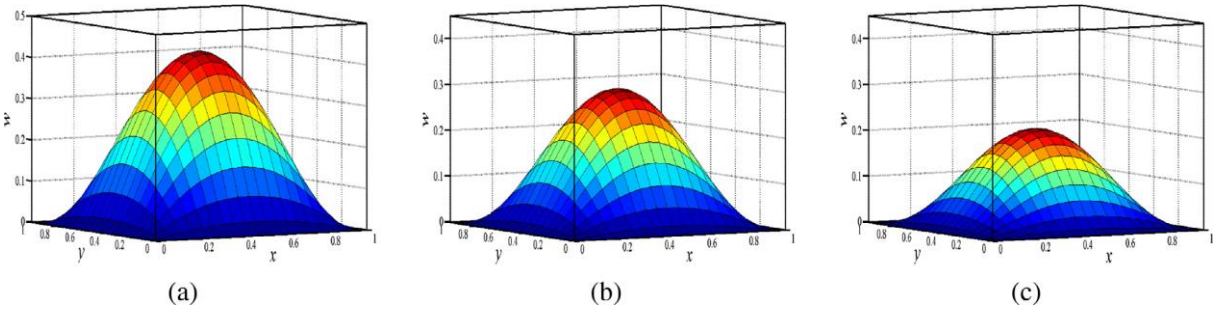

Figure 1.1: Velocity profile in 3-D for various coupled stress parameters[15].

1.3.2 Complex channels

1.3.2.a Newtonian fluids

The increasing number of experimental and numerical studies interest in complex systems like valves, pumps, mixers, reactor to achieve better and more dedicated performance satisfyingspecific requirements in different application areas. In accordance with this development, Fellouah, et al [16] presented the Dean instability of Newtonian fluids in laminar secondary flow in 180 ◦ curved channels, by using CFD code. They showed the effects of the curvature ratio (from 5.5 to 20) and aspect ratio (from 0.5 to 12) on Dean instability. Their results indicated that the critical value of the Dean number decreases with the increasing duct curvature ratio.

A numerical study of rapid chaotic mixing of two fluids flowing in a planar serpentine convergent–divergent mini-channel (see figure 1.2) was presented by Kuo-Wei Lin and Jing-Tang Yang [17]. Their approach is to create chaotic trajectories with flow in a planar serpentine channel at an appropriate Dean number which determines the degree of induced secondary flow. They tracked the trajectories of particles using visualization methods, these are smooth, and exhibit little disturbance in the z-direction as seen in figure 1.3. Their results reveal that the pattern of the alternating convergent–divergent cross sections induces corner Dean cells with much increased Dean numbers; the stretching and folding of interfaces is hence effectively enhanced, and a superior chaotic mixing of two fluids was consequently achieved, see figure 1.4.

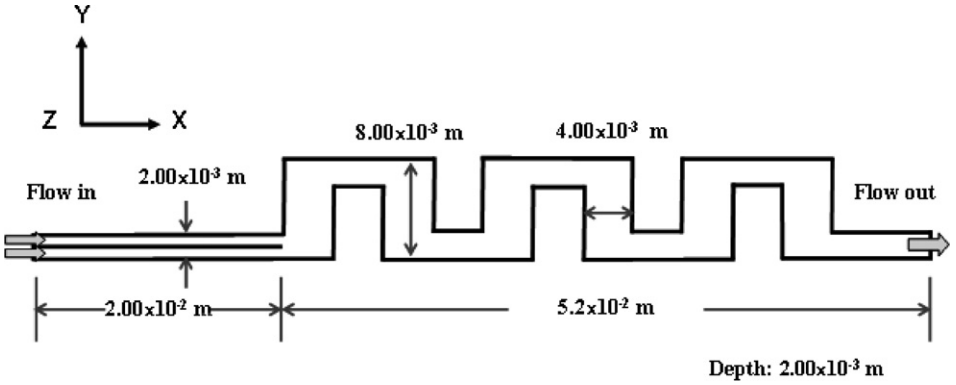

Figure 1.2: Schematic diagram of the mixing channel [17].

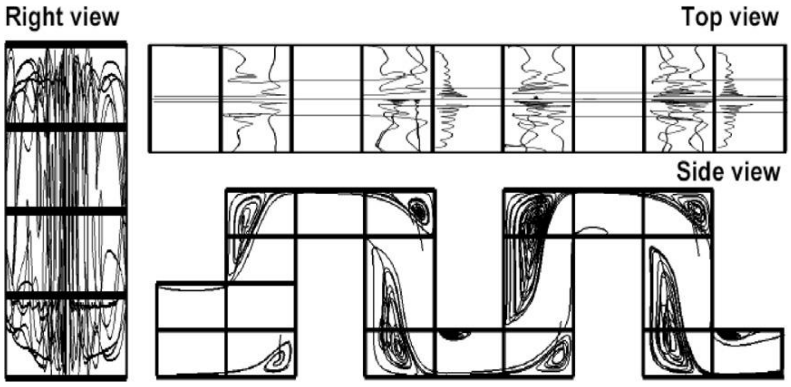

Figure 1.3: Three views of the fluid trajectories of corner flow [17].

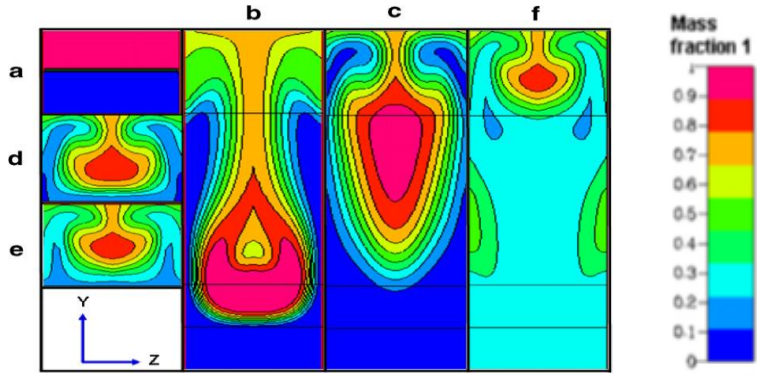

Figure 1.4: Fluid distribution at six analyzed cross sections of the channel [17].

Tet al [18] proposed a passive mixing device of two fluids in laminar regime.They achieved better mixing performance under the effects of chaotic advection. They results showed an enhancement of mixing by adding a periodic external force working on a single rigid particle, which changes the trajectory of the fluid particle.
Recently,Paulo et al [19]developed a numerical simulation using finite difference technique for solving the closure constitutive model in fully developed channel flow.Theyillustrate the effects of varying Reynolds number and the Weissenberg number on the resulting flow patterns.
Saatdjian el al [20] obtained numerical solutions for mixing fluids by chaotic advection in three-dimensional complex geometry (as shown in figure 1. 5). They showed that the key mechanism of chaotic advection isstretching and folding originating from the hyperbolic perturbationinduced by the particles and the rotational motion of theparticles.

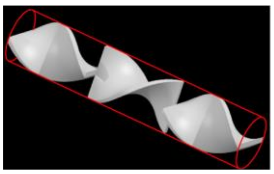

Figure 1.5: Standard helical twisted tape inserts of the static mixer [20].

Mixing performance of micro-channel T-junction with wavy structure relatives to the conventional straight micro-channel T-junction were numerically studied by Nita Solehati et al [21].They numerical results suggest that the mixing quality (M_d) improves significantly for micro-channel T-junction with wavy structure, especially at higher Reynolds number, see figure 1.6.

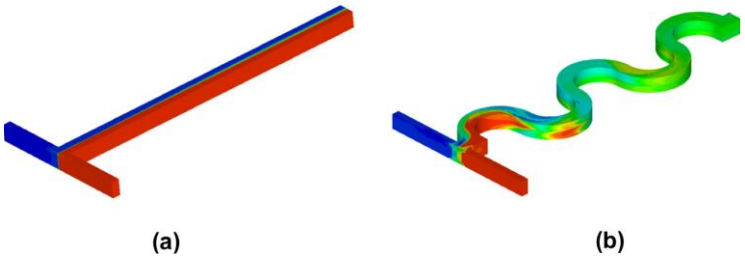

Figure 1.6: Mixing performance of micro-mixer T-junction designs for (a) conventional straight (M_d= 0.018) and (b) wavy structure (M_d= 0.578) at Re = 200 [21].

More recently, Lasbet et al [8] studied the influence of the geometry scale on the kinematic behaviorof the fluid flow for C-shaped channel. The modification of the geometric scale presented an easy and adequate solution to increase these parameters, which examined for different values of the Reynolds number. Theirresults illustrate that the geometry with the smallest hydraulic diameter is the more favourable to increase the considered parameters.

1.3.2.bNon-Newtonian fluids

Many works are currently available on the laminar flow of shear-thinning and shear-thickening fluids, which are frequently modelledby the simple power-law model [22-24]

over a curved or coil ducts. Their results presented the velocity magnitude contours, axial velocity profile and friction factor as function of the Reynolds number.
Castelain and Legentilhomme[25]used Pseudoplastic fluid inside of helically coiled and chaotic systems toshowthe evolution of the flow fraction in the two configurations as function of generalized Reynolds number,(see figure 1.8).

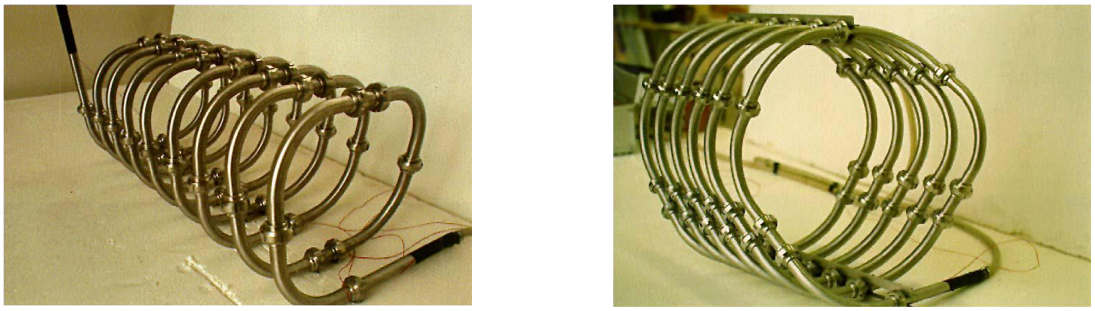

(a) **(b)**

Figure 1.7: Two different systems: (a) helically coiled tube; (b) chaotic configuration [25]

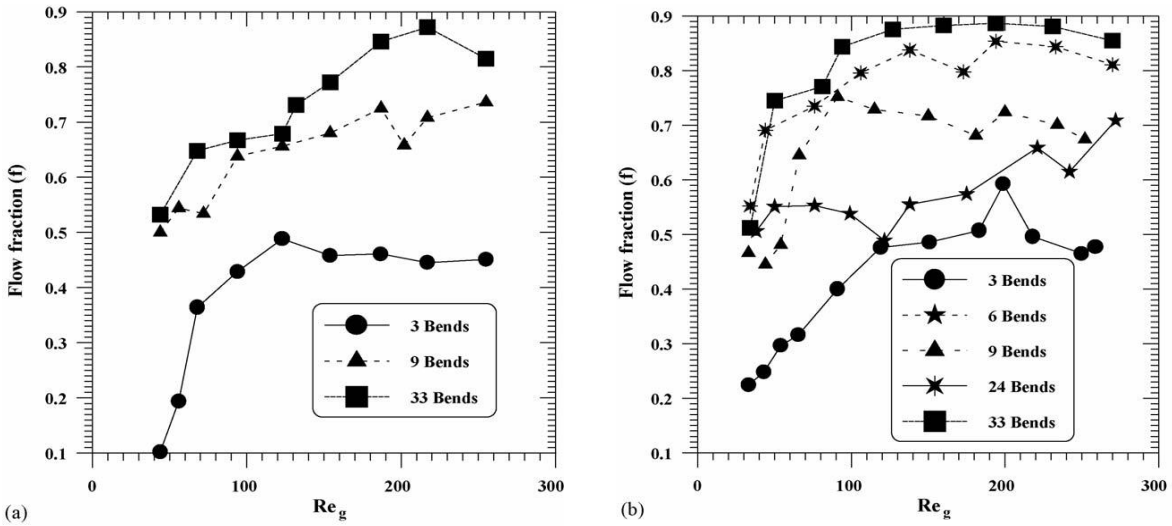

. **Figure 1.8:** Variation of the flow fraction as function of Reynolds number: (a) helically coiled configuration; (b) chaotic configuration [25].

Mohammed et al [26] numericallyinvestigated secondary motion of CMC solution induced by curved channel. They found that two steady Dean cells which developed to four-cell pattern when the centrifugal forces become significant,see figure 1.9.

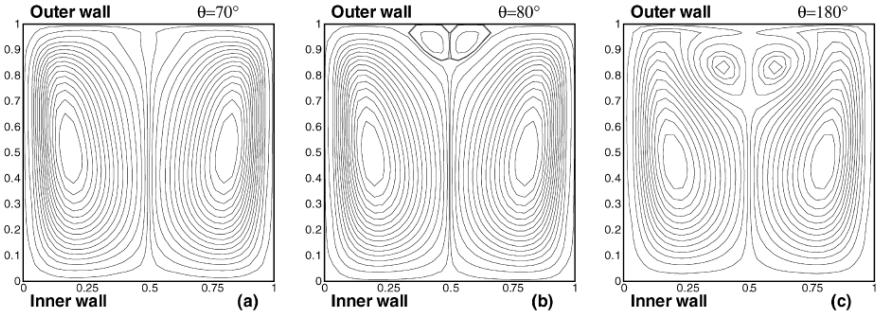

Figure 1.9: Stream function at outlet section of curved duct for non-Newtonian fluid, with different cross sections, (a): $\theta = 70°$, (b): $\theta = 80°$ and (c) $\theta = 180°$[26].

Fellouah et al [27]experimentally and numerically investigated the detail motion of laminar flow of power-law and Bingham fluids in a curved channel in order to understand the effect of rheological fluid behavior on Dean instability. The same phenomena was performed for a curved square duct by Ali Salehi et al [28]. The objective of their work was to examine how a fluid's non-Newtonian viscous behavior affects the onset of Dean instability in a curved square duct, as shown in figure 1.10.

(a) **(b)**

Figure1.10: The effect of power-law index, n, on the velocity vectors of curved channel: (a) n = 0.8, (b) n = 1.2[27].

HosseinHamedi et al [28] modeled a non-Newtonian fluid using Lattice Boltzmann Method (LBM) through complex geometries. Their solutions was validated for both Newtonian and the shear thinning fluids. Their results show the pressure drop along the channel, axial velocity profiles and the effects of pseudo-plasticity for various power-law index (n = 0.5 to 1), as show in figure 1.11.

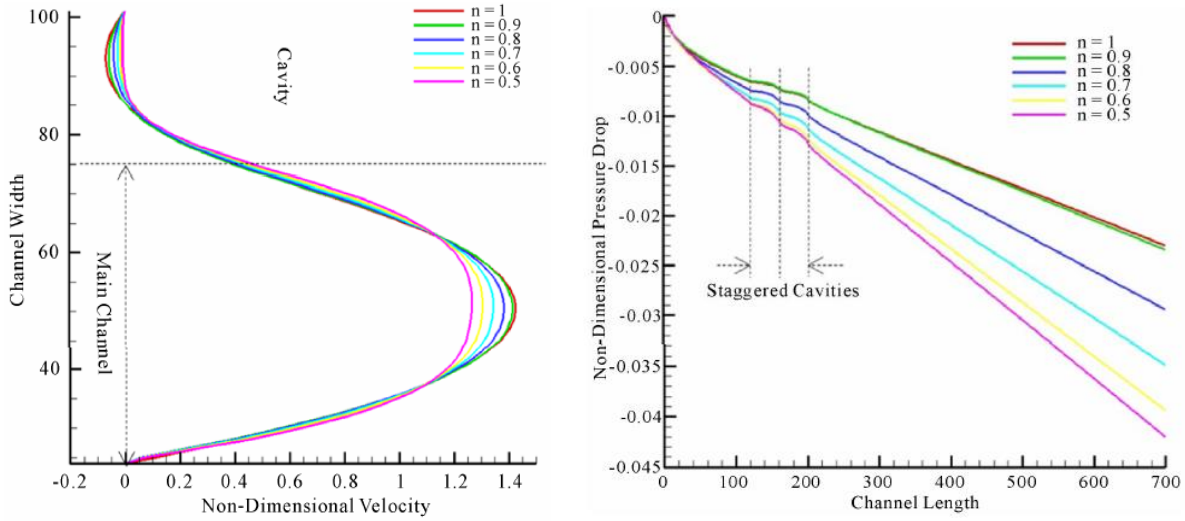

(a) **(b)**

Figure 1.11: (a) Non-Dimensional velocity and (b) Non-Dimensional pressure drop for the shear-thinning fluid[29].

Lattice Boltzmann simulations for Bingham and Casson model fluids through complex channels were investigated by Mitsuhiro et al [30].They considered the flow of viscoplastic fluids passing through rectangular obstacle as shown in figure 1.12.

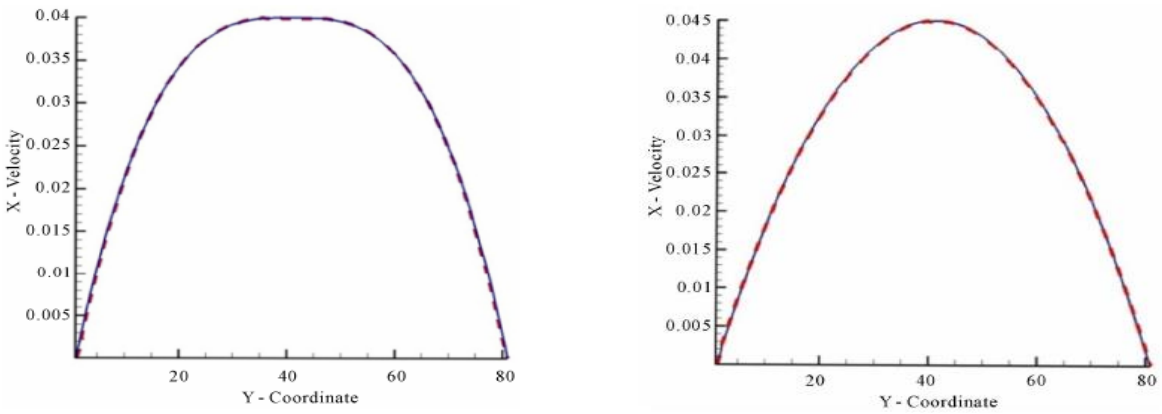

Figure 1.12: axial-velocity profile for (a): Newtonian fluid n = 1 and (b): non-Newtonian fluid n = 0.5 [30].

The Papanastasiou (modified Bingham) model [31] and the modified Casson model was employed in their Lattice Boltzmann simulations. They showed numerical visualizationof viscosity profile and velocity field depending on the fluid type for systems (a): figure 1.14, and system (b): figure 1.15.

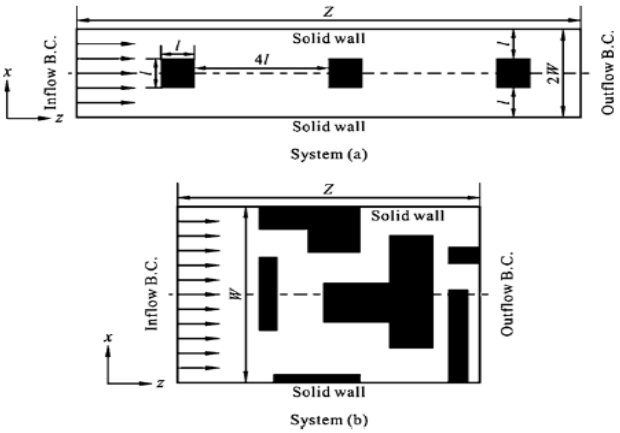

Figure 1.13: Computational system for non-Newtonian fluid flows in the flow channel including rectangular obstacles [30].

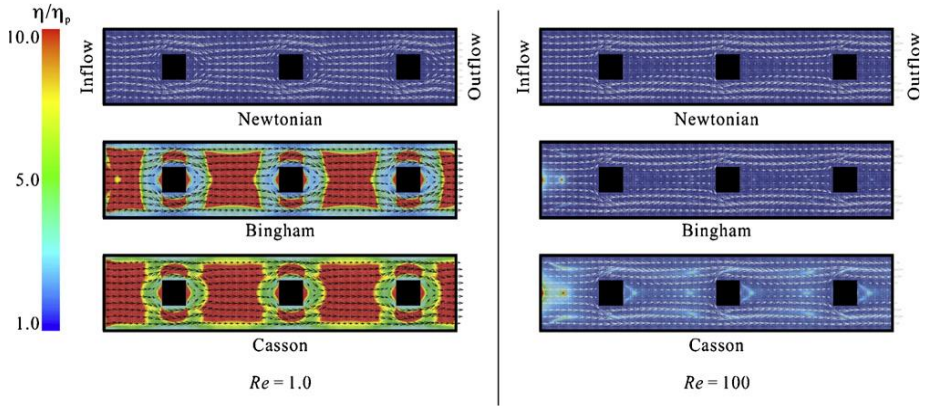

Figure 1.14:Viscosity profile and velocity field for viscoplastic fluids flowing through the flow channel with 3-square obstacles under the condition of Re = 1.0, Bn= 10 (left) and Re = 100, Bn= 0.1 (right)[30].

They results showed that the viscosity for both the viscoplastic fluids was largely decreased around solid obstacles when the fluids flowed around solid obstacles, therefore, the Bingham model fluid exhibited more rapid fall in the viscosity at high shear-rate regions than the Casson model.

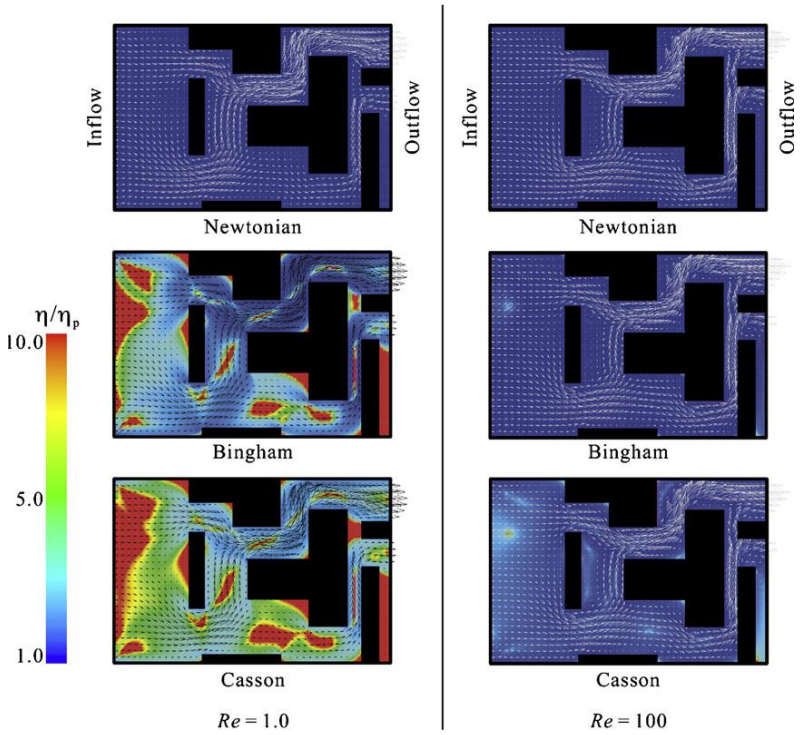

Figure 1.15 Viscosity profile and velocity field for viscoplastic fluids flowing through the complicated flow channel under the condition of Re = 1.0, Bn= 20 (left) and Re = 100, Bn= 0.2 (right) [30].

Ching-Chang Cho et al [32] performed numerically the flow characteristics of non-Newtonian fluids in rough microchannels with a complex-wavy surface. They presented the effect of flow behavior index of the non-Newtonian transported fluids on the local velocity profiles as shown in figure 1.16, and the effects of the wave amplitude on the flow field characteristics.

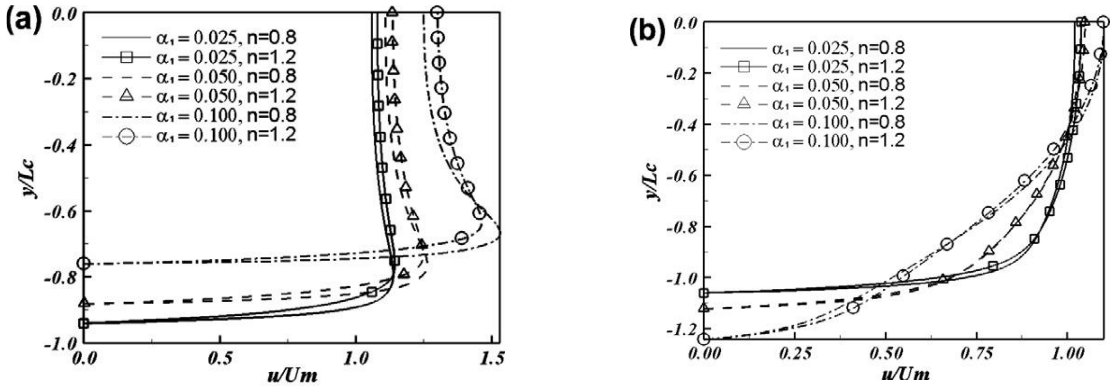

Figure 1.16: Non-dimensional u-velocity profiles in (a) wave crest and (b) wave trough regions of wavy-surface for various wave amplitudes and flow behavior index [32].

Arshad Afzal et al [33] numerically analyzed the mixing flow of non-Newtonian fluids in straight and serpentine microchannels using ANSYS CFX©software. They used the Carreau-Yasuda and Casson non-Newtonian blood viscosity models to capture the non-Newtonian characteristics.

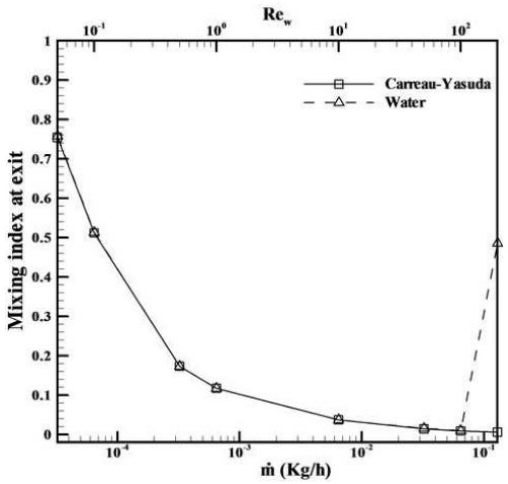

Figure 1.17: Mixing index as function of flow rate at the outlet section of T-junction straight channel for Newtonian fluid (water) and non-Newtonian fluid (Carreau-Yasuda model) [33].

Their results showed that for low mass flow rate, the mixing performances of both the fluids were found to be nearly equivalent, and decreased with flow rate, as shown in figure1.17. Then, they compared the mixing flow between the T-shaped channel and the serpentine channel for blood and water fluids, as shown in figure 1.18. Moreover, they showed a flow visualization comparison of volume fraction at the outlet section between the straight T-junction and serpentine channels, see figure 1.19.

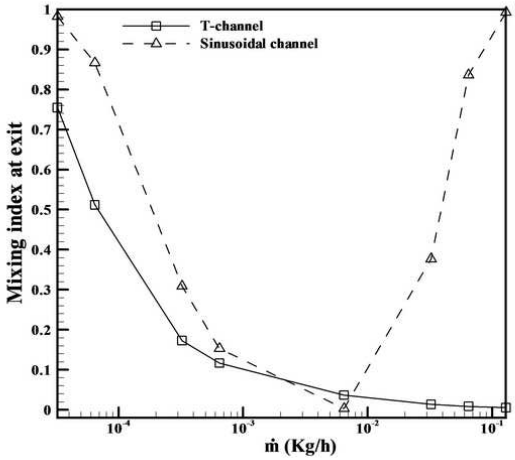

Figure 1.18: Mixing index as function of flow rate at the outlet section for T-channel and serpentine channel for non-Newtonian fluid (Carreau-Yasuda model) [34].

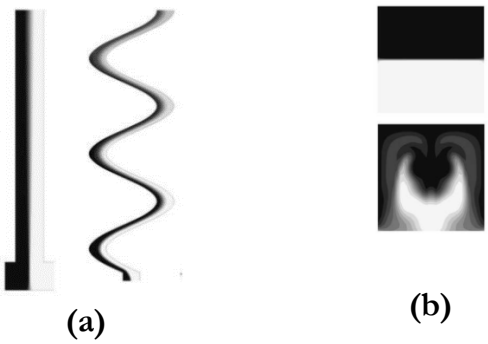

Figure 1.19: Volume fraction of non-Newtonian blood model for T-junction and serpentine channels, (a): longitudinal section and (b): outlet cross-section [33].

Vinit Khandelwal et al [34] presented numerical results for laminar flow of shear-thinning fluids in a T-channel. The flow fields have been explained by streamline contours for all cases of shear thinking fluid, see figure 1.20.

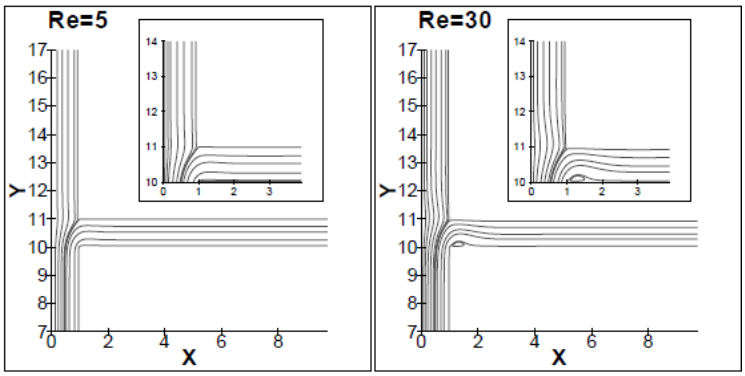

Figure 1.20: Stream function contours in a T-channel at different values of Reynolds number [34].

They results showed that for a particular n, length of recirculation zone increases in the side branch with increasing Reynolds number.

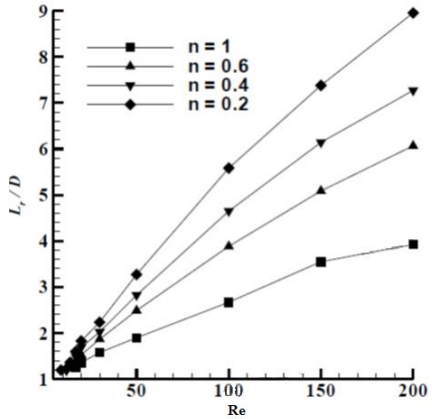

Figure 1.21: Variation of dimensionless recirculation length (*Lr/D*) with Reynolds number at different values of power-law index [34].

1.4Thermal behavior

1.4.1Straight ducts

1.4.1.a Newtonian fluids

Many researchers have studied the heat transfer phenomena of Newtonian fluid flows in straight ducts. Some studies reviewed by Shah and London [35] [36] and Shah and Bhatti [37] for laminar flow. They used the finite differencemethod to obtain numerical solutions for fullydeveloped conditions.

Sehyun et al [38] numerically studied the laminar heat transfer withtemperature dependent fluid viscosity in a 2:l rectangular duct. The H1 thermal boundary condition corresponding to axially constant heat flux was adopted for the configuration. They proposed a new correlation for local Nusselt numbers in the straight duct, which covers boththermally developing and thermally fully developed regions.

Effect of viscous dissipation on laminar mixed convection in a vertical channelwas analyzedby Barletta [39]in the fully developed region. The temperature, velocity field and the Nusselt numbers were obtained for Brinkman numbers. Then, the same work was investigated for the reversal flow with one or more isotherm walls [40].The author analytically discussed the velocity, temperature profiles and friction factor witch dependent on the ratio between the Grashof number and the Reynolds number. After that, Barletta [41] [42] obtained the Nusselt number and Poiseuille under the effect of wall heat flux on vertical rectangular duct, while the effect of the choice of the reference fluid temperature was considered. They found that the choice of the reference temperature affects both the velocity profiles and the axial change of the difference between the pressure and the hydrostatic pressure.

Muzychka and Yovanovich [43] investigated the laminar forced convection in the combined for fully developed flow of straight ducts. They developed a new model for predicting Nusselt numbers for both isothermal and wall flux boundary conditions. The agreement between the proposed modeland numerical data is within 15%.

An exact analytical solution for heat transfer characteristics in straight ducts with rectangular cross-sections wasdevelopedby Mohammad and Mahmoud [44], which validated for both H1 and H2 boundary conditions. The authors obtained the local and mean Nusselt numbers asfunctions of the aspect ratio.

Recently, Sphaier and Barletta [45] analyzed the unstablemixed convection in a horizontal heated duct for laminar flow of Newtonian fluid. Their analysis confirmed that longitudinal rollsindeed lead to most unstable situations, for different the Rayleigh numbers.

1.4.1.b Non-Newtonian fluids

Non-Newtonian flows and heat transfer were studied in early years by Seppo[46], and Ray and Misra [47] who showed that the effects of fluid behavior index on laminar forced convection in straight channels. James and Milivoje [48] investigated the heat transfer of Newtonian and non-Newtonian fluidsin rectangular ducts.

Sayed-Ahmed and Kishk [49] used the finite differencemethod to investigate laminar flow and heattransfer non-Newtonian fluids in a rectangular duct. They considered two thermal boundary conditions (T and H2)and the effects of the aspect ratio, the Prandtl number, velocity, and pressure on the temperature and the Nusselt number.

Sayed-Ahmed and Karem [50] presented a numerical solution for combined laminar fluid flow and heat transfer of Herschel–Bulkley fluid in a rectangular duct. The authors studied the problem in the entrance region of a rectangular duct.

Numerical investigation on performance comparison of non- Newtonian fluid flow in vertical heat exchangers combined helical baffle with elliptic and circular tubes (figure 1.22) was performed by Zhenbin He el al [51].Their found that the thermal performance factor enhances by 30–35%, which demonstrates that the elliptic tube can effectively improve the heat transfer performance of non-Newtonian fluid flowing in the helical baffle heat exchanger when compared to the circular tube.

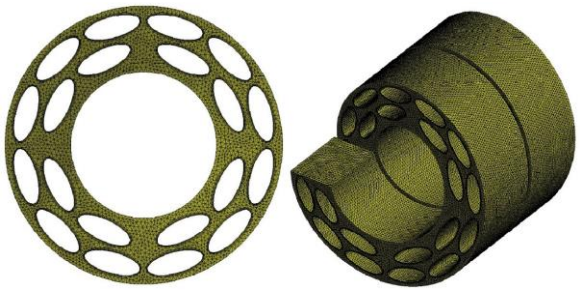

Figure 1.22: Layout pattern of tubes: Elliptic tubes [51].

Two new correlations, for the friction factor and the Nusselt number of the heat exchanger, were proposed:

$$Nu_0 = 0.089 Re_0^{0.6992} Pr_0^{1/3} \ (R^2 = 0.9993)$$

$$f_0 = 0.5989 \ Re_0^{-0.1574} \ (R^2 = 0.9994)$$

Gharraei et al [52]numerically investigated the power-law non-Newtonian flow and heat transfer characteristics of multiple impinging square jets. Their results reveal that jet-to-plate spacing have important effects on the flow structure and local Nusselt number (Figures 1.23 and 1.24). The size of peripheral vortices was increased by increasing the power-law index. By decreasing the jet-to-plate spacing, the effect of walls becomes considerable, therefore the size of peripheral entrainment vortices decreases. On the other hand, by increasing the power-law index, the wall Nusselt number increased which was the result of higher inlet velocity for fluids with higher power-law indices.

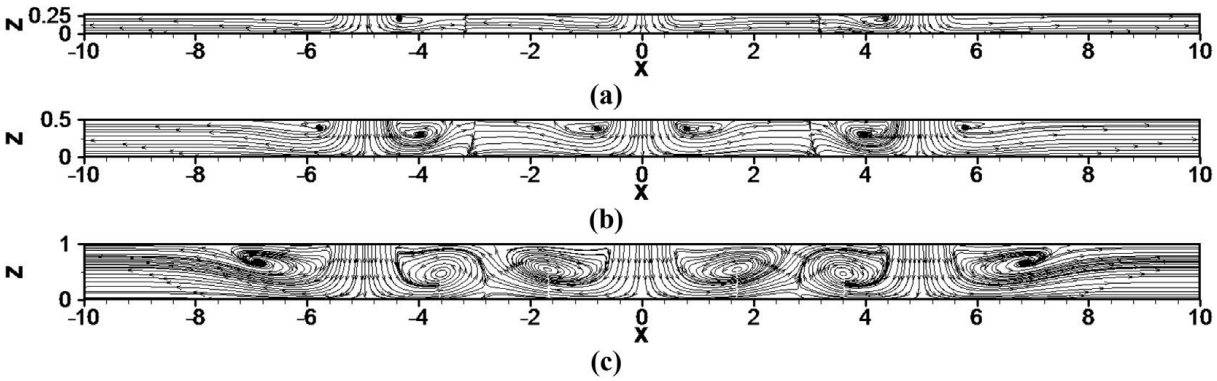

Figure 1.23: Streamlines for Reynolds number Re =100, and power-law index (a) n = 0.4, (b) n= 1 and (c) n = 1.6 [52].

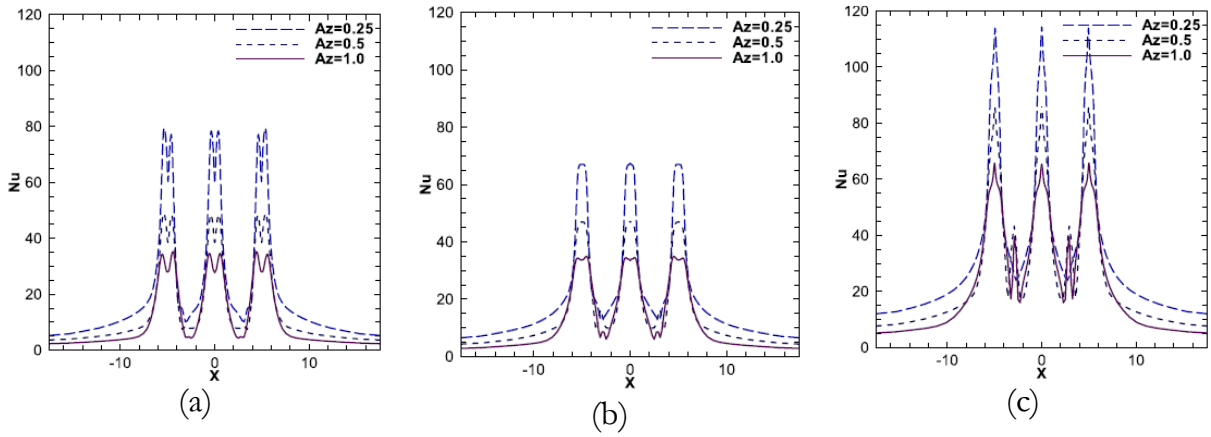

Figure 1.24: Distribution of local Nusselt number for Reynolds number Re= 100, and power-law index (a) n = 0.4, (b) n= 1 and (c) n = 1.6 [52].

1.4.2 Complex channels

1.4.1.a Newtonian fluids

In complex channel structures or chaotic geometries, laminar flow of Newtonian fluids has been the subject of many investigations for different configurations such as planar serpentine, chaotic channels [53] [6] and zigzag channels [56] and helical ducts [54]. Their heat performance was considerably improved compared to that when the flow is regular (straight channel).

Convective heat transfer in chaotic configuration (coiled tube with bends) of laminar flow regime at different values of Dean number with constant wall flux was investigated by Vimal Kumar [53]. The effects of Dean number on the development of average friction factor and Nusselt number were presented in figure 1.25. The results show that the chaotic configuration shows a 25–36% enhancement in the heat transfer due to chaotic mixing while relative pressure drop is 5–6% compared to the coiled tube.

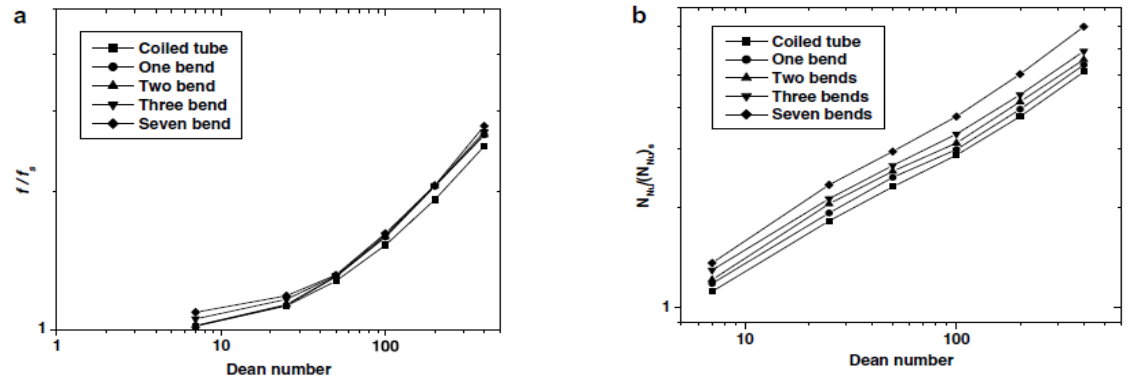

Figure 1.25:(a) Friction factor variation and (b) Nusselt number variation in coiled tube and chaotic configuration [53].

Lasbet el al [5] [6] considered four chaotic geometries (square-wave mixer geometry, C-shaped, V-shaped, and B-shaped geometries) to enhance the heat transfer and mixing fluids in laminar Newtonian flow. They found that the C- channel geometry significantly improves convective heat transfer over that ofregular straight or square-wave mixer channels, see table1.1.

Table 1.1: Comparison of the average Nusselt number, average Poiseuillenumber, and the Po/Nu ratio for the considered geometries [6].

	Average Nusselt number	Average Poiseuille number	Ratio (Po/Nu)
Straight channel	3.0	62	20.7
Square wave mixer	11.0	126	11.5
C-shaped	20.0	160	8
B-shaped	13.0	93	7.2
V-shaped	13.1	89	6.8

Jung et al. [54] studied the friction factor and the heat transfer of a helical heat exchanger. The heat exchanger is composed of a helical tube with rectangular cross section and two cover plates. In the experiment part, the radial flow was air and the helical flow was water. The Reynolds numbers were in the range 307– 2547. They results indicate that the Darcy friction factor of the radial flow increases with the channel spacing and decreases with an increase of the Re, and Nusselt number increases with the Reynolds number and the channel spacing.

Charbel Habchi et al [55] carried out the influence of several arrays of vortex generators mounted inside a complex geometry on mixing flow of two fluids which heated by different temperature (300 and 320). Two flow configurations are considered in which the arrays are in-line and rotated periodically by an angle of 90°,see figure 1.26. Each vortex generator creates a pair of stream-wise vortices, which enhances the mixing performance in the flow cross section.

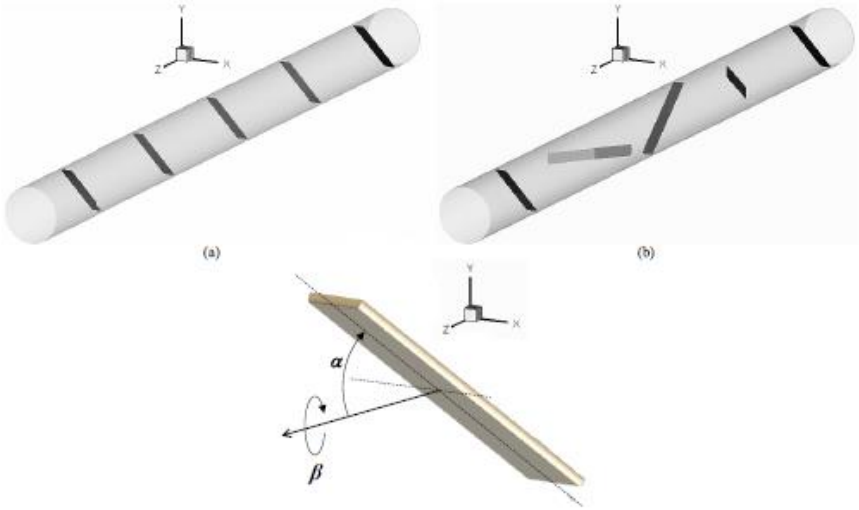

Figure 1.26: Isometric views of the (a) in-line and (b) alternate configurations and (c) of one tab with the main rotation angles. The flow is in the z axisdirection [55].

Their results showed that the alternate configuration, in which the vortex generators are rotated periodically by an angle of 90°, enhances the mixing process relative to the in-line one due to the generation of chaotic advection flow, while in the in-line configuration the flow is regular and the mixing process is only caused by the convective motion of the longitudinal vortices. By exploring the Poincaré sections and the Lagrangian trajectories projections of different passive tracers, it is found that chaotic advection takes place in the alternated configuration while the flow in the in-line configuration stays regular, as shown in figure 1.27 and figure1.28, respectevley. Then, the authors found that the thermal mixing flow clearly enhanced by the fact that the chaotic advection is better distributed at the flow cross section, as shown in figure 1.29.

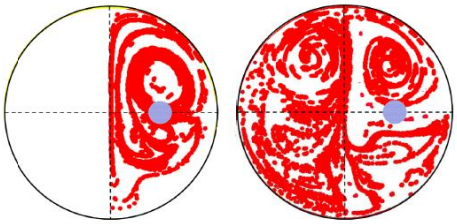

Figure 1.27: Poincaré section for (left) in-line and (right) alternate configurations for initial 5000 particles injected at (x_0= 5 mm, y_0= 0 mm)[55].

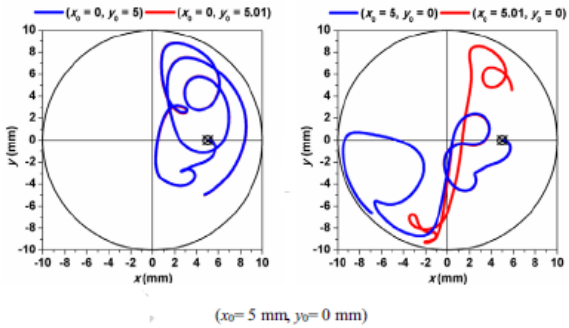

(x_0= 5 mm, y_0= 0 mm)

Figure 1.28: Projections of the Lagrangian trajectories for different initial positions for the (left) in-line and (right) alternate configurations [55]

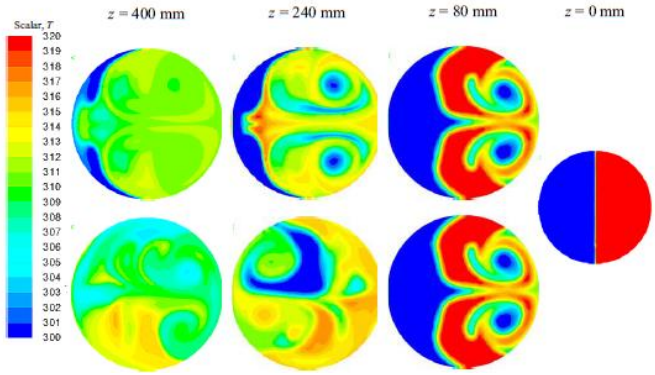

Figure 1.29: Scalar *T* contours on different cross sections for (top) in-line and (bottom) alternate configurations [55].

ZhanyingZheng et al [56] studied the laminar flow and heat transfer for Periodic Zigzag channel with square cross-sections, considering the effect of chaotic advection. They used the Poincare section, for Re = 150, to present the stretching and folding of the tracer particle. Then, they showed, for Re = 400 (Figure 1.30), the tracer particles witch almost covered the entire area of the cross-section. Also, They presented a streaklines, and secondary flow vectors, axial velocity fields (d and e), see figure 1.31.

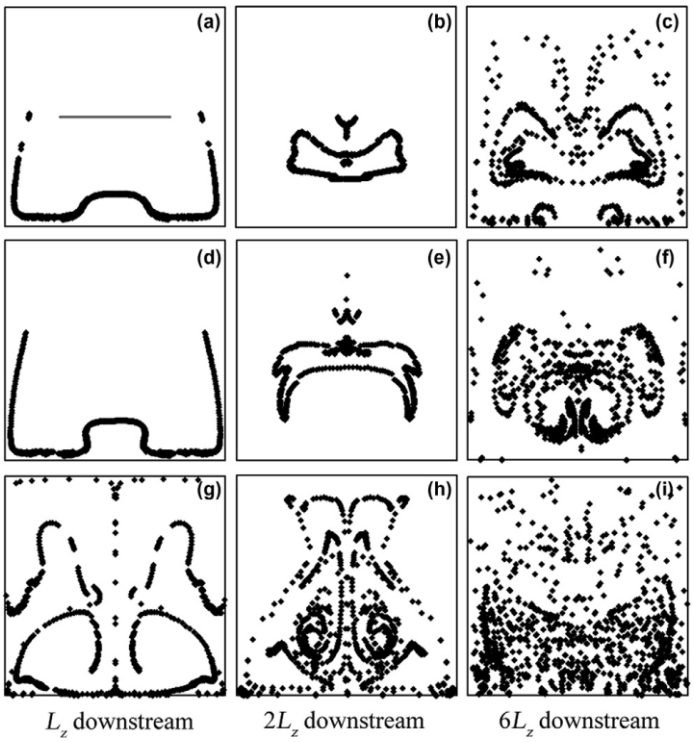

Figure 1.30: Poincaré sections at locations Lz(half unit), 2Lz and 6Lz downstream of the initial plane for Reynolds numbers of 150 (a–c), 200 (d–f) and 400 (g–i) [56].

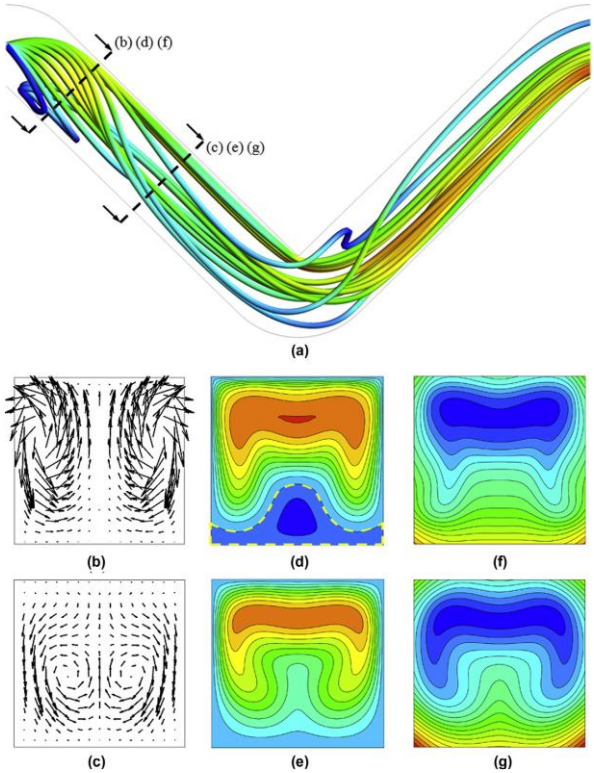

Figure 1.31: Streaklines (a), secondary flow vectors (b and c), axial velocity fields (d and e) and non-dimensional temperature fields (f and g) in a fully-developed periodic flow unit at Re = 200 [56].

The red color indicates regions of high velocity or non-dimensional temperature and the blue color indicates regions of low velocity or non-dimensional temperature. The yellow dotted line demarcates the region of reverse flow [56].

Tohidi et al [57] have numerically investigated the effects of chaotic mixing on heat transfer through modifications in the geometry of helical heat exchangers, see figure 1.32.

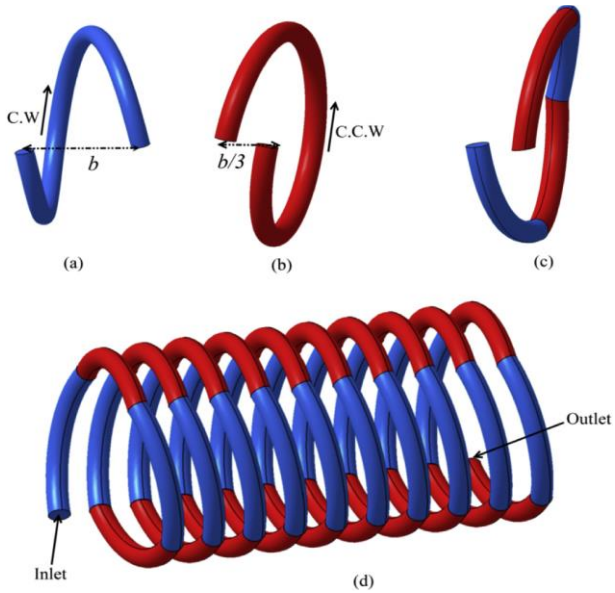

Figure 1.32:(a) Coil with clockwise orientation; (b) coil with counterclockwise orientation; (c) one period of the chaotic configuration; (d) 10 periods of the chaotic configuration [57].

They presented the Heat transfer performance by isotherms contours in different cross-sections, see figure 1.33. Their numerical solutions revealed that the chaotic coil configuration displayed heat transfer enhancement of 4-26% relative to the fully developed Nusselt numbers in the regular coil with only 5-8% change in the pressure drop.

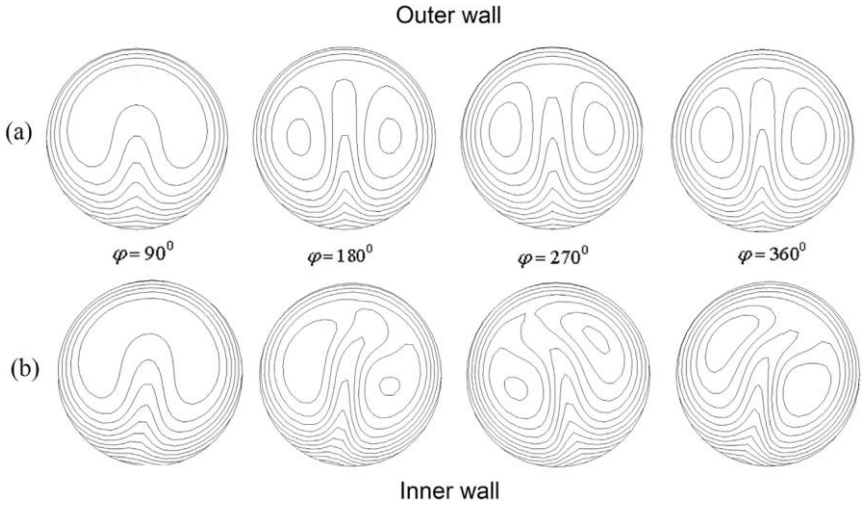

Figure 1.33: Velocity contours at different cross-sections in (a) normal coil and (b) chaotic coil at first pitch of coil with Re =200 [57].

Tian and Mostafa[58] used the chaotic advection to enhance the continuous heat-hold-cool sterilisation process. They geometry was meshed with hexahedral cells using CFX 14.5, as shown in Figure 1.34. The authors compared the physical model with the results of a numerical study of EesaandBarigou, [59].Their results indicated that the chaotic flow process leads to faster nearly-uniform heating and cooling.

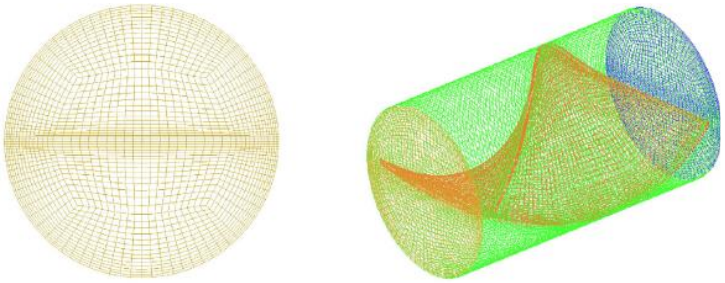

Figure 1.34: Computational mesh: [58]

1.4.1.b Non-Newtonian fluids

Several works can be found regarding the coupling between chaotic mixing for rheologically complex fluids and heat transfer (El Omari et al [61] and Lester et al [60], Ping Li et al [62] and Waleed et al [64]. Since most fluids involved in industrial processes are non-Newtonian (e.g., food or chemical products), there is a crucial need to focus on the application and study of chaotic advection for mixing and heat transfer for these fluids.

El Omari et al. [61] investigated numerically the enhancement of both mixing and heat transfer in a two-rod mixer for highly viscous non-Newtonian fluids (shear-thinning, shear-thickening and Newtonian fluids). Chaotic flows were obtained by imposing the temporal modulations of the rotational velocities of the walls. The authors confirmed that chaotic mixing is suitable for shear thickening fluids for which it is observed a clear enhancement of the thermal mixing (heat extraction and homogenization), see figure 1.36.

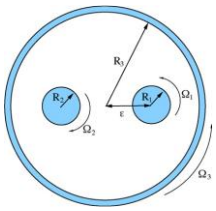

Figure 1.35: Sketch of the two-rod mixer [61].

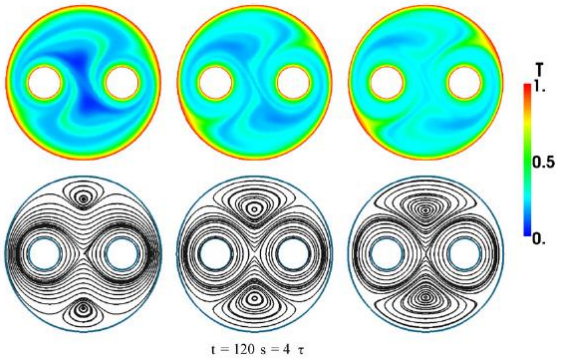

Figure 1.36: Temperature fields and streamlines at instants t = 120 s [61].

Lester et al [60] studied the asymptotic scalar transport (temperature or concentration) within both Newtonian and non-Newtonian fluids over the control parameter space of a chaotic flow, the Rotated Arc Mixer (RAM). The goal of their analyses was to utilize the composite spectral method to quantify and optimize heat or mass transfer within a chaotic configuration.

Shear-thinning fluid and heat transfer effects for laminar flow in heat sinks with dimples and protrusions were numerically investigated by Ping Li et al [62]. They showed that the heat and mass transfer enhancement due to the behavior of non-Newtonian fluids is mainly because of the variation of dynamic viscosity of working substances and the secondary flow in the dimpled/protruded passage with flow separation.

More Recently, Waleed et al [63] experimentallystudied the characteristics of convective heat transfer and fluid flow within a square cross-section serpentine channel for two types of polymeric fluids, shear-thinning and constant-viscosity Boger solutions. They found that the normalized values of non-dimensional pressure drop increase monotonically with increasing Weissenberg number.

1.5 Entropy generation

1.5.1 Straight ducts

1.5.1.a Newtonian fluids

Recently, entropy generation has been used as an index for evaluating the significance of irreversibility related to heat transfer and fluid friction in a thermal engineering. Based on the concept of efficient exergy use and minimal entropy generation principal, optimal designs of thermodynamic systems have been widely proposed from the viewpoint of thermodynamic second law [64].To enhance the heat transfer efficiency of Newtonian fluid in ducts, the rate of entropy generation must be effectively controlled. Bejan [64] presented a method for calculating the entropy generation in a flow field and proposed a minimum entropy generation principle.

Entropy generation and second law analysis for the laminar flow passing through straight duct was studied by Yilbas et al [65]. They developed the dimensionless quantities for the entropy generation, heat transfer and irreversibility. They found that the irreversibility increases with increasing Prandtl number.

Extended performance criteria based on the augmentation entropy generation numbers for enhanced heat transfer surfaces for ducts with constant wall temperature was developed by Zimparov [66].

Abbassi et al. [67] reported the entropy generation in straight channel flow. They found that the maximum entropy generation is localized at areaswhere heat exchanged between the walls. In the similar manner, Nourullahi et al. [68] analyzed the entropy generation and Nusselt number in Poiseuille–Benard channel flow. Their result showed that the Nusselt number changes very slightly and it is almost constant for low values of inclination angle. The heat transfer entropy generation is localized at areas where heat exchanged between the walls and the flow has a maximum value.

Chen et al [69] performed a numerical study of entropy production of mixed convection flow in a vertical channel. Their numerical results showed that the entropy generation rate had a minimal value near the centerline of the channel.

Chen et al [70] studied a the heat transfer and entropy generation within a fully developed flow in a vertical duct. Their simulations focus specifically on the effects of the mixed convection dimensionless parameter, Brinkman number on the velocity distribution, temperature distribution, Nusselt number and entropy generation through the channel.

Yang, and Wu [71] numerically investigated the mixed convection flow and heat transfer in a vertical rectangular duct under the effect of assisted buoyancy at a constant Prandtl number. They found that the reversal flow to occur in the entrance region when buoyancy parameter exceeds a certain critical value, which strongly affects the temperature field. Then, they presented the effect of the opposed buoyancy force on the global entropy generation due to heat fluid friction.

Chen [72] studied the heat transfer performance and entropy generation characteristics of a mixed convection in a vertical subject to viscous dissipation effects. Their results showed that the presence of the magnetic field increases the Nusselt number. Moreover, the average entropy generation number also reduces when a magnetic field is applied.

1.5.1.b Non-Newtonian fluids

Since there are many applied applications related to non-Newtonianfluids, the valuation of their heat transfer characteristics isvital for accomplishing successful thermal system designs. Mahmud and Fraser [73] [76] carried out the second-law analysis of heat transfer inducts for non-Newtonian fluids. They neglected the viscous dissipation term in the energy equation. The rationale of neglectingviscous dissipation effect in the energy equation (first-lawanalysis) isdubious as the fluid friction irreversibility due to frictional heating ofviscous dissipation plays a vital role in the second-law analysis.

Luna et al. [74] reported a steady stateanalysis of a power law fluid in the entrance region of a thermallydeveloped flow with uniform heat flux.

Entropy production due to the flowof a non-Newtonian fluid withvariable viscosity in a straight pipe carried out by Yilbas and Pakdemirli [75]. They presented analytical solutions for velocity and temperature distributions. Then, theycomputed the entropy generation number for different non-Newtonian parameters, viscosity parameters, and Brinkman numbers.

Numerical simulations to examine wall slip effects on Newtonianand non-Newtonian fluid flows in microchannelswere performed by Sunarso et al [77]. They showed that the different vortex growth could be observed in micro scale due to theinclusion of wall slip, which qualitatively matched with experimentalresults. Barkhordari and Etemad [78] analyzed a numericalstudy on convective heat transfer in microchannels at both constant wall temperature and constant wall heatflux boundary conditions. Their computational results showed thata change in the slip coefficient decreased Poiseuille number whileincreasing local Nusselt number.

Second low analyses of non-Newtonian fluids for laminar and fully developedflow in straight channel with viscous dissipation effects provided by Saouli and Aiboud [79]. Effect of Brinkman number and flow behavior index on velocity, temperature and entropy generation rate were discussed. They found that the entropy generation irreversibility dominated in Pseudoplastic fluid by the heat transfer, whereas, for dilatant fluid irreversibility due to fluid friction is more dominated.

An analytical study of entropy generation for fully developed non-Newtonian flow through microchannels, in which the effects of viscous dissipation on the entropy production were investigated by Hung [80]. Their results indicated that under certainconditions the viscous dissipation effect on entropy generation in microchannels is significant and should notbe neglected.

Ragueband Mansouri[81] proposed a numerical analysis to study the heattransfer characteristics of a laminar flow of a power law fluidwith viscous dissipation. They found that in the fully developedregion, Nusselt number increases with increase in aspect ratio.

Chen et al. [82] studied heat transfer characteristics of non-Newtonian powerlawfluid flow in a straight channel and reported dimensionless temperaturedistributions and fully

developed Nusselt numbers for differentparameters such as flow behavior index, ratio of Joule heating to surface heatflux, and Brinkman number.
Vishal [83] investigated the viscous dissipation effect on entropy generation for non-Newtonian fluids in laminar fluid flow through a microchannels subjected to constant heat flux. He investigate the effect of various friction coefficients of the slip laws on entropy generation rate and Bejan number.

1.5.2 Complex channels

1.5.2.a Newtonian fluids

As a good heat-exchanger passage, the chaotic channels should provide the most effective heat transfer performance so that the available energy can be utilized efficiently. However, the heat transfer enhancement in a thermal system is always achieved at the expense of the increase of friction loss. Some typical examples include: the irreversibility analysis in various irregular geometries for Newtonian fluids with constant wall heat flux and laminar flow performed by Sahin [84] [85]; the optimizing work for the helical coils or double-sine duct by Ko and Ting [87] [88].
Second law of thermodynamics for laminar convection inside an inclined wavy enclosure was numerically performed by Shohel [86]. They presented the contours of Bejan to understand the development of entropy generation under the effects of inclination angle, see figure 1.37.

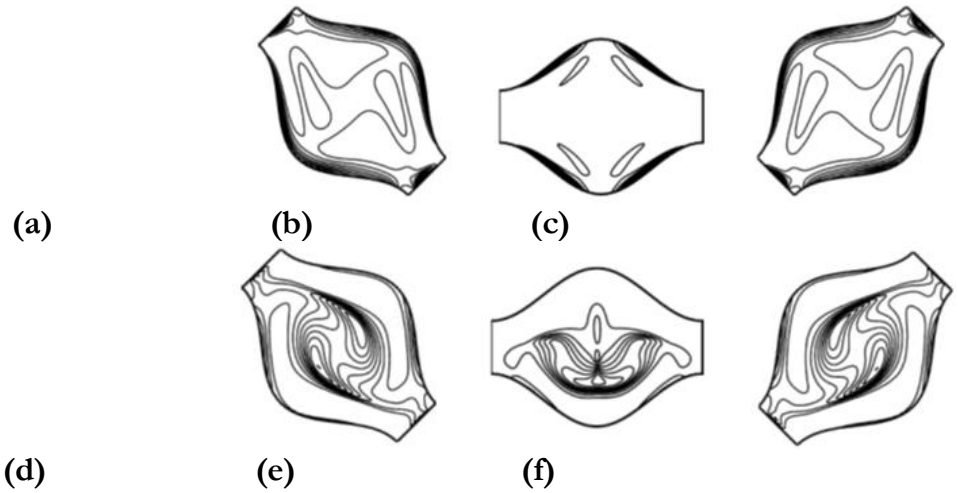

Figure 1.37: Contours of Bejan numberatdifferent angles of inclination (a) $\theta = 45°$, $Be_{max}= 1$, $Be_{min}= 0.82$; (b) $\theta = 90°$, $Be_{max}= 1$, $Be_{min}= 0.97$; (c) $\theta = 135◦$, $Be_{max}= 1$, $Be_{min}= 0.82$; (d) $\theta = 255◦$, $Be_{max}= 1$, $Be_{min}= 0.19$; (e) $\theta = 270◦$, $Be_{max}= 1$, $Be_{min}= 0.21$; (f) $\theta = 315◦$, $Be_{max}= 1$, $Be_{min}= 0.19$. [86]

Computational Fluid Dynamics simulation of entropy generation were investigated by Ko and Ting [89] for incompressible laminar shear flows in heated curved rectangular duct. They present the effects of three important factors, including Dean number, external wall heat flux and cross-sectional aspect ratio, on entropy generated from frictional irreversibility and heat transfer irreversibility. They compared various rib arrangements

and discovered that mounting a single rib on the heated wall could reduce the entropy generation most effectively. They results reveal that the major source of entropy generation in the flow fields with larger Dean number and smaller wall heat flux comes from frictional irreversibility; whereas for the flow fields with smaller Dean number and larger wall heat flux the entropy generation is dominated by heat transfer irreversibility, as shown in figure 1.38.

Zimparovet al [90] optimized the performance of several classes of assumed laminar and fully developedflow, consisting of T- and Y-shaped ducts. Maximum thermodynamic performance is acieved by minimization of the entropy production for each geometry.

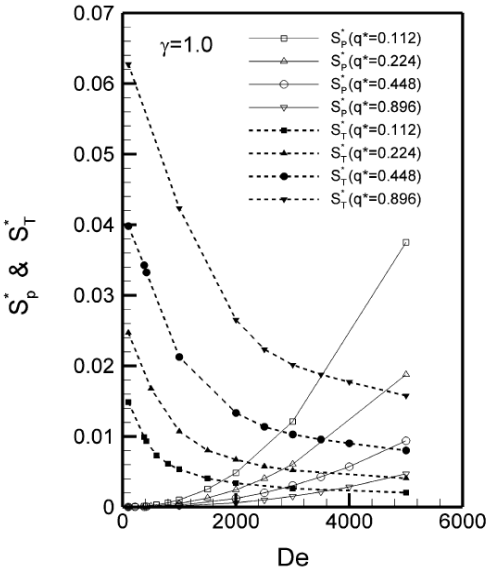

Figure 1.38: The effects of *De* on entropy generation induced from heat transfer (S^*_T) and fluid friction (S^*_P) [89].

Yonghua et al [91] studied the second low thermodynamics for laminar thermal augmentation with conical strip inserts in horizontal circular tubes. They use horizontal circular tubes fitted with non-staggered and staggered conical strip inserts as physical model, see figure 1.39. Comparisons of local entropy generation rates between non-staggered alignments and staggered ones were conducted, see figure 1.40. They found that the tubes with non-staggered strips behave better than those with staggered ones.

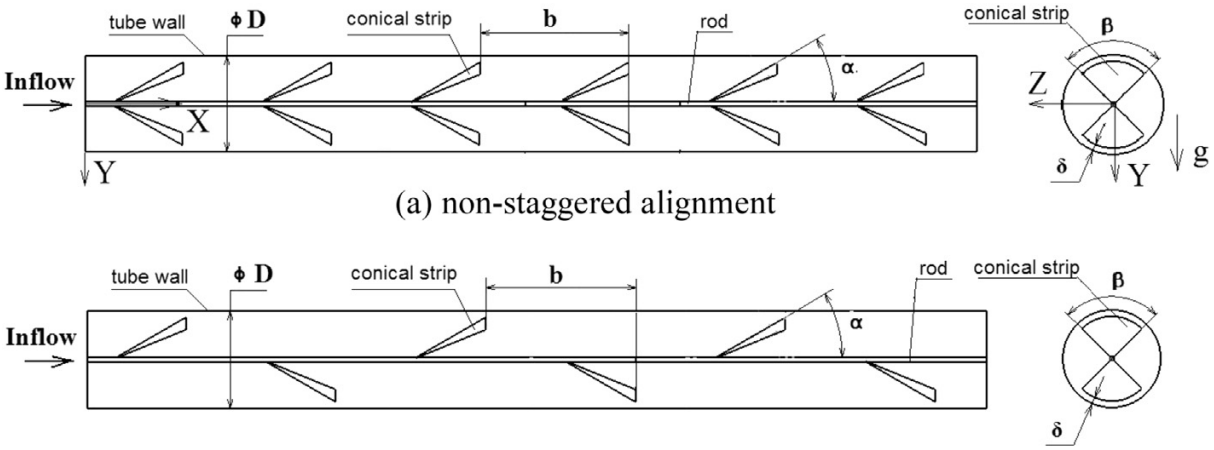

Figure 1.39: Schematics of enhanced tubes with conical strip inserts. (a) Non-staggered alignment; (b) staggered alignment [91].

Mohammad et al [92] investigate the entropy generation in a helically coiled tube in laminar flow under a constant heat flux. Their results showed that the effect of different flow conditions such as mass velocity, saturation temperature, and heat flux on contributions of pressure drop and heat transfer in entropy generation.

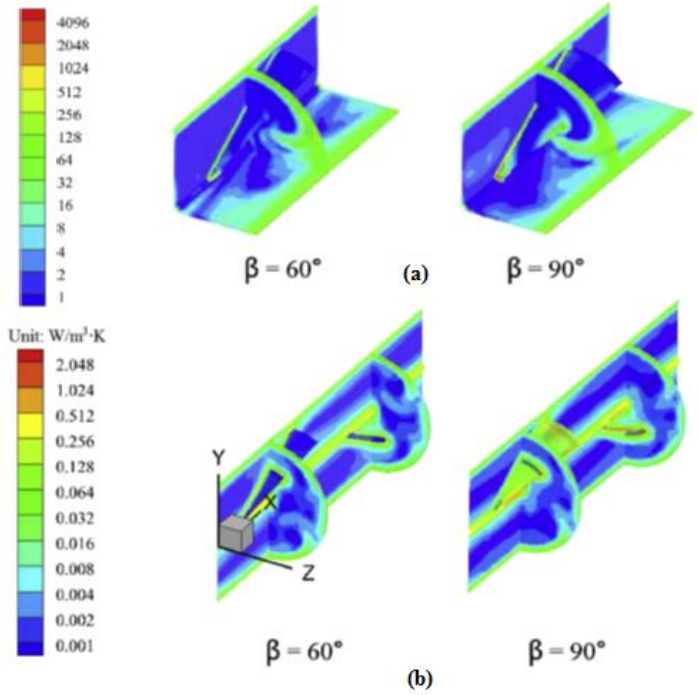

Figure 1.40: Contours of local entropy generation rate induced by viscous flow at longitudinal plane and cross sections for enhanced tubes with (a): staggered strips and (b): non-staggered strips of different geometry angles [92].

Recently, Jundika et al [93] numerically investigated the heat transfer and entropy generation of laminar flow in helical tubes with various cross sections, see figure 1.41.. They summarized the advantages and disadvantages of straight and coiled tubes for various cross-sectio8n channels, as shown in table 1.2.

Table 1.2: Advantages and disadvantages of straight and coiled tubes heat exchanger [93].

Straight tube	Coiled tube
Lower heat transfer performance Circular < ellipse < square	Higher heat transfer performance Circular < ellipse < square
Lower pressure drop (pumping power) Circular < ellipse < square	Higher pressure drop (pumping power) Circular < ellipse < square
Higher total entropy generation Circular < ellipse < square	Lower total entropy generation Circular < ellipse < square
Higher entropy generation due to heat transfer Circular < ellipse < square	Lower entropy generation due to heat transfer Circular < ellipse < square
Lower entropy generation due to viscous dissipation Circular < ellipse < square	Higher entropy generation due to viscous dissipation Circular < ellipse < square

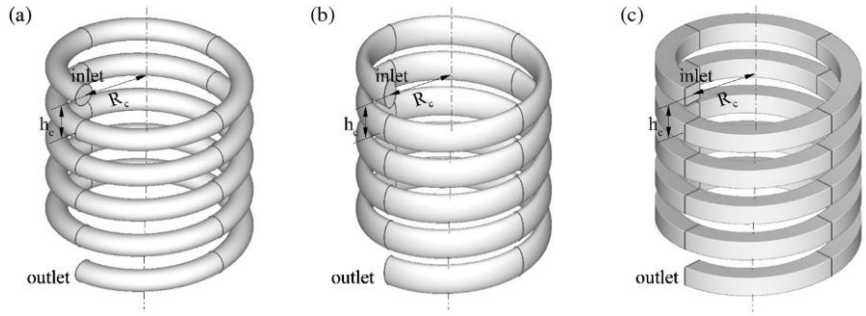

Figure 1.41: Schematic representation of (a) helical circle, (b) helical ellipse, (c) helical square tubes [93].

1.5.2.b Non-Newtonian fluids

Effects of temperature-dependent viscosity on entropy generation in curved square micro-channel for laminar flow were numerically investigated by Jiangfeng [94]. They demonstrated the variations of heat transfer entropy generation number with the mass flow rate for the cases of aniline heated and cooled, see figure 1.42. They found that entropy generation number due to heat transfer decreases as the mass flow rate increases.

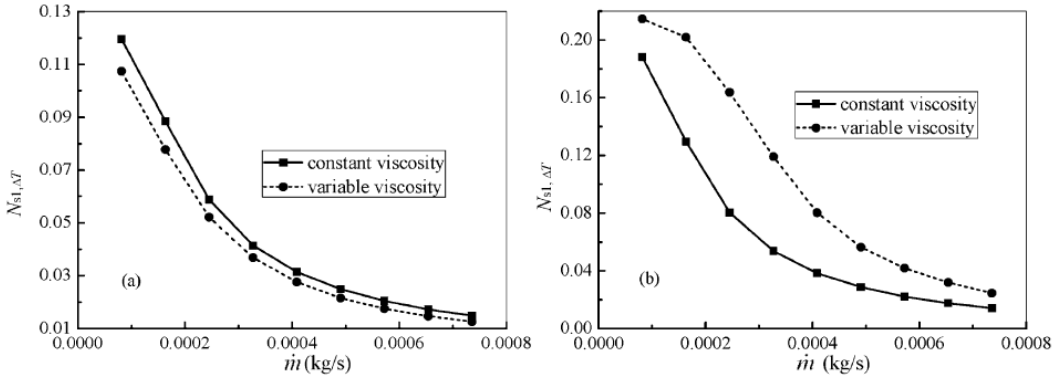

Figure 1.42: The relations of heat transfer entropy generation number with the mass flow rate in the cases: (a) aniline is heated and (b) aniline is cooled [94].

1.6 Conclusion

In conclusion, this literature review has illustrated some analytical, numerical and experimental works for laminar flow of non-Newtonian fluids as working fluids in strait, curved and complex geometries. Most experimental and numerical studies regards the effect of fluid behavior on the flow control, thermal mixing by chaotic advection, and the effect of external flow on the enhancement of heat transfer and second law analyses have been also outlined.We see that the literature is very in rich with the papers that dealing the behavior of the Newtonian fluids in straight and complex geometries while the papers which treat the behavior of the non-Newtonian fluids in complex geometry are very few. So our contribution in this thesis is to outline the behavior of the non-Newtonian fluids in complex geometry called here C-shaped geometry.

CHAPTER 2

Geometries Description and Numerical Methodology

2.1 Introduction

In this chapter, theoretical bases and numerical methodology are introduced. First, the considered geometries and the governing equations are discussed. Then, numerical methodology is described and mesh methodology is investigated.

2.2 Description of the geometry

Three dimensional chaotic geometry and straight channel are considered for laminar non-Newtonianfluid. Each geometry is characterized by a square cross-section, and the hydraulic diameter D_h is 1.5 cm. The unfolded length of one period C-shaped geometry is equal to 13.5 cm.Figure 1 presents the basic elements of the two considered geometries called period(C-shaped and the straight channels).

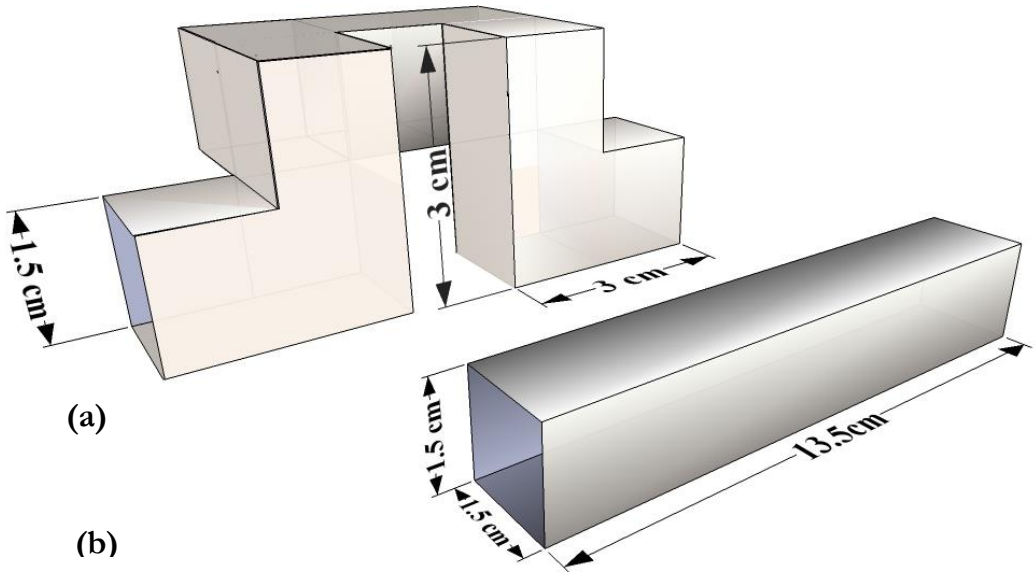

Figure 2.1: Schematic representation of the studied geometries: (a) straight channel, (b) C-shaped geometry.

2.3 Governing equations

The mass conservation and Navier–Stokes equations were numerically solved using the commercial CFD code Fluent© and are given by the following equations respectively [95]:

$$div\vec{V}=0 \tag{2.2}$$

Where $V$is the velocity vector.

(b)

$$\vec{V}.\vec{\vec{\nabla}}\vec{V} = -\frac{1}{\rho}\vec{\nabla}P + div\,\tau \tag{2.3}$$

Where ρ is fluid density, τ(Pa) is the shear stress and P is the pressure.

$$\rho c\vec{V}.\vec{\nabla}T = \lambda\Delta T \tag{2.4}$$

The constitutive relation between the shear stress, τ, (Pa) and the shear rate,$\dot{\gamma}$, (s^{-1}) can be described by a simple power-lawexpression [96]:

$$\tau = k\,\dot{\gamma}^{n} \tag{2.5}$$

Where, **k** ($Pa.s^{-1}$) is the power-law consistency index (k=0.1$Pa.s^{-1}$) and n is the power-law index which varies between 0.3 to 1 (Carboxymethyl cellulose (CMC) 7H4C at a mass concentration of 1%) [25].

The apparent viscosity of the work fluid is given by:

$$\mu_{app} = \mathrm{k}\,\dot{\gamma}^{\mathrm{n-1}} \tag{2.6}$$

The applied boundary conditions are:

- at the inlet section, uniform velocity profile equal to the mean velocity and the temperature equal to Ts = 300 k.
- at solid walls, no–slip conditions and a uniform wall heat flux (q" = 100 k/m^3).
- at the outlet section, the pressure outlet condition is considered.

2.4 Generalized Reynolds number

For the case of laminar non-Newtonian power-law flow, Kozicki et al [98] has proposed a parametric method to generalize the Reynolds number for complex section flow. This method based on the generalization of Rabionwich-Mooney equation with two parameters geometric, including the special case of power-law fluids in arbitrary ducts having a constant cross section. For rectangular section, they introduced a new generalized Reynolds number as flow:

$$\mathrm{Re_g} = \frac{\rho U_i^{2-n} D_h^n}{\left[8^{n-1}\left(b^* + \frac{a^*}{n}\right)^n k\right]} \tag{2.7}$$

Where, a* and b* equal 0.2121and 0.6771 respectively, for square channel, ρ is thedensity of fluid (kg m^{-3}), n is the power-law index, $k$is the power-law consistency index and U_i (m/s) is the inlet velocity. Table 2.1 presents these values for a rectangular channel as a function of the aspect ratio α*.

Table 2.1: Geometric constants a* and b* for rectangular ducts [99]:

α*	a*	b*	α*	a*	b*
1.00	0.2121	0.6771	0.45	0.2538	0.7414
0.90	0.2129	0.6785	0.35	0.2809	0.7750
0.80	0.2155	0.6831	0.25	0.3212	0.8183
0.75	0.2178	0.6870	0.20	0.3475	0.8444
0.70	0.2208	0.6921	0.15	0.3781	0.8745
0.65	0.2248	0.6985	0.10	0.4132	0.9098

2.5Pressure losses characteristics

The pressure losses of both straight and C-shaped channels are characterized by the evolution of the friction coefficient. The hydrodynamic performance of all geometries is characterized by the evolution along the curvilinear coordinate s of the local friction coefficient *f*, defined as [99]:

$$f = \frac{2\left(\frac{dp}{ds}\right)D_h}{\rho U_i^2} \tag{2.8}$$

Where dp/ds is the local pressure gradient along the curvilinear coordinate of the channel. Because this parameter depends on the generalized Reynolds number, it is preferable to follow the evolution of the local Poiseuille number:

$$Po_{local} = f.\mathrm{Re}_g \tag{2.9}$$

The mean Poiseuille number is calculated as:

$$Po_{mean} = \frac{1}{L}\int_0^L Po_{local}\,ds \tag{2.10}$$

Where L is the total length of the geometry and s is the axial coordinate.
On the other hand, Wheeler and Wissler [9] investigated an analytical expression of Poiseuille number for the fully developed laminar flow of a non-Newtonian power-law fluid (0.4 < n < 1.) through a square straight duct:

$$Po_{mean} = 1.873\left(\frac{1.7330}{n} + 5.8606\right)^n \tag{2.11}$$

2.6 Convective heat transfer characteristics

Heat transfer coefficient,h, for wall heat flux boundary condition is given as:

$$h = \frac{q''}{(T_b - T_w)} \tag{2.12}$$

Where, q'' (w/m^2) is the wall heat flux, T_b(k) is the mean bulk temperature fluid over the cross-sectional area and T_w(k) is perimeter average wall temperature.
These two temperatures are defined as:

$$T_w(s) = \frac{1}{P}\int_P T_w\,dp \tag{2.13}$$

$$T_b(s) = \frac{1}{AU_i}\iint_A \vec{V}.\vec{n}T.\,dA \tag{2.14}$$

The mean heat transfer coefficient,h_{mean}, defined as:

$$h_{mean} = \frac{1}{L}\int_0^L h(s)ds \tag{2.15}$$

The local Nusselt number given by the following equation:

$$Nu_{local} = h(s)\frac{D_h}{\lambda} \tag{2.16}$$

Where, $\lambda$is the thermal conductivity of the fluid$(\lambda = 0.614W.s^{-1}.K^{-1})$.
And the mean Nusselt number is defined by:

$$Nu_{mean} = \frac{1}{L}\int_0^L Nu_{local}ds \tag{2.17}$$

2.7 Thermal Mixing efficiency

2.7.1 Probability density function PDF (T)

The probability density function PDF (T) is the probability (in %) of the scalar temperature T to be present between two values; the PDF (T) in an interval [T_a, T_b] at the outlet is equal to the number of mesh cells in which T values are within [T_a, T_b] divided by the total number of cells on the outlet cross section.

2.7.2 Mixing degree (M_d)

Mixing degree (M_d)of two fluids (hot and cold), given in the following equation is an efficient parameter for quantifying scalar mixing:

$$M_d = 1 - \frac{\sqrt{\frac{1}{N}\sum_{i=1}^{N}(T_i - \bar{T})^2}}{\sigma_0} \tag{2.18}$$

Where N is thenumberofpointsontheplane, $T_i$is temperature at the node i, $\overline{T}$ is the mean temperature at the cross section and $\sigma_0$is the standard deviation at the inlet section. The values of $M_d$range from zero for the no mixture case, to 1for fully mixed flows.

2.7.3 Ratio of mixing

A second criterion to quantify the thermal mixing by the calculation of the ratio over flow cross-section (and calculated from the entry section). Therefore, we proposed the normalized ration (R):

$$R = \left(\frac{\frac{T_{min}}{T_{max}} - R_0}{1 - R_0}\right) \tag{2.19}$$

WhereR_0 is the ration at the inlet section.For a fully mixed flow, R = 1. The uniformity of mixing in flow cross-sections is qualified by examining of the temperature contours.

2.8 Numerical methodology

The conservation equations for mass, momentum and energy were solved by using computational fluid dynamics (CFD) code, ANSYS Fluent®. The standard scheme is

used for pressure discretization, and the SIMPLE scheme is employed for pressure-velocity coupling. The momentum and energy equations are solved with second-order up-wind scheme. The computations were considered to be converged once all the scaled residuals are less than 10^{-7} and the global imbalances, representing overall conservation don't exceed 10^{-5}.

2.8.1 Grid mesh sensibility

To perform grid independence studies, four grids were used for simulations of non-Newtonian fluid flow in the C-shaped geometry considering a steady laminar flow and forced convection, at a given generalized Reynolds number Re_g = 200and power-law index n = 0.5. All the structured elements used were quadrilateral for a three-dimensional chaotic geometry, as shown in figure 2.2.

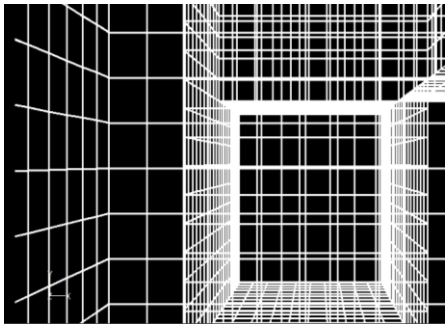

Figure 2.2a: Inside view of the grid on the wall chaotic geometry.

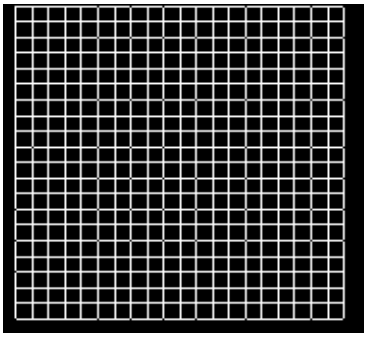

Figure 2.2b: Grid of the model geometry cross-section.

The grids are ranging from 30 to 60 nodes in the x and y direction, and from 30 to 60in the z direction. The Nusselt number, the Poiseuille number, velocity and temperature profiles were assessed for increasing mesh densities.
Figures 2.3 and 2.4 show the evolutions of static temperature and the axial velocity versus x and y coordinates for various grids at the center line of the outflow section. It can be seen that the temperature profiles in both x and y directions are superimposed for all mesh densities. This illustrates that the temperature profiles are not affected by the grid mesh. However, it can be observed that the velocity profiles are sensitive to the grid mesh except for the mesh densities (50x50x50) and (60x60x60) where no significant difference is seen. As consequence, the (50x50x50) grid is chosen as the optimal grid mesh for the computation.

Table 2.2 presents the mean values of the Poiseuille number between inlet and outlet sections of the C-shaped geometry and the values of the local Nusselt number at the outlet section for all grid densities. It shows that the differences between the two grids mesh (50*50*50) and (60*60*60) of the Poiseuille and the Nusselt numbers change by less than 0.24% and 1.4% respectively. This presents another argument to select the (50*50*50) grid mesh as the optimal mesh density for the rest of the computations.

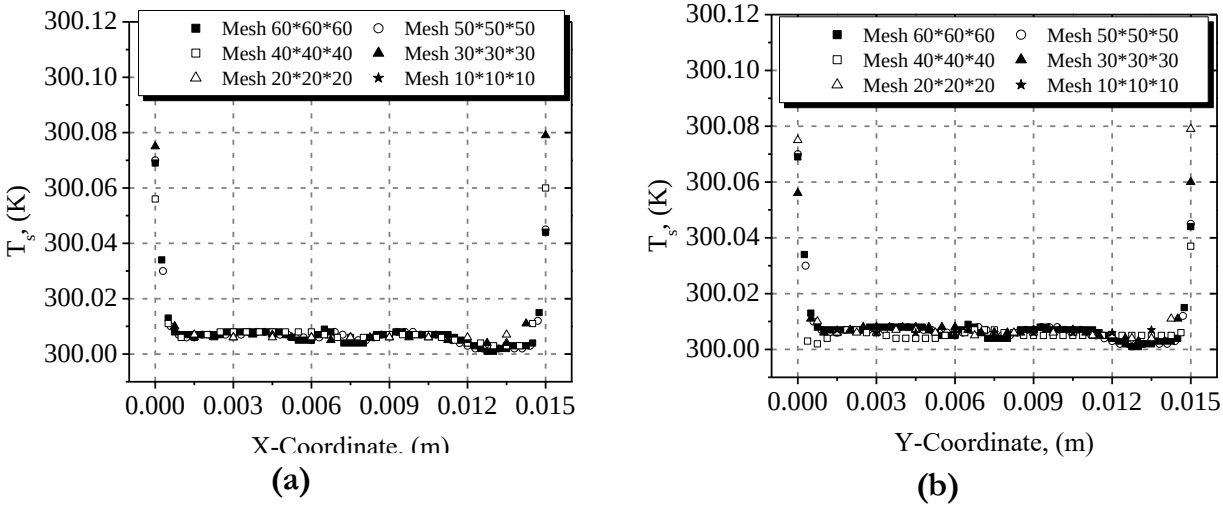

Figure 2.3: Temperature profiles for different mesh densities for n = 0.5 and Re_g = 200 at the outlet section of the C-shaped channel, (a) X-Coordinate (b) Y-coordinate.

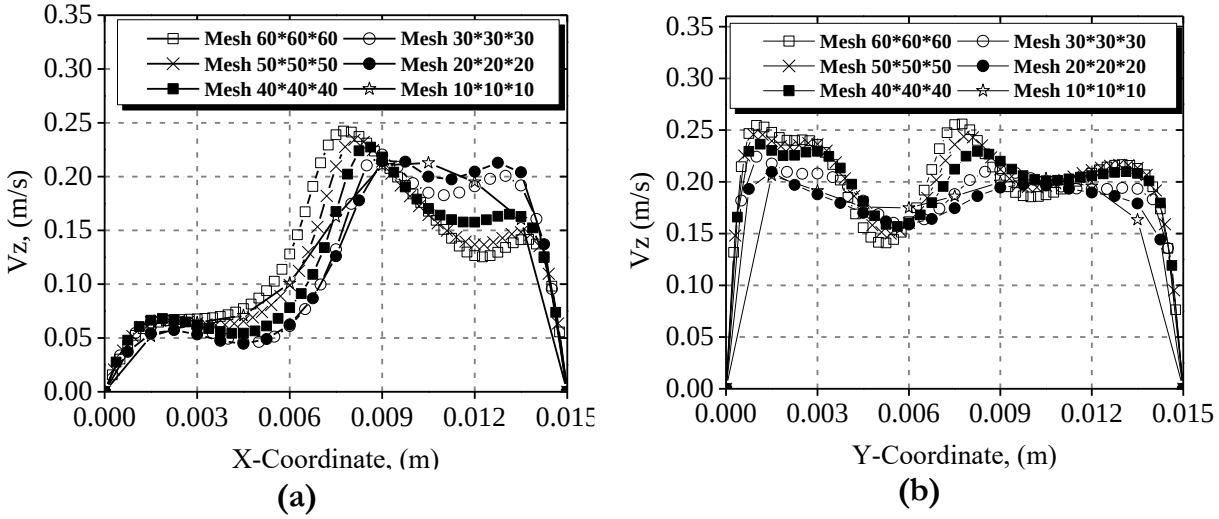

Figure 2.4: Axial velocity profiles for different mesh densities for n = 0.5 and Re_g = 200 at the outlet section of the C-shaped channel, (a) X-Coordinate (b) Y-coordinate.

Table 2.2: Mean Poiseuille number and local Nusselt number for different mesh densities for n = 0.5 and Re_g = 200 in the C-shaped channel.

Mesh	Po_{mean}	Error/ 60	Nu_{local}	Error/ 60
30x30x30	218.270	0.13%	41.741	13.56%
40*40*40	219.270	- 0.32%	45.8307	5.09%
50*50*50	219.099	- 0.24%	47.6098	1.41%
60*60*60	218.561	0.00%	48.2904	0.00%

2.9 Conclusion

In this chapter, geometrical description and the governing equations are presented. Then, numerical methodology and the gridmesh sensibility are discussed for hydrodynamic and the heat transfer characteristics of C-shaped channel for non-Newtonian laminar flow.

CHAPTER 3

Hydrodynamic, heat transfer, and thermal mixing performances

3.1 Introduction

In this chapter, flow and thermal performances for power-law non-Newtonian fluid are studiedin detail for the straight and the C-shaped geometries. These performances are investigated as function of generalized Reynolds number ranging from 50 to 200 and different power-law index ($n \leq 1$).

3.2 Validation

In order to check the reliability and the precision of the CFD computation, a comparison with other results provided in the literature is carried out for hydrodynamic and thermal flow cases.

3.2.1 Hydrodynamic flow problem

Fully developing laminar steady flow of shear thinning fluid in straight channel is considered. Figure 3.1 presentsanumerical profiles of laminar flow in straight circular tube witch compared with the analytical profile for different power-law index (n = 1 and 1/3). The numerical profile tends towards a theoretical value. The comparison is quite good for both cases of power-law index.

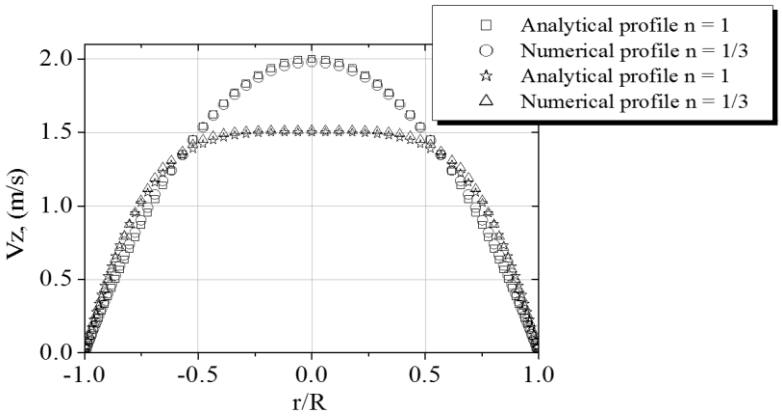

Figure 3.1: Axial velocity profiles for n = 1 and 1/3.

Moreover, another numerical study for validation of results have been performed for the case of fully developed laminar flow in straight square channel, and found to agree quite well number, as shown in Table 3.1.

Tables 4.1 presents a comparison of the values of the Poiseuille number obtained in the present study and those provided in the literature for large range of a power-law index

(n= 0.3-1).The numerical values barely differ from the case of the theoretical values where the maximum difference is less than 0.5%. These values are in fair agreement and the comparison is satisfactory and reveals a very good concordance.

Table 3.1: Poiseuille number, Po, of fully developed laminar flow in square straight channel for different power-law index (n = 0.3-1).

n	1	0.9	0.8	0.7	0.6	0.5	0.4	0.3
Present work	56.90	47.47	39.32	33.00	27.52	22.90	18.99	15.66
Wheeler and Wissler [9]	56.92	47.53	39.67	33.07	27.54	22.89	18.97	15.65
Seppo [46]	56.90	47.52	39.65	33.06	27.53	22.88	18.96	15.64
Simsoo et al [11]	56.90	47.89	40.29	33.89	28.49	23.91	20.01	-
Kozicki et al [98]	56.91	47.88	40.26	33.82	28.37	23.75	19.82	-
Sayed-Ahmed [50]	56.90	-	-	-	-	22.88	-	-
Ray [47]	56.90	-	-	-	-	-	-	-
Shah [36]	56.90	-	-	-	-	-	-	-
Error (%)/ [9]	0.007	0.09	0.82	0.17	0.05	-0.06	-0.14	-0.14

3.2.2 Thermal flow problem

The numerical solution procedure of heat transfer characteristics has been reported andvalidated thoroughly by comparing the present results with the results of Cotta [103] and Wheeler and Wissler [9], for fully developed laminar flow of Newtonian and non-Newtonian fluids in straight square ducts, subjected to wall heat flux. Where the comparison regarding the local Nusselt number (Nu) for straight circular duct, as shown in figure 4.2 and mean Nusselt number for straight square duct, as shown in table 4.2 for different power-law index with the corresponding results available in the literature.

An excellent agreement is seen to exist between the present numerical values and the literature values of Nusseltnumber. Based on these comparisons, it is perhaps reasonable to conclude that the present results are reliable to within ±0.4%. Deviations of this order are not at all uncommon in numerical studies and arise due to the differences in the flow schematics, problem formulations, grid and/or domain sizes, discretization schemes, numerical methods, etc.

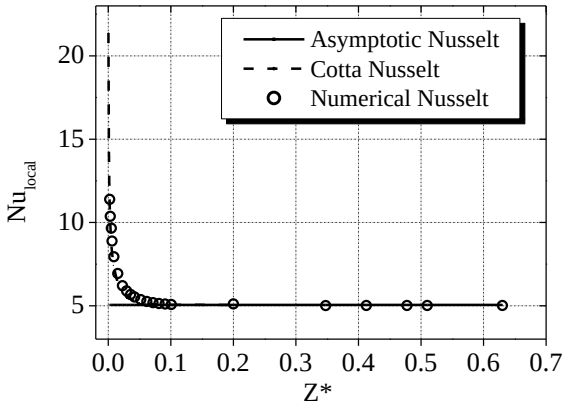

Figure 3.2: Local Nusselt number of fully developed laminar flow in circular straight channel for n = 1/3.

Table 3.2: Mean Nusselt number of fully developed laminar flow in square straight channel for different power-law degree (n = 0.5-1).

N	1	0.9	0.8	0.7	0.6	0.5
Present work	3.0704	3.1140	3.1463	3.1832	3.228	3.2818
Wheeler and Wissler [9]	3.0950	3.106	3.135	3.171	3.216	3.274
Error (%)/[9]	0.2407	- 0.258	- 0.360	- 0.386	- 0.373	- 0.238

3.3 Behavior of the Local Physical Process of the velocity field

The velocity field depends greatly to the velocity gradient components $(\partial U_i)/(\partial x_j)$. Consequently, these components contribute to the fluid kinematic flow such as vorticity rate, deformation rate, rotation rate and stretching/compression of the vorticity. It should be noted that these parameters either they do not exist or they are very small in the straight channel because the flow is laminar and establishment. The main phenomena that can occur in the Straight channel, where the regime is established and laminar, are the shear stress and/or rotation of the particle around itself. This weakens the level of heat transfer in the fluid because the transfer mode is limited to the heat conduction way.

3.3.1 Stretching /compression of the vorticity

The transport equation of the vorticity is given by:

$$\partial\vec{\Omega}/\partial t + \vec{V}.\vec{\vec{\nabla}}\vec{\Omega} = \vec{\Omega}.\vec{\vec{\nabla}}\vec{V} + \nu\Delta\vec{\Omega} \qquad (3.1)$$

The term $\vec{\Omega}.\vec{\vec{\nabla}}\vec{V}$ induces formation of vortex structures in the flow with different sizes by generating the stretching and compression (folding) vortex in the flow [100], see figure 3.3. The stretching and compression phenomena act simultaneously on the vortex dimensions. At a given time, the stretching operation, increases the vortex length and decreases its cross section, while the compression decreases the vortex length and increases its cross section. These phenomena are generated as a consequence of the conservations of the mass and angular momentum.

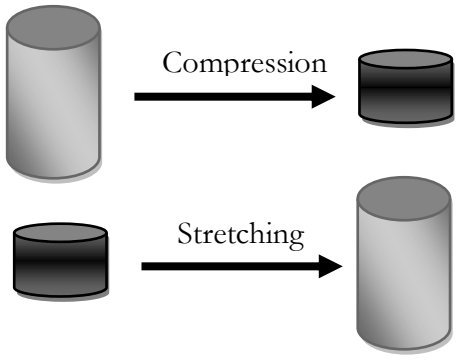

Figure 3.3: Illustration of the stretching and compression operations

The appearance of the stretching and folding in the flow often gives rise to chaotic behavior. Stretching results in nearby points diverging, folding results in distant points being mixed together. These operations in the flow destroy the thermal and dynamic

boundary layers and prevent its reformation. The boundary layer being a barrier against the parietal thermal transfer, its destruction enhances considerably the heat transfer [61]. On the other hand, these operations increase the contact area between fluids to be mixed even in the existence of the interfacial barrier as surface tension [55]. To characterize this behavior in the flow, the stretching and compression coefficients of the vortex $\alpha$was estimated. It is defined by the following expression:

$$\alpha = \frac{\vec{\Omega}.\overline{\overline{D}}.\vec{\Omega}}{\Omega^2} \tag{3.2}$$

Where $\overline{\overline{D}}$ is the deformation tensor and $\vec{\Omega}$ is the vorticity vector. At any location where $\alpha > 0$, the vortex stretching prevails on vortex compression [100]. α^+ presents the arithmetic average of the positive values of the stretching coefficient and α^- presents the arithmetic average of the negative values of the compression coefficient.

Figures 3.4 and 3.5, present respectively the evolutions of vortex stretching coefficient (α^+) and compression coefficient (α^-) as function of generalized Reynolds number Re_g for different power-law index n ranging from 0.5 to 1.

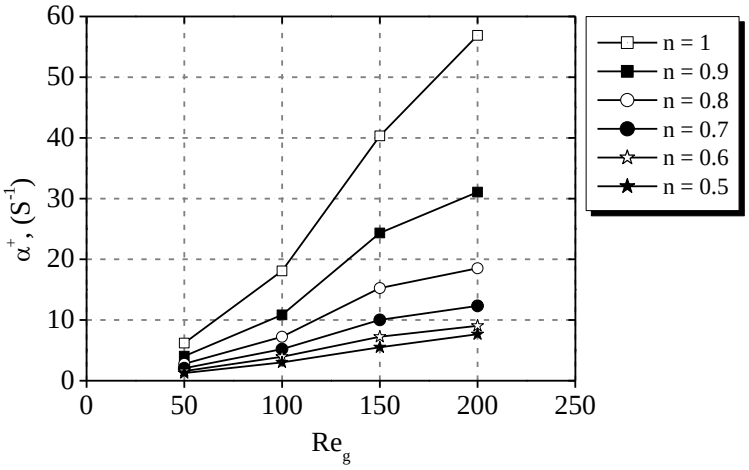

Figure 3.4: Evolutions of the vortex stretching in the fluid flow with generalized Reynolds number in the C-shaped channel for varying n.

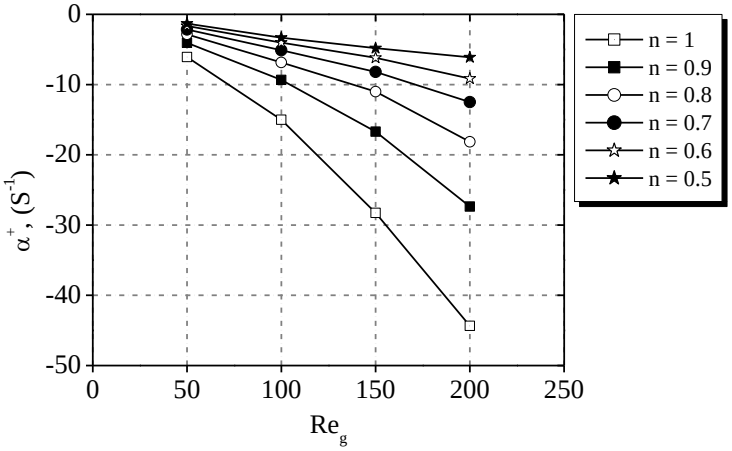

Figure 3.5: Evolution of the vortex compression in the fluid flow with generalized Reynolds number in the C-shaped channel for varying n values.

These coefficients increase constantly with the increase of the generalized Reynolds number. While going towards the great values of n, the stretching and folding processes become very important. Because when the n values are small the fluid is more viscous and the fluid needs an additional energy to create a significant agitation in the fluid. At low generalized Reynolds number values, the chaotic behavior is not yet active and so these phenomena are identical for all values of n.

3.3.2 Deformation (Strain rate) and rotation

Both mechanisms (deformation and rotation) are complementary in the mixing operations. The rotation process gives rise to three-dimensional movements of the fluid particles and it can transport the fluid particles to regions of high shear rates. The rotation process realizes a good macroscopic mixing while the deformation process achieves a good quality of mixing by molecular diffusion. For this aim, the chaotic geometry can be a potential solution for increasing the deformation and rotation rates at once. An examination of the fluid behavior index effect on the deformation and rotation rates is performed. Evolutions of the mean deformation and rotation rates ($\mathrm{D_{mean}}\ and\ \Omega_{\mathrm{mean}}$) in the C-shaped channel as function of the generalized Reynolds number ranging from 50 to 200 are presented in figure 3.6 and 3.7. The two parameters, rotation and deformation, are defined by the following equations [101]:

$$D = \left[2\left(\frac{\partial u}{\partial x}\right)^2 + 2\left(\frac{\partial v}{\partial y}\right)^2 + 2\left(\frac{\partial w}{\partial z}\right)^2 + \left(\frac{\partial u}{\partial y} + \frac{\partial v}{\partial x}\right)^2 + \left(\frac{\partial u}{\partial z} + \frac{\partial w}{\partial x}\right)^2 + \left(\frac{\partial v}{\partial z} + \frac{\partial w}{\partial y}\right)^2\right]^{\frac{1}{2}} \quad (3.3)$$

$$D_{\mathrm{mean}} = \frac{1}{\mho}\int S d\mho \quad (3.4)$$

$$\Omega = \frac{1}{2}\left[\left(\frac{\partial w}{\partial y} - \frac{\partial v}{\partial z}\right)^2 + \left(\frac{\partial u}{\partial z} - \frac{\partial w}{\partial x}\right)^2 + \left(\frac{\partial v}{\partial x} - \frac{\partial u}{\partial y}\right)^2\right]^{\frac{1}{2}} \quad (3.5)$$

$$\Omega_{\mathrm{mean}} = \frac{1}{\mho}\int \Omega d\mho \quad (3.6)$$

Where $\mho$ represents the total volume of the fluid in the channel.

Figure 3.6 shows the evolutions of the deformation rate for different generalized Reynolds number (Reg = 200 to 50) in C-shaped channels. As can be seen from this figure, the deformation increases by an increase in generalized Reynolds number, where the deformation rate is maximum for the Newtonian case (n = 1). This explains that this behavior is kinematic and is accentuated by the fluid behavior index.

As the power-law index increases, the deformation rate becomes larger inside the geometry. Therefore, the deformation rate is higher for the Newtonian case (n = 1).

Evolutions of the mean rotation rate (Ω_{mean}) in the C-shaped channel as function of the generalized Reynolds number ranging from 50 to 200 are presented in figure 3.7.

As it can be observed, when the power-law index increases, these parameters are more vigorous, and the flow becomes more agitated and sheared. Besides, the flow in the Newtonian case (n = 1) exhibits very high rates of rotation compared to the other non-Newtonian cases (n = 0.5 to 0.9). At high values of generalized Reynolds number, the

rotation rates are more important in Newtonian case compared to the other fluid. The cases of low values of Re_g and n have qualitatively the same behavior in terms of deformation and rotation rates. The difference becomes noticeable when the Reynolds number exceeds the value of 50.

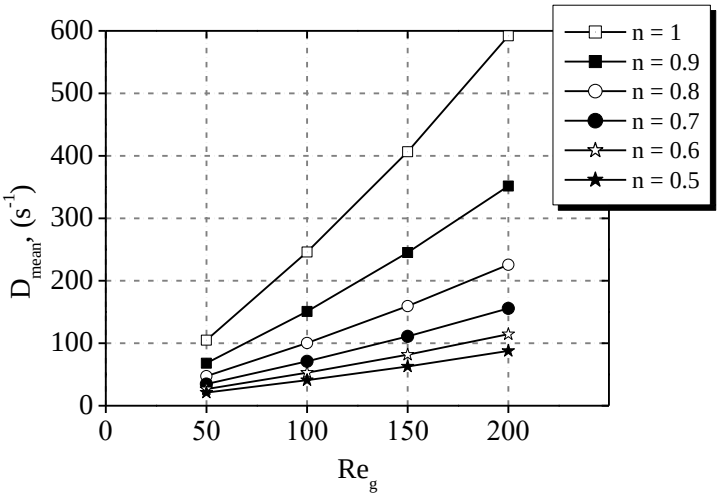

Figure 3.6: Evolution of the deformation rate with different generalized Reynolds number in C-shaped channel.

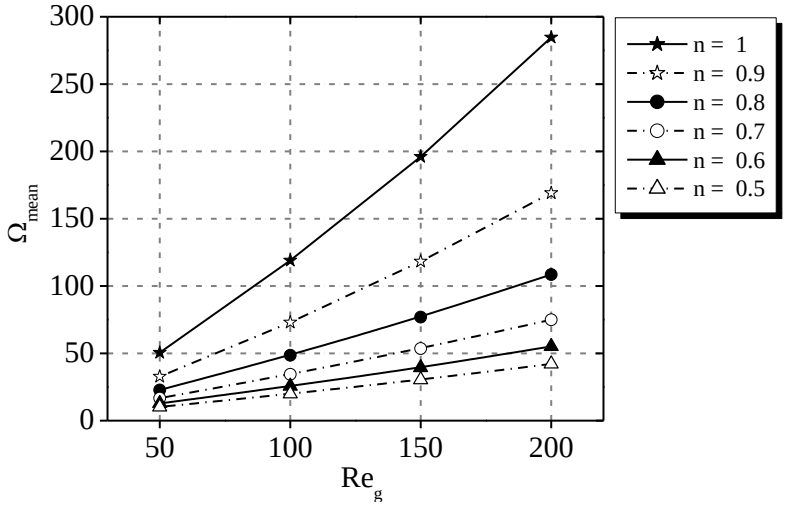

Figure 3.7: Evolution of the rotation rate in the fluid flow with generalized Reynolds number for different power-law index.

3.3.3 Vortex intensity

When the fluid passes through the geometrical perturbation in the considered channel, a secondary flow is created by the presence of a centrifugal force. The secondary flow is more intense for the disturbance having a complex shape. In order to estimate the secondary flow, the vortex intensity was calculated at the exits of the C-shaped channel as defined by [101]:

$$\Omega_{\text{average}} = \frac{1}{S}\int |\Omega_z| dS \tag{3.7}$$

S is the cross section area and Ω_z is the vorticity at the flow cross section. Due to the secondary flow effect, the transversal movements of the particles increases and the axial dispersion decreases, which consequently enhanced the heat transfer [101].

In order to show the effect of power-law index and generalized Reynolds number Re_g (n) on the vortex intensity, the figure 3.6 presents the evolutions of the vortex intensity for different generalized Reynolds numbers with power-law index ranging from 0.5 to 1. It is noticed that the vortex intensity increases with the growth of the generalized Reynolds number. For the cases of n = 0.5 and n = 0.6, the change of the maximum absolute of vortex intensity is changed with generalized Reynolds number by about 23%. Therefore, the maximum vorticity are given at high power-law index (Newtonian case). However, the existence of much great secondary flows in Newtonian fluid case compared to those exhibited in the cases of non-Newtonian fluid. For low generalized Reynolds number and low power-law index, the evolutions are very close to each other. Therefore, the magnitude of the vortex intensity has less effects of secondary flow, and the fluid can easily flow inside the geometry and thus a vortex is not created.

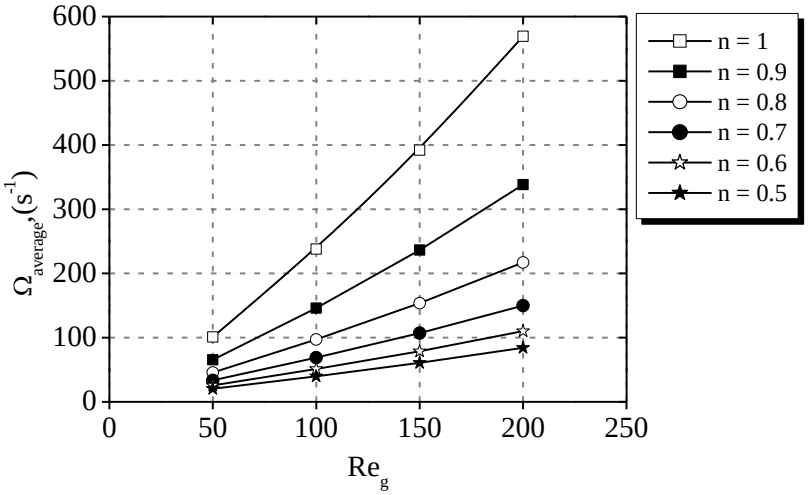

Figure 3.8 : Variations of the vortex intensity with generalized Reynolds number for the different power-law index at the outlet section.

3.3.4 Helicity

The Helicity, defined as the inner product of velocity and vorticity, characterizes the helical motions. Non zero-Helicity declares that the fluid particles move along their axis of rotation and the flow might be expected to be less complex than flows withzero Helicity.

$$H = \frac{\vec{V}.\vec{\Omega}}{V\Omega} \tag{3.8}$$

Dimensionless Helicity is used in the present work to describe the nature of the secondary flows (chaotic or regular), which occur at the exit of each perturbation area (middle and outflow sections). The dimensionless Helicity value is bounded between -1 and +1. For both limit values -1 and +1, the fluid flow is considered fully chaotic. Figures 3.9 shows the dimensionless Helicity contours of the C–shaped channel, for various generalized Reynolds numbers with different values of power-law index (n = 0.5 and 1).

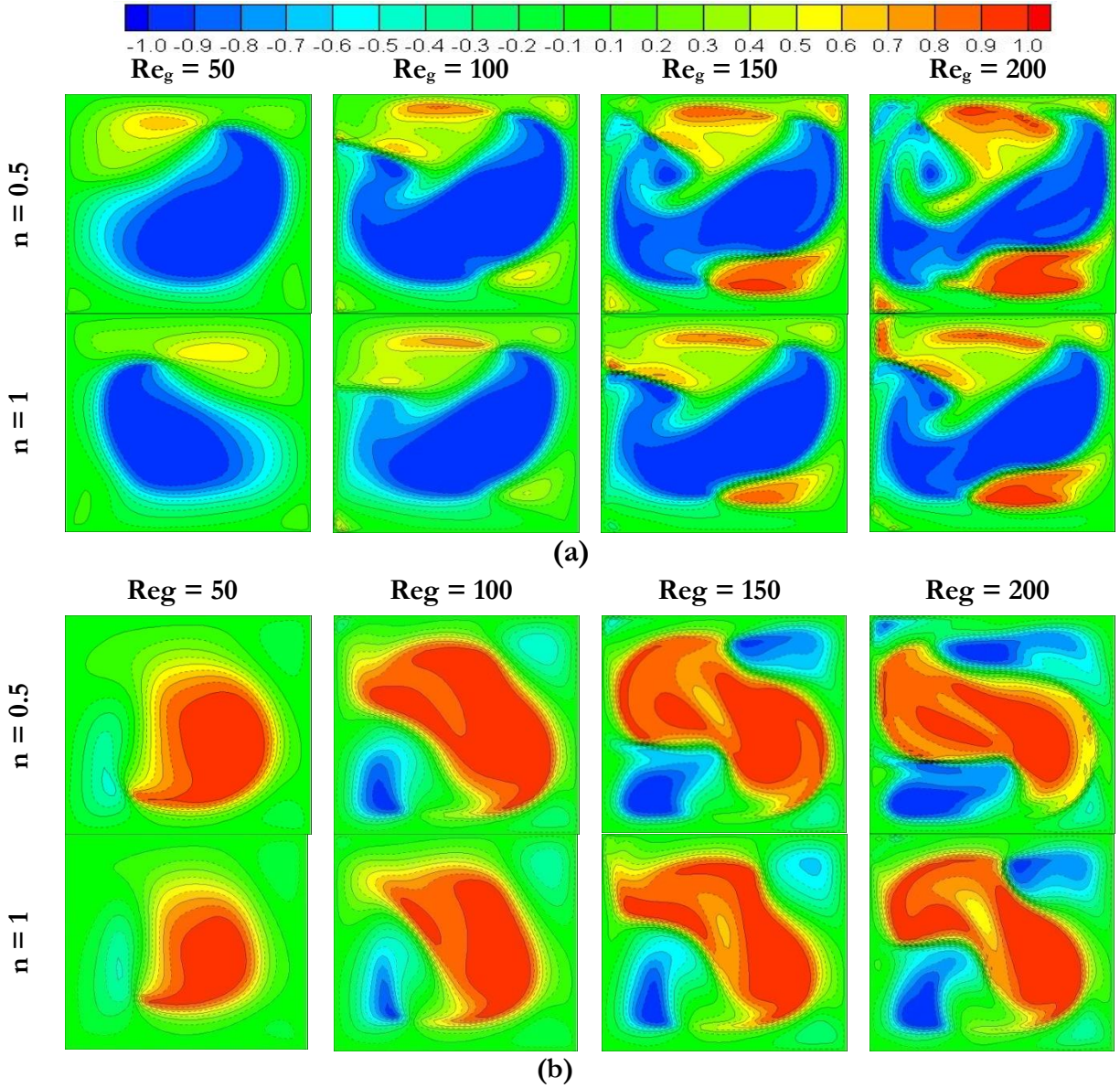

Figure 3.9: Helicity contours, (a) middle cross section (b) outlet section.

3.4 Flow characteristics

In this section, the effects of power-law index (n) and generalized Reynolds number (Re_g) on velocity field for each cross section within straight and C-shaped channels are investigated.

3.4.1 Influence of power-law index on axial velocity

To discuss the velocity field, contour maps of the axial velocity distributions of different cross sections are presented, for given generalized Reynolds number Re_g = 100 and power-law index (n = 0.5 to 1) is increases as fluid behavior index.

Figure 3.10 presents the axial velocity contours for generalized Reynolds number Re_g = 100 and power-law index ranging from 0.5 to 1, in outlet cross section of the straight duct.

It can be seen clearly that, there is no secondary flows appeared in the outlet cross section. So, the momentum transfer is limited only to the molecular diffusion mode for all cases of the power-law index (n).

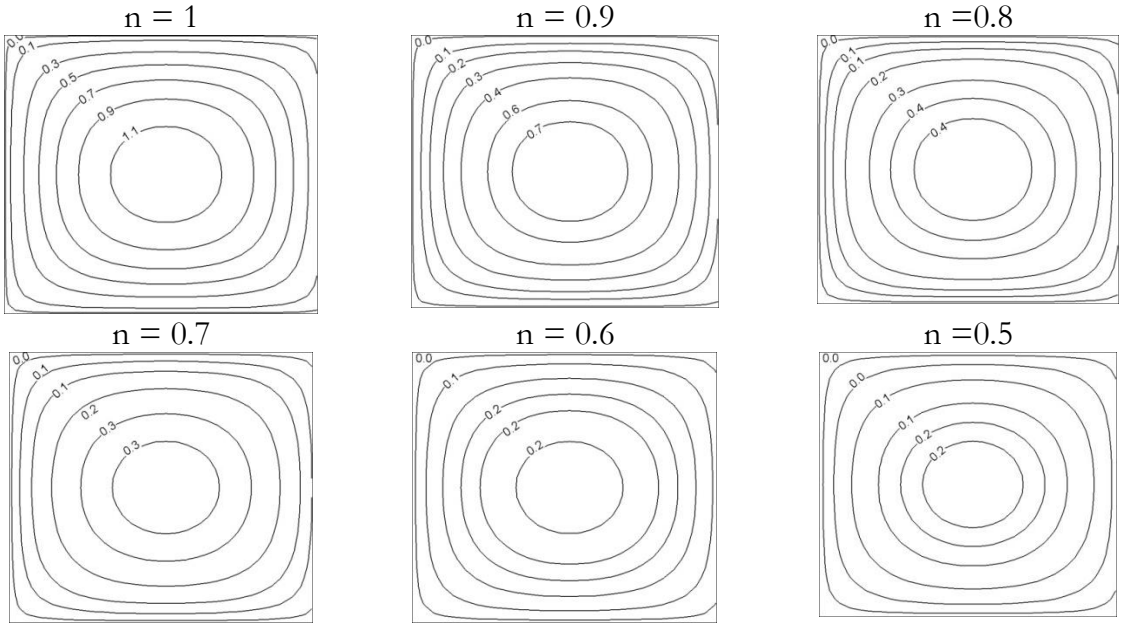

Figure 3.10: Axial velocity contours at the outlet section of the straight channel for generalized Reynolds number $Re_g = 100$, with n = 0.5 to 1.

Figure 3.11 shows the axial velocity contours of C-shaped channel for generalized Reynolds number $Re_g = 100$ and power-law index ranging from 0.5 to 1, in three different cross sections (S1: inlet, S2: middle and S3: out flow sections). For all cases of different power-law index, the bulk induced fluid flow throughout the middle sections and two small cells is formed at the top wall and the opposite one, where the flow pattern is changed drastically in out flow section.

The fluid particles in outlet section have larger centrifugal force than other regions due to the chaotic advection. The intensity of secondary flow increases with increase in the value of n. It is evident from the figure that as the secondary flow becomes more skewed toward the wall of the geometry. These changes in pattern for different power-law index and their physical implications are discussed in the next section.

Figure 3.11 shows the secondary flow vectors of fluid particles from central to near wall regions in the outflow section for the straight andthe C-shaped channels at given generalized Reynolds number ($Re_g = 100$) with diffferent power-law index (n = 0.5 and 1). Figure 3.12 displays that there is no secondary flows appeared in the outlet cross section. So, the momentum transfer is limited only to the molecular diffusion. The recirculation observed in C-shaped geometry is related to the sudden change of the direction due to the specific geometrical feature of the chaotic channel. Hence, the principal direction of the vectors is transformed through 90° in a short distance. Meanwhile, the vectors are seen to cross over each other, indicating the fluid particles are being mixed in the tangential direction and a significant secondary flow is formed, which

is able to provide an extra advantage to heat transfer perfarmance and mixing flow compared with flow in a straight channel, as shown in the next parts.

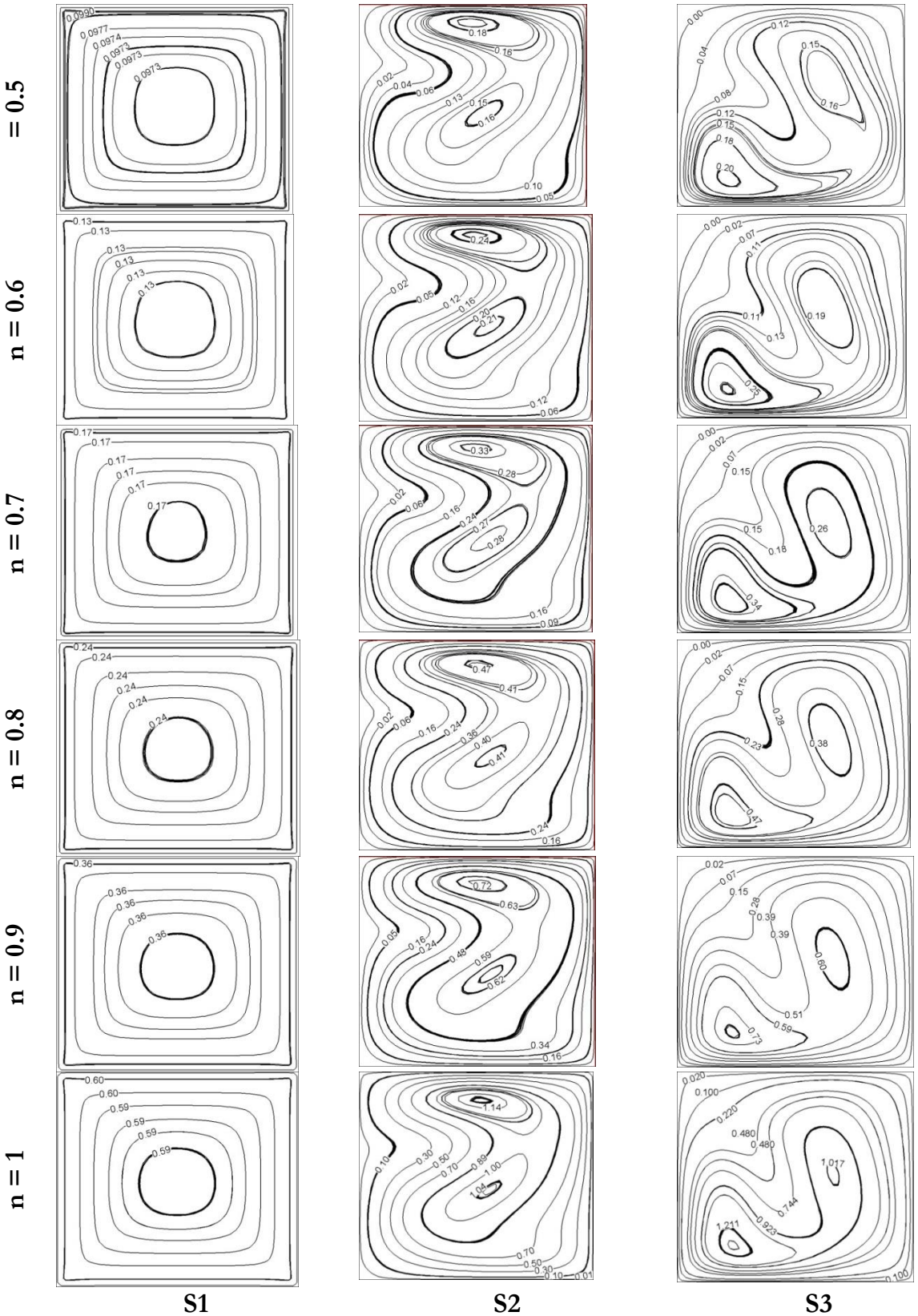

Figure 3.11 : Axial velocity countours of C-shaped channel for generalized Reynolds number Re_g = 100 with power-law index n = 0.5 to 1.

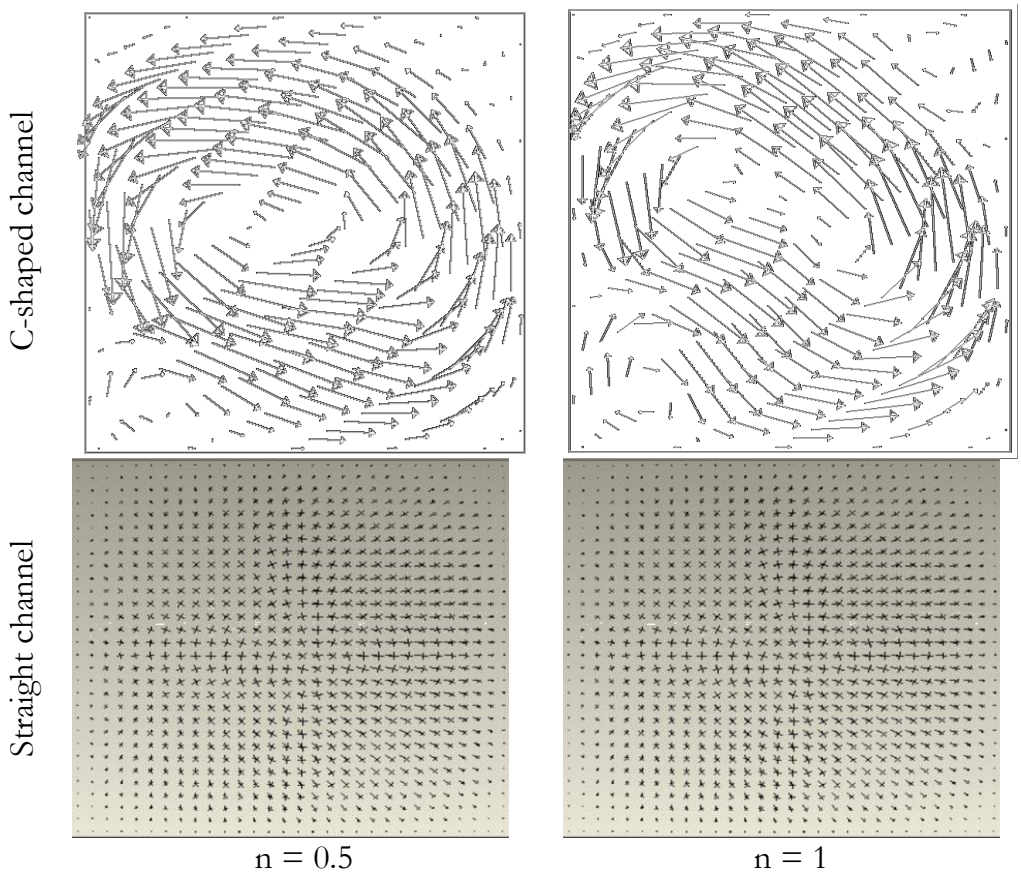

Figure 3.12 : Secondary flow vectorsat a cross section of the C-shaped channel for Re_g = 200 with n = 0.5 and 1.

Figure 3.13 and figure 3.14 show the evolutions of the axial velocity profiles with x and y coordinates at the center line of the straight channel outlet section for power-law non-Newtonian fluid for two generalized Reynolds number 50 and 150, respectively. The power-law-index varies from 0.5 to 1. The profiles of the velocity are symmetric and parabolic. The maximum velocity is located in the center of the cross section and it increases considerably with the increase of the power-law index. It can be seen clearly that, with this type of flows, particles trajectories are parallel resulting in no motion of the fluid particles in the transverse direction of the flow. So, the momentum transfer is limited only to the molecular diffusion mode.

Figure 3.15 and figure 3.16 show the evolutions of the axial velocity with x and y coordinate at the center line of the outlet section in the C-shaped geometry for power-law non-Newtonian fluid for two generalized Reynolds number 50 and 150.The velocity distributions within the channel highlight the flow complexity where the symmetric nature of the velocity profile is disrupted under the effect of the secondary flows. The velocity profiles in the central core region are more latter compared to that in the straight channel. The location of the maximum velocity point in this type of geometry is of interest. One can gain the general idea about the secondary flow pattern and the intensity of secondary flow.

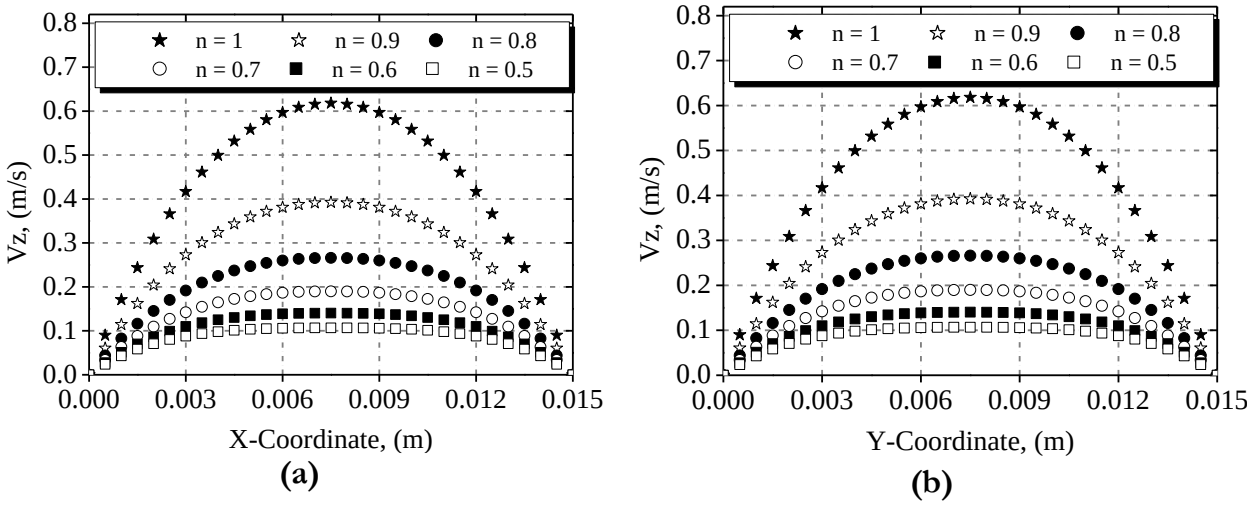

Figure 3.13: Axial velocity profiles at the outlet section of the straight channel for Re_g=50, with n = 0.5 to 1, (a) X-Coordinate and (b) Y-Coordinate.

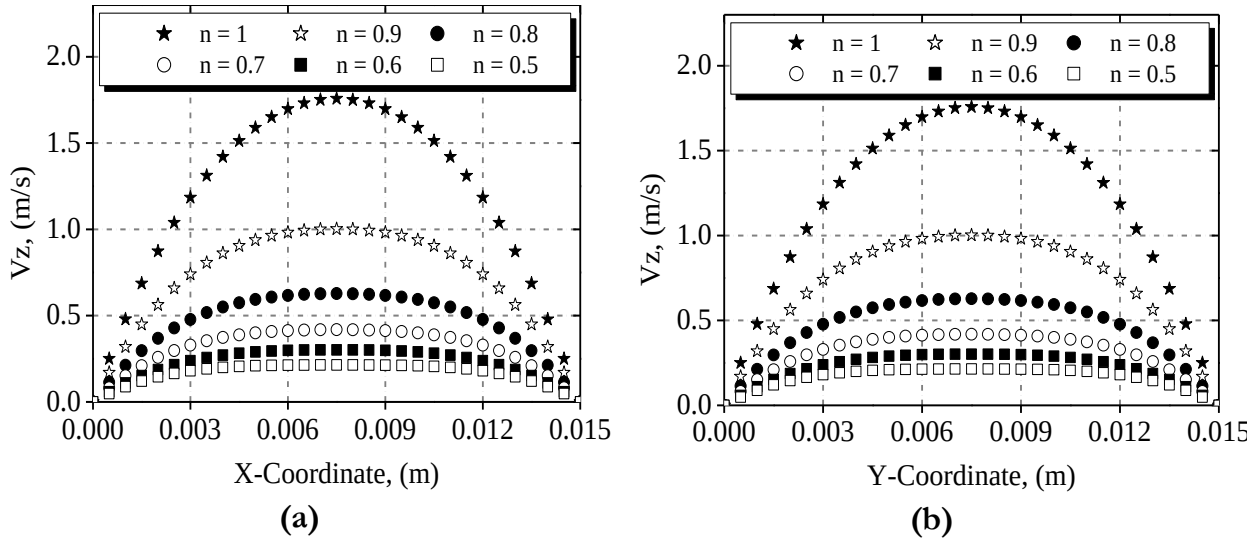

Figure 3.14: Axial velocity profiles at the outlet section of the straight channel for Re_g = 150, with n = 0.5 to 1, (a) X-Coordinate and (b) Y-Coordinate.

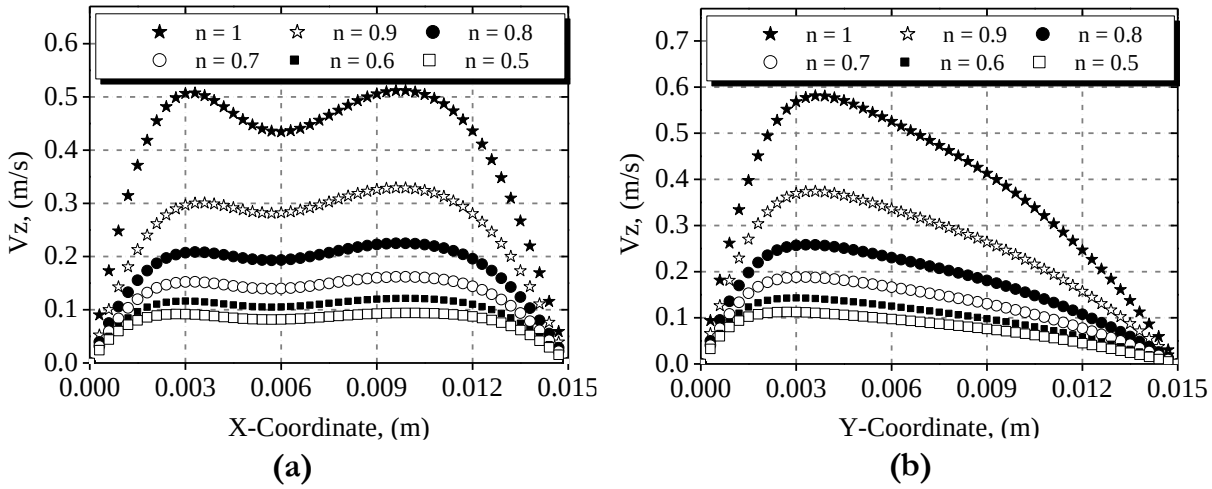

Figure 3.15: Axial velocity profiles at the outlet section of the C-shaped channel for Re_g = 50, with n = 0.5 to 1, (a) X-Coordinate and (b) Y-Coordinate.

The results show clearly that the effect of the secondary flows is to shift the location of the maximum value toward the walls. In addition, the maximum value increases as the value of the power-law index increases.

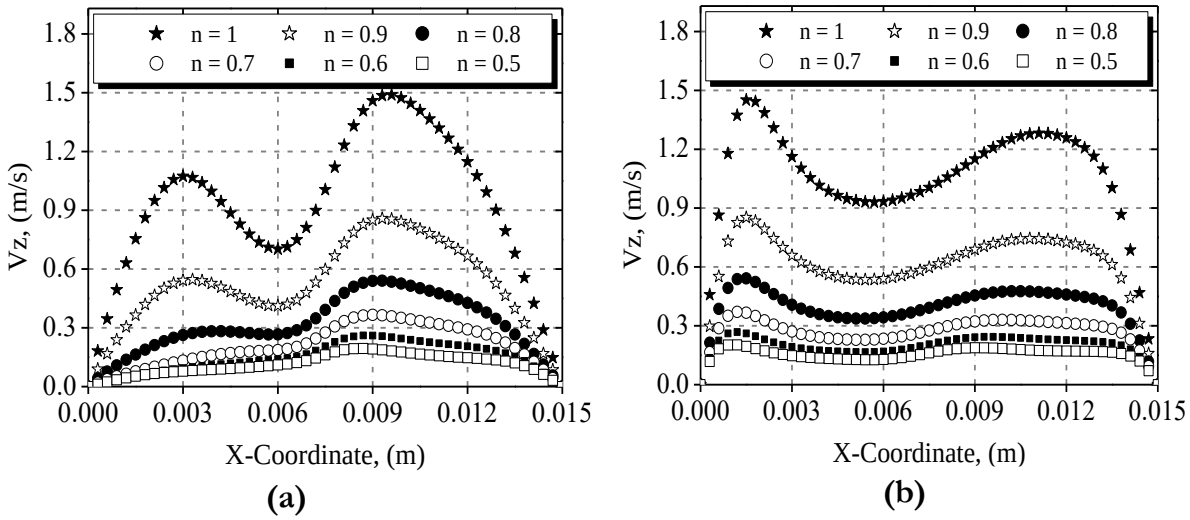

Figure 3.16: Axial velocity profiles at the outlet section of the C-shaped channel for Re_g = 150, with n = 0.5 to 1, (a) X-Coordinate and (b) Y-Coordinate.

3.4.2 Influence of generalized Reynolds number on axial velocity

In this section, a different power-law index is considered and generalized Reynolds number is changed to plot the flow velocity profiles for each cross sectional geometry.
Figure 3.17 present axial velocity profiles for different generalized Reynolds numbers Re_g = 50 to 200 and power-law index n = 0.5 and 1, corresponding to pseudoplastic and Newtonian fluid behaviors, respectively. As can be seen in this figure, the generalized Reynolds number strongly affects the velocity profiles in the C-shaped channel.
The stream lines in the case of Newtonian fluid were much more twisted compared to the non-Newtonian fluid, thereby indicating the development of stronger secondary motion in the Newtonian fluid. For high generalized Reynolds number Re_g = 200, the vortex structure switches from a two-cell structure to a three-cell structure. The new vortex rotates in a direction opposite to that of their corresponding main vortices. The cells become larger in size by an increase in the generalized Reynolds number, Re_g. This suggests that the level of mixing in C-shaped channel is strongly affected by the extensional-flow behavior of non-Newtonian fluids.
Figure 3.18 and figure 3.19 show the axial-velocity profiles for horizontal and vertical centerlines at the outlet section of C-shaped channel for Newtonian and non-Newtonian fluids, respectively, with various values of generalized Reynolds number (Re_g = 50 to 200). The velocity profile value steadily decreases due to decreased values of generalized Reynolds number for both Newtonian and non-Newtonian fluids, the flow field is a bit unstable for Re_g = 50. The velocity profiles for non-Newtonian fluid show a marked decrease with decreasing of generalized Reynolds number in centerline axial velocities in

comparison to the Newtonian fluid, due to the increasing effect of the centrifugal force in the flow pattern.

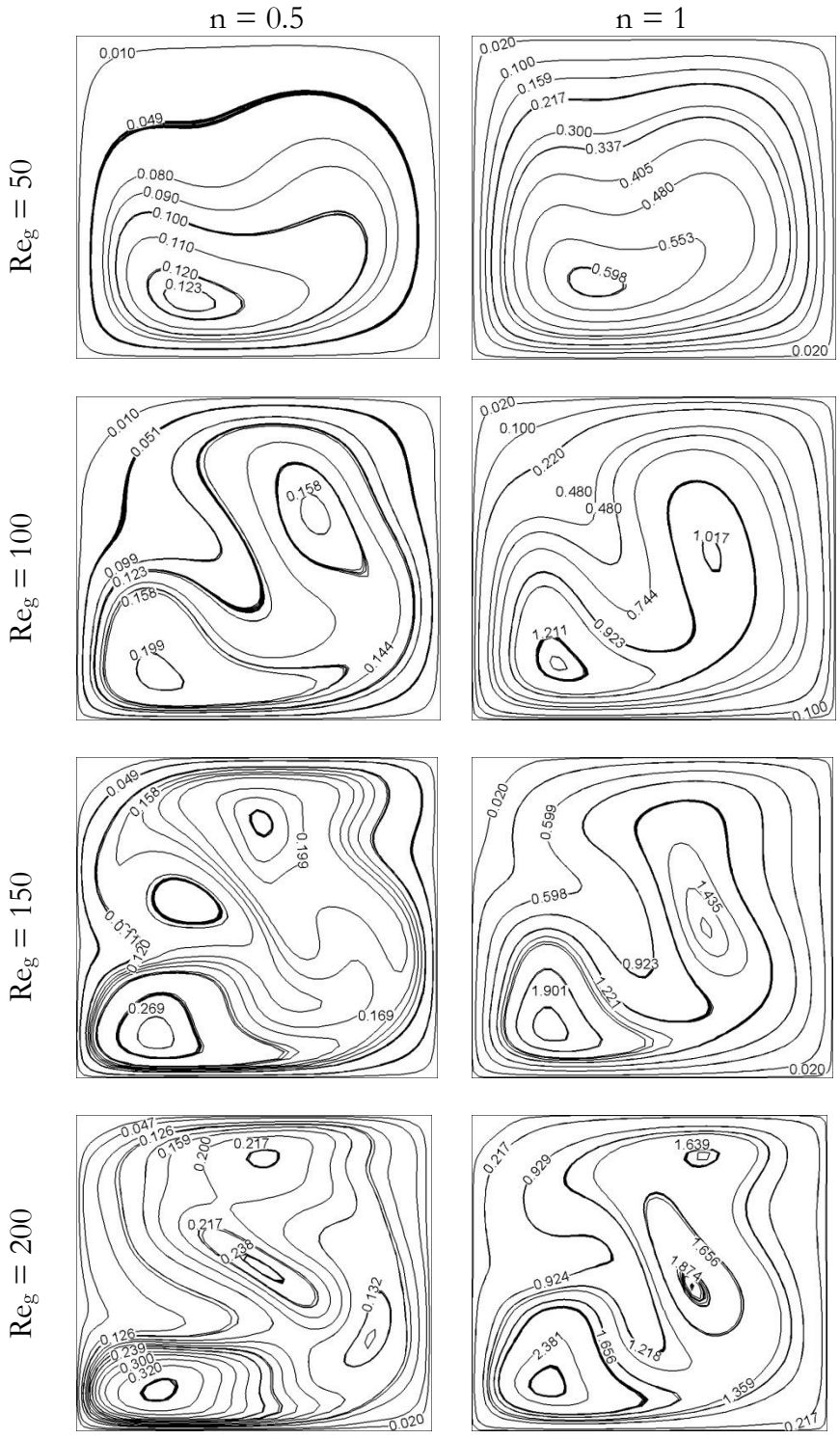

Figure 3.17 : Axial velocity countours of C-shaped channel for power-law index n = 0.5 and 1 with generalized Reynolds number Reg = 50 to 200.

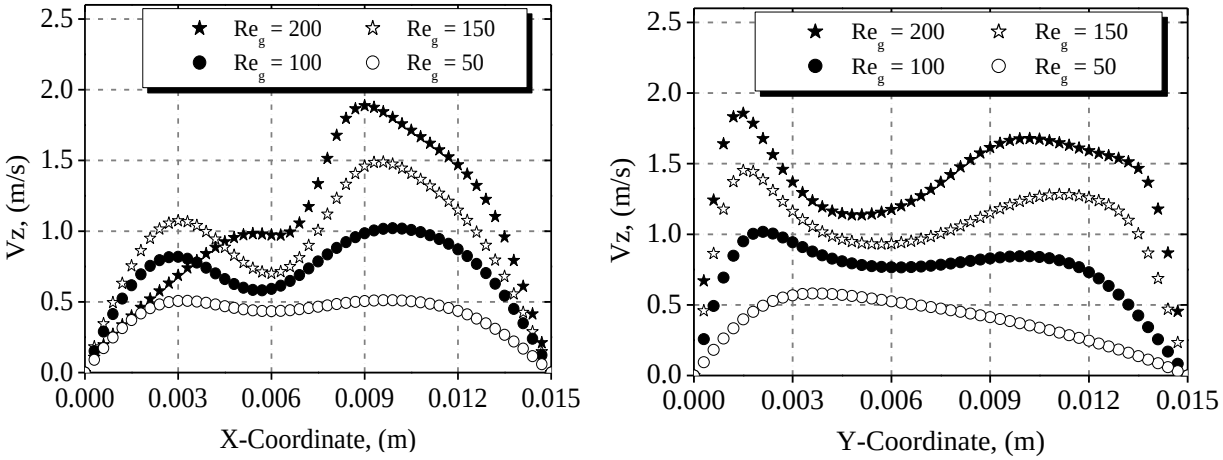

Figure 3.18: Axial velocity profiles at the outlet section of the C-shaped channel for Re_g = 50 to 200, with n = 1, (a) X-Coordinate and (b) Y-Coordinate.

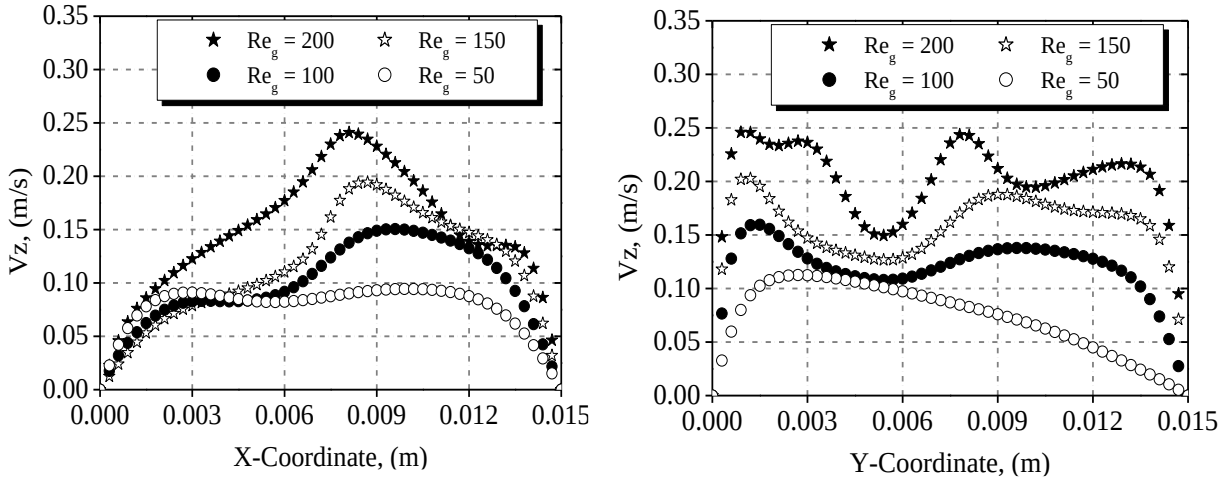

Figure 3.19: Axial velocity profiles at the outlet section of the C-shaped channel for Re_g = 50 to 200, with n = 0.5, (a) X-Coordinate and (b) Y-Coordinate.

3.4.3 Periodic flow

Axial Velocity profiles of in three periods of C-shaped channel are presented in figure 3.20 and figure 3.21, respectively. For both Newtonian and non-Newtonian cases, the same velocity profiles are taken in the second and the third period. Therefore, the pressure loss is even more important that the axial velocity of the flow is low. By conservation of volume flow, the maximum of axial velocity profiles are reduced due to the formation of fluid cells, which generate an increase in the secondary flow.

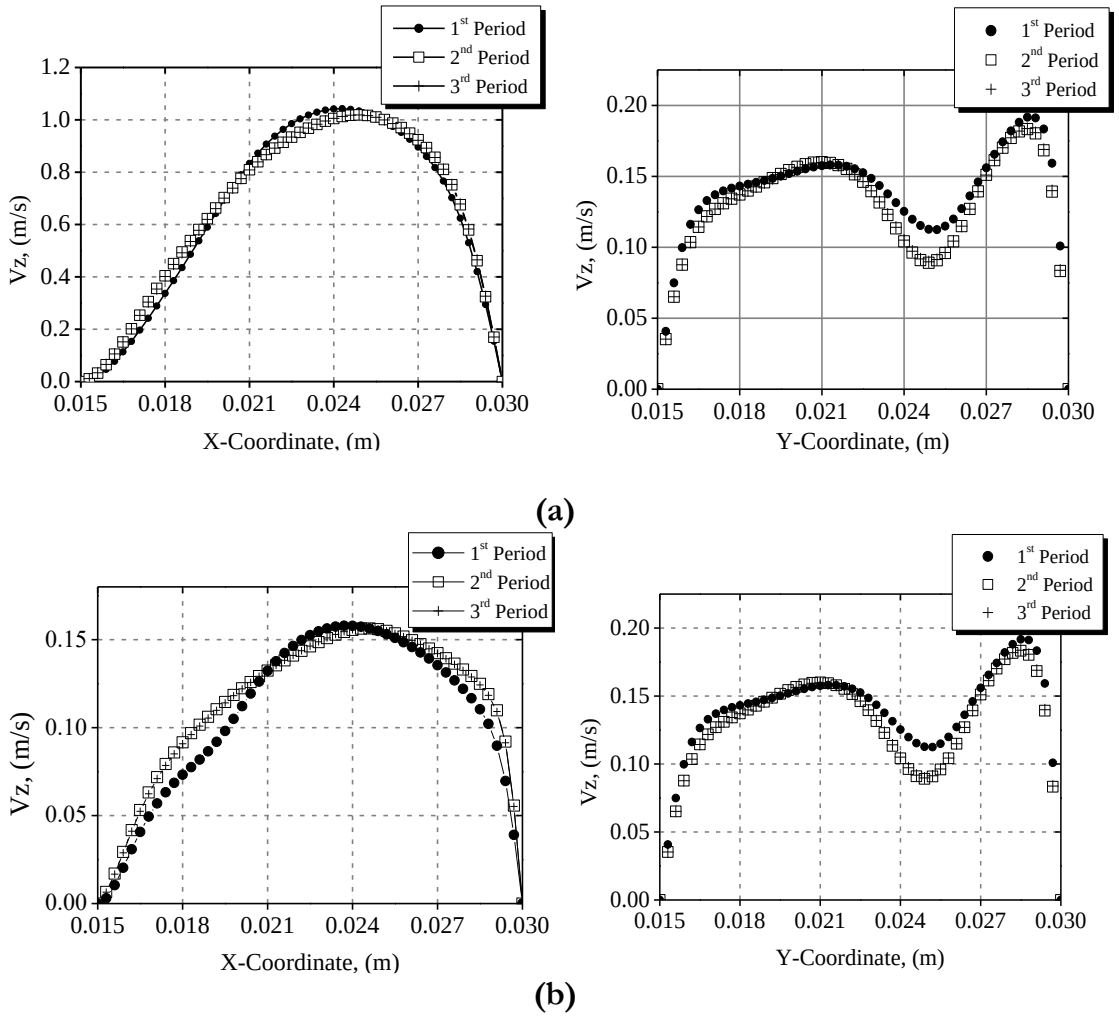

Figure 3.20: Axial-Velocity profiles of the C-shaped channel at the middle section of each period, as function of (left) X-coordinate and (right) Y-coordinate for: (a) n = 1and (b) n = 0.5.

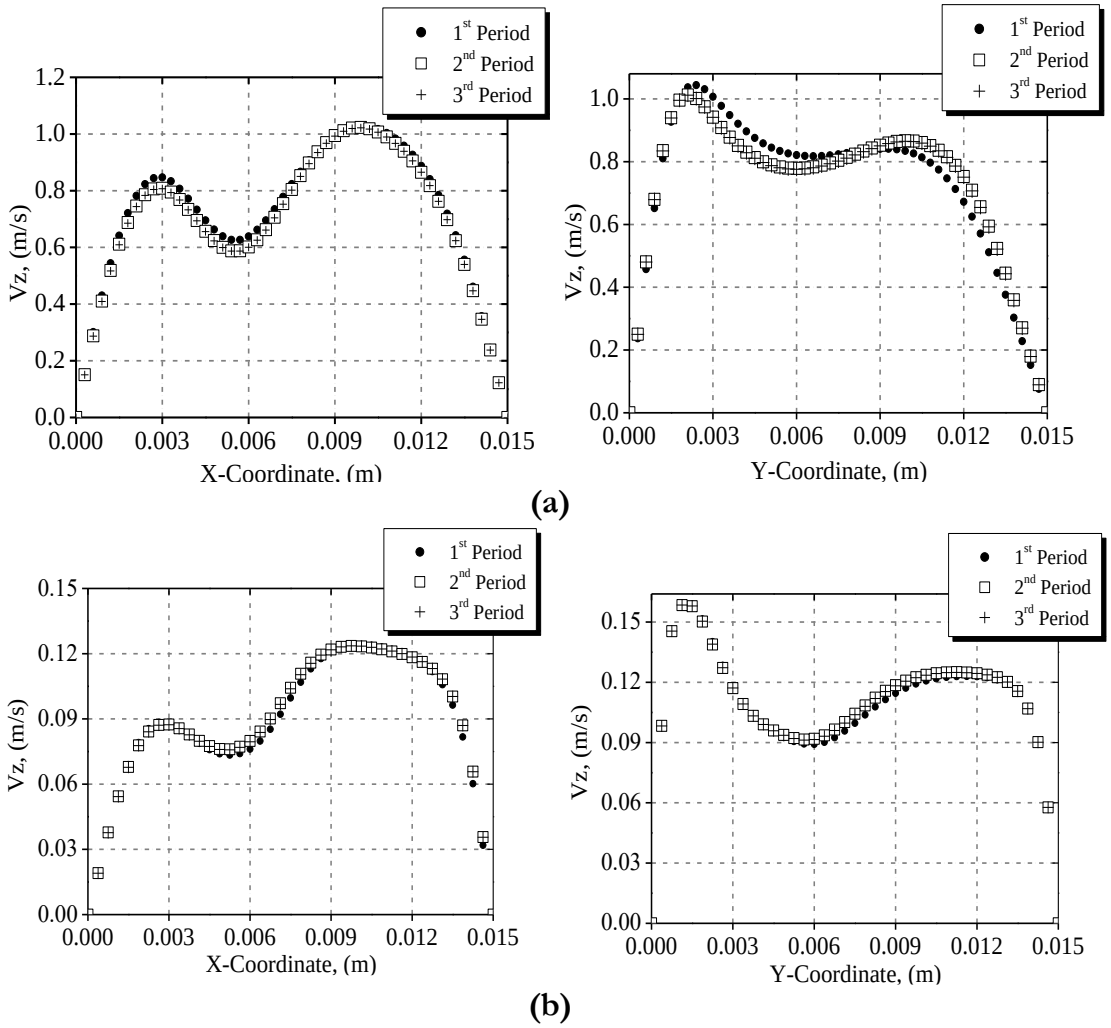

Figure 3.21: Axial-Velocity profiles in the C-shaped channel at the outlet section of each period, as function of (left) X-coordinate and (right) Y-coordinate for: (a) n = 1and (b) n = 0.5.

3.5 Poiseuille number

Figure 3.22 presents the evolutions of the local Poiseuille number with the curvilinear coordinate for a generalized Reynolds number equal to 100 and for two values of the power-law index 0.5 and 1 in three periods of the straight and C-shaped channels.

Because the flow is regular in the straight channel, the local Poiseuille number decreases rapidly at the entrance of the channel as function of the curvilinear coordinate and it tends towards an asymptotic value once the flow is established. This value increases with the power-law index n. In the C-shaped geometry and from the second period, the variation of the local Poiseuille number is periodic. This is explained by the fact that the velocity field is itself periodic (figure 3.23). The flow is enough disrupted due to the existence of the geometrical perturbations, which prevents the establishment of the boundary layer. This phenomenon on increases strongly the pressure drop.

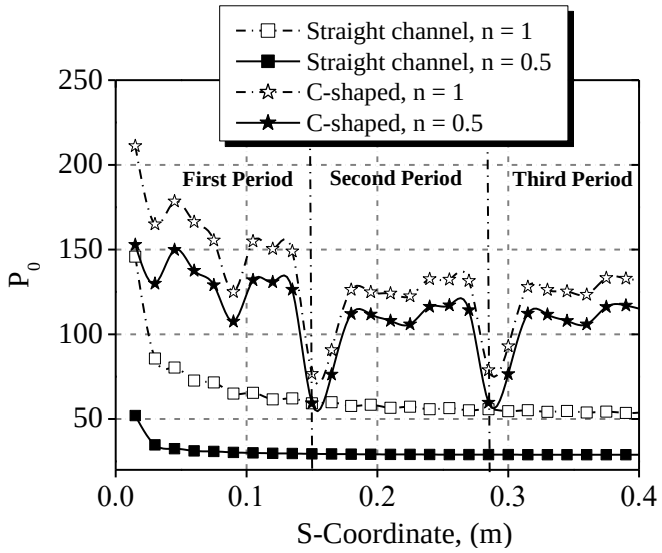

Figure 3.22: Evolutions of the local Poiseuille number with the curvilinear coordinate for the two geometries for a power-law index of 0.5 and 1 (Re_g =100).

Figure 3.16 presents the evolutions of the mean Poiseuille number with generalized Reynolds number for the two considered geometries and for power-law index ranging from 0.5 to 1.In the straight channel when the flow regime is established, the mean Poiseuille number keep a constant value whatever the generalized Reynolds number for a given value of power-law index n. This parameter (Po_{mean}) increases with the growth of the power-law index. As mentioned to above, the pressure drops are influenced by the intense secondary flows and accentuated with the increase of the generalized number and the power-law index. So, the mean Poiseuille number is very significant in the C-shaped than that calculated in the straight channel.

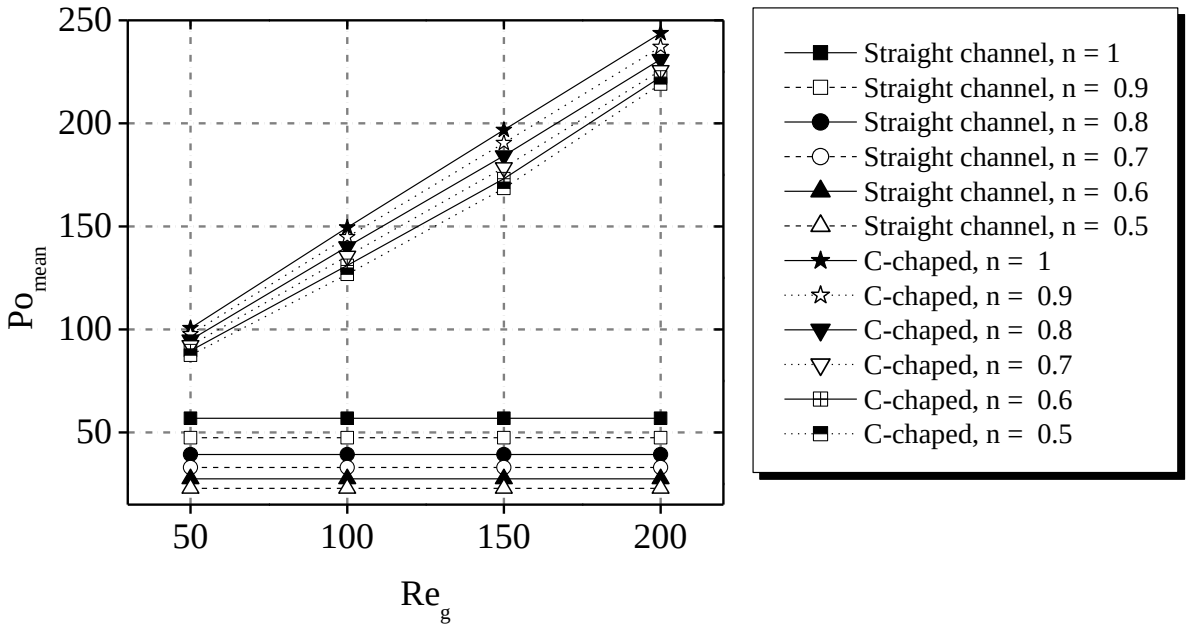

Figure 3.23: Evolutions of the mean Poiseuille number with generalized Reynolds number in straight and C-shaped channels.

3.6 Heat transfer characteristics

The axial variation of the local Nusselt number with respect to power-law index n = 1 to 0.5, is depicted in Figure 3.24. The local Nusselt number sharply decreases at the entry and then fluctuates for all cases of Newtonian (n = 1) and non-Newtonian (n = 0.9 to 0.5) fluids. This observed phenomenon is different from that of straight channel, and these oscillations are caused by the flow pattern which is affected by the centrifugal and viscous forces inducing thermal boundary layer formations at the entrance, see figure 3. 18.

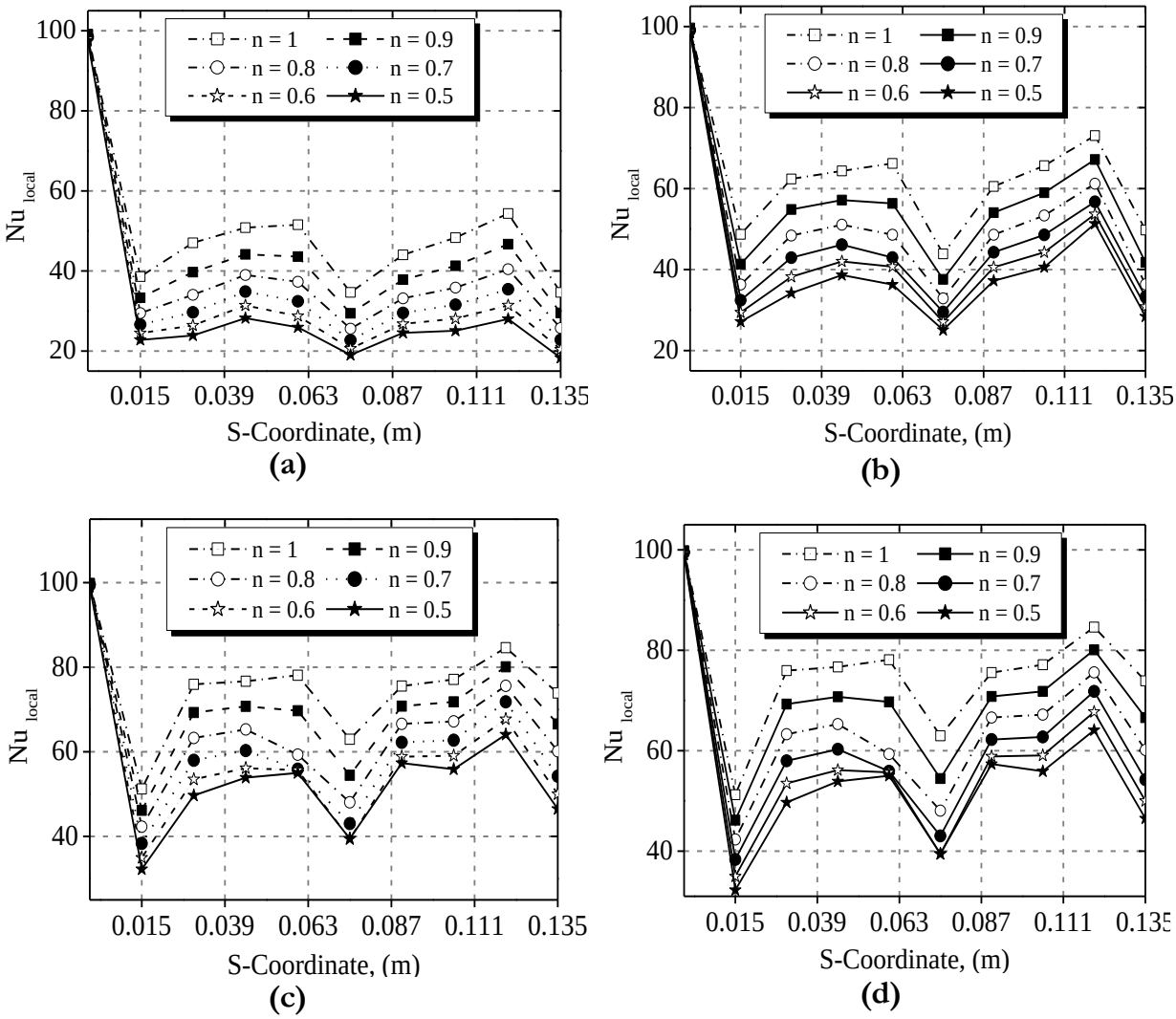

Figure 3.24: Evolutions of the local Nusselt number as function of the curvilinear coordinate (S) in the C-shaped channel for n = 0.5 to 1 with: (a) Re_g = 50, (b) Re_g = 100, (c) Re_g = 150 and (d) Re_g = 200.

In the entrance length of the straight channel, the local Nusselt number decreases strongly to reach an asymptotic value which depends on the power-law index (Figure 4.25). However, in the C-shaped geometry, the chaotic behavior exhibits a marked influence on heat transfer distributions in the system. Due to the continuous effect of the boundary layer destruction, the local Nusselt number evolves periodically with the curvilinear coordinate, which allowed us to make the computation in one period. Consequently, the

thermal boundary layer in the chaotic channel became thin and the heat transfer is very sensitive to temperature changes between the wall temperature and the mean bulk temperature. The maximum variation of the local Nusselt number is very considerable and it is around 40.

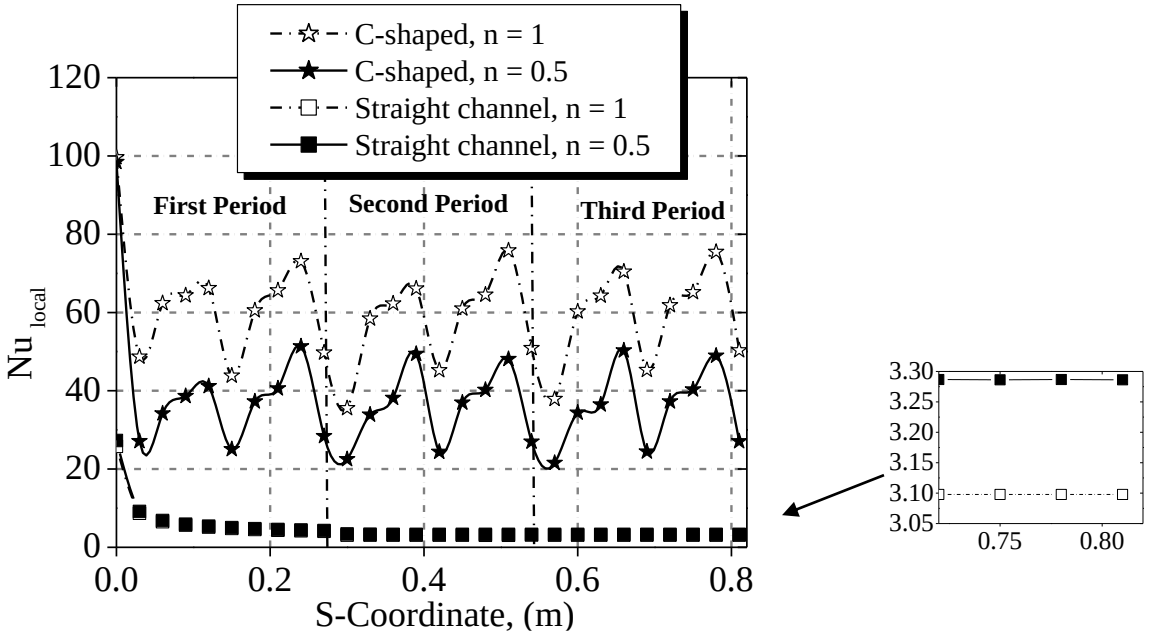

Figure 3.25: Evolutions of the local Nusselt number with the curvilinear coordinate in the two geometries for two values of the power-law index 0.5 and 1 (Re_g = 100).

In order to compare the heat transfer performances between the two geometries, the variation of the mean Nusselt number as function of generalized Reynolds number for several power-law index values ranging from 0.5 to 1 is estimated (figure 3.26).

In the straight channel, the mean Nusselt number is independent of the generalized Reynolds number and keeps a constant value, which increases with the power-law index value n. This is due to the effect of the chaotic kinematics of the fluid flow. With a view to examine the increase of heat transfer rate rather than the decrease of pressure drop, we present on the figure 3.27 the evolutions of the ratio Nu_{mean}/Po_{mean} with the generalized Reynolds number for the power-law index values. When this ratio is high, the compromise (improving heat transfer- diminution pressure losses) is the best. In the straight channel, this parameter has a constant value for a given power-law index and is lower when n = 1.

However, in the C-shaped geometry, the ratio Nu_{mean}/Po_{mean}becomes higher with the increase of the power-law index but it decreases with the generalized Reynolds number. As conclusion, the compromise (improving heat transfer- diminution pressure losses) provided by the C-shaped is very significant in comparison with that calculated in the straight channel.

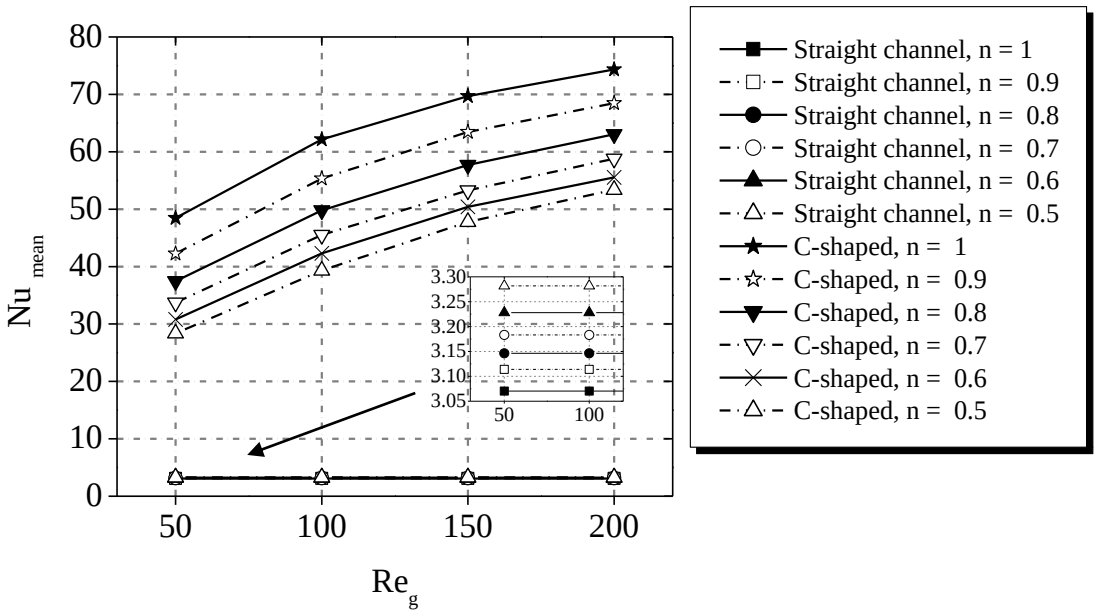

Figure 3.26: Evolutions of the mean Nusselt number with generalized Reynolds number in straight and C-shaped channels power-law index (n = 1 to 0.5).

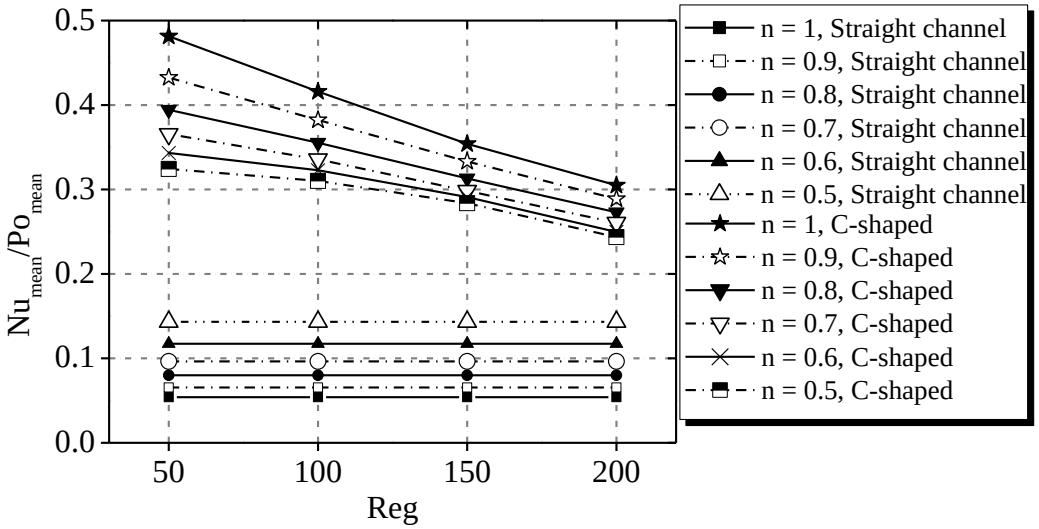

Figure 3.27: Evolutions of the ratio of the Poiseuille number to the Nusselt number with different power-law index for straight channel and C-shaped geometry.

3.7 Thermal mixing performances

The thermal mixing (temperature homogenization) between hot and cold non Newtonian fluids is considered for two injections modes (horizontally and vertically). For this, the inlet cross section of each geometry is divided in two parts. The hot fluid is injected in one part at 330K and the cold fluid is injected in the other part at 300K, see figure 3.28. In this paper, we estimate the mixing performances in the chaotic geometry (C-shaped geometry) and its performances will be compared to those of the classical geometry, Straight channel.

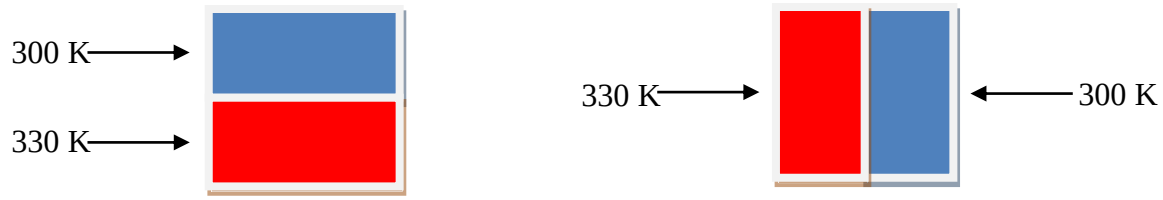

(a) Horizontal injection **(b)** vertical injection

Figure 3.28: Temperature at the inlet cross section.

3.7.1 Temperature contours

Figures 3.29, 3.30, 3.31 and 3.32 present the temperature contours in five cross sections in the Straight channel for different power-law index (n = 0.5, 0.8 and 1) and for two generalized Reynolds numbers equal to 50 and 150 and for two injection modes, horizontally and vertically. In the straight channel, the trajectories are parallels for which there is no transfer of fluids in the transverse direction. So, the thermal mixing between the two fluids is located at the interface and it is achieved only by molecular diffusion (conduction). Because the heat transfer level in the straight channel depend to the residence time, the thermal mixing for generalized number equal to 50 is better than that obtained when generalized Reynolds number equal to 150 for both horizontal and vertical injections. As known, the increase of the power law index gives a significant role of a molecular diffusion. In other words, when the power law index n is high the fluid became more viscous and consequently the momentum transfer by conduction dominates.

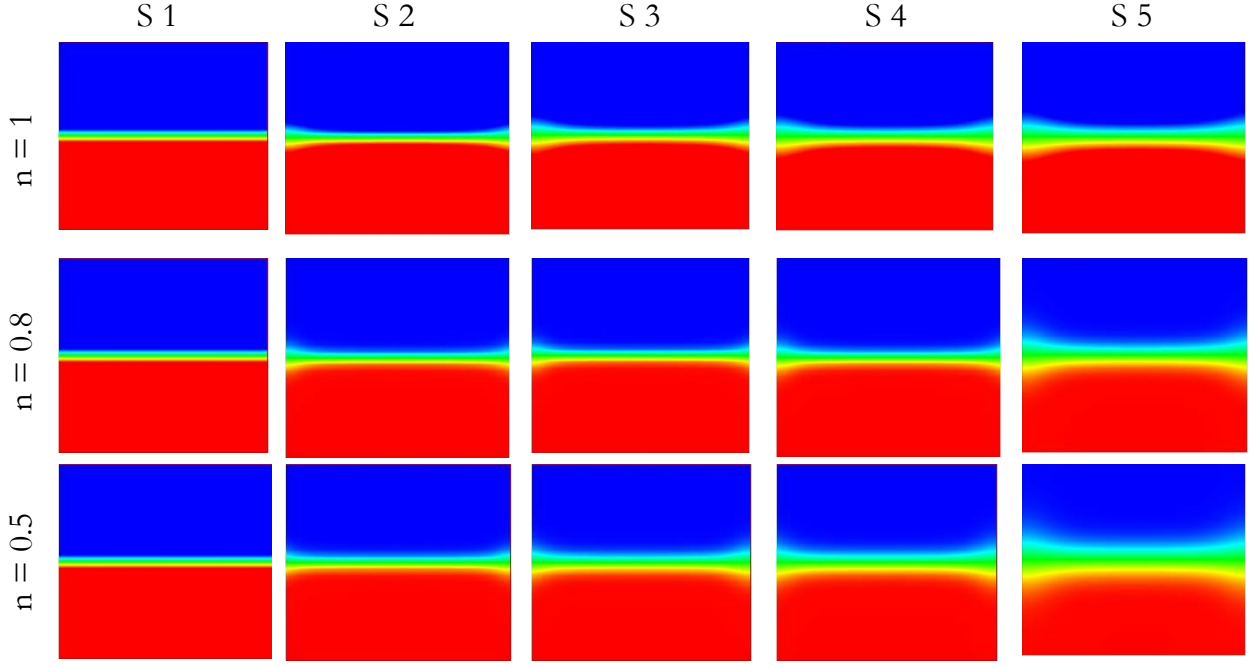

Figure 3.29: Temperature contours in the Straight channel for different power-law index (n : 0.5, 0.8 and 1) with horizontal injection (Re_g = 50) at five cross sections: S1: inlet section, S2: middle of the first period, S3: outlet of the first period, S4: middle of the second period and S5: outlet of the second period.

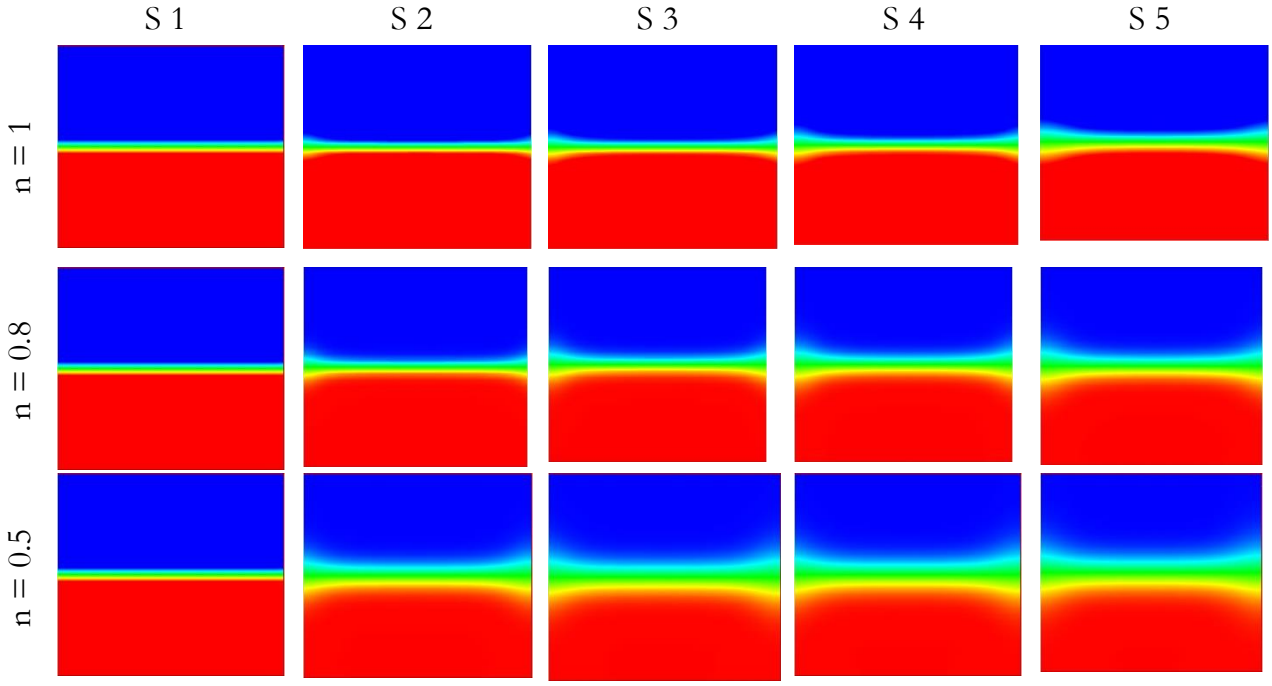

Figure 3.30: Temperature contours in the Straight channel for different power-law index (n : 0.5, 0.8 and 1) with horizontal injection (Re_g = 150) at five cross sections: S1: inlet section, S2: middle of the first period, S3: outlet of the first period, S4: middle of the second period and S5: outlet of the second period.

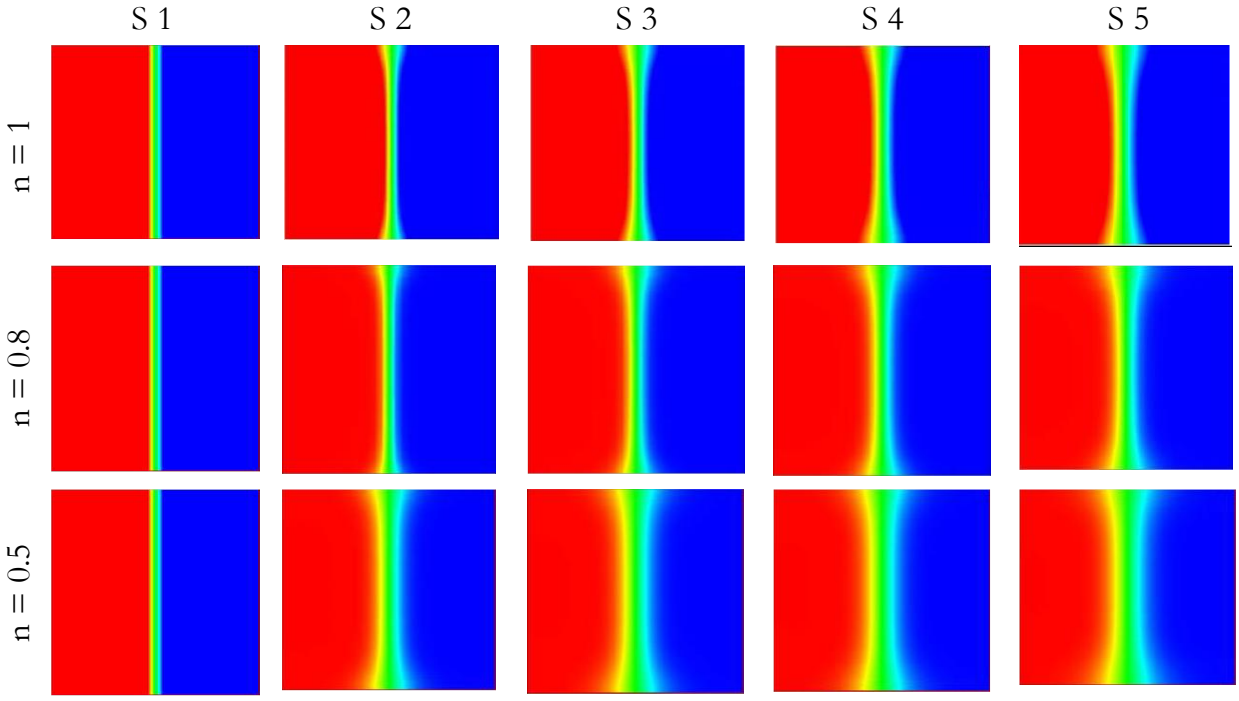

Figure 3.31: Temperature contours in the Straight channel for different power-law index (n : 0.5, 0.8 and 1) with vertical injection (Re_g = 50) at five cross sections: S1: inlet section, S2: middle of the first period, S3: outlet of the first period, S4: middle of the second period and S5: outlet of the second period.

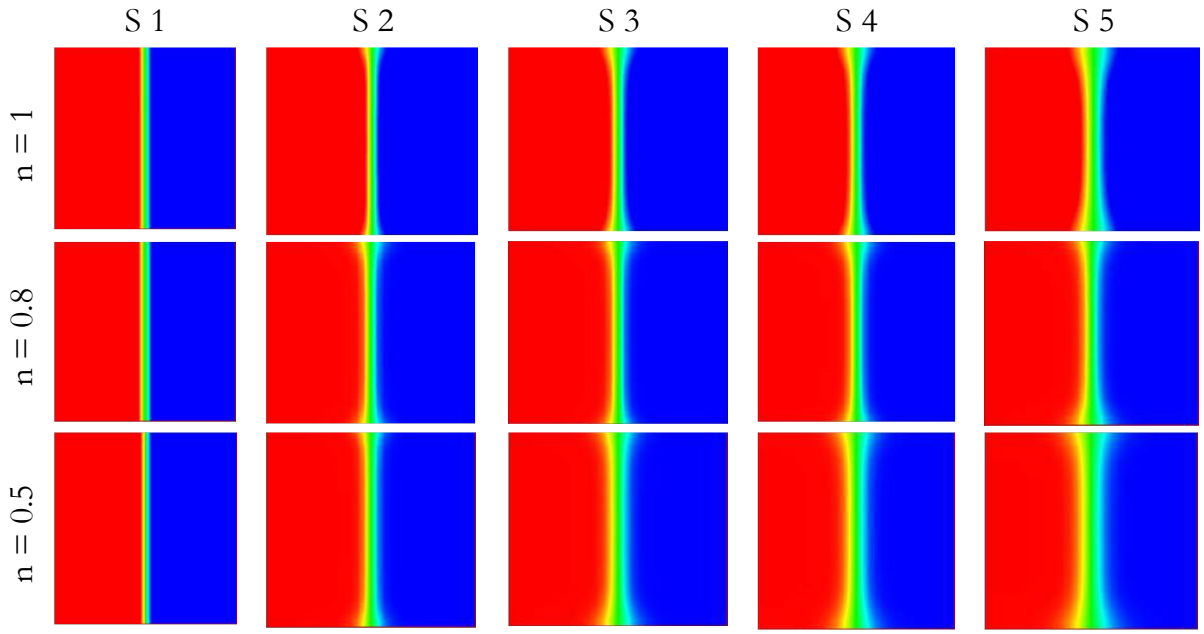

Figure 3.32: Temperature contours in the Straight channel for different power-law index (n : 0.5, 0.8 and 1) with horizontal injection (Re_g = 150) at five cross sections: S1: inlet section, S2: middle of the first period, S3: outlet of the first period, S4: middle of the second period and S5: outlet of the second period.

For a given value of generalized Reynolds number, if the power law index n increase, the velocity increase too. Contrary to the power law index n effects, the increase of the velocity begets the decreasing of the mixing level. So, there is a competition between the two effects. For example, we remark that for mixing is better for n=0.5 than that obtained for n=0.8 which explain that the effect of the velocity on the mixing is dominated and vice versa.

Figures 3.33, 3.34, 3.35 and 3.36 present the temperature contours in five cross sections in the C-shaped channel for different power-law index (n = 0.5, 0.8 and 1) and for two generalized Reynolds numbers equal to 50 and 150 and for two injection modes horizontal and vertical. Unlike what is given by the Straight channel, the preview of the temperature contours at each cross section situated along the C-shaped geometry indicates that the mixing quality is not affected by the power law index n for a given generalized Reynolds number Re_g either horizontally or vertically injections. So, the power law index has not any effect on the mode of momentum transfer in the flow. For a given value of the power law index and on the same cross section, the mixing quality is more vigorous when the generalized Reynolds number is more important. The increase of the generalized number enhances highly the dynamic of the flow and the kinematic of the fluid particles changes considerably and the mixing level will be improved.

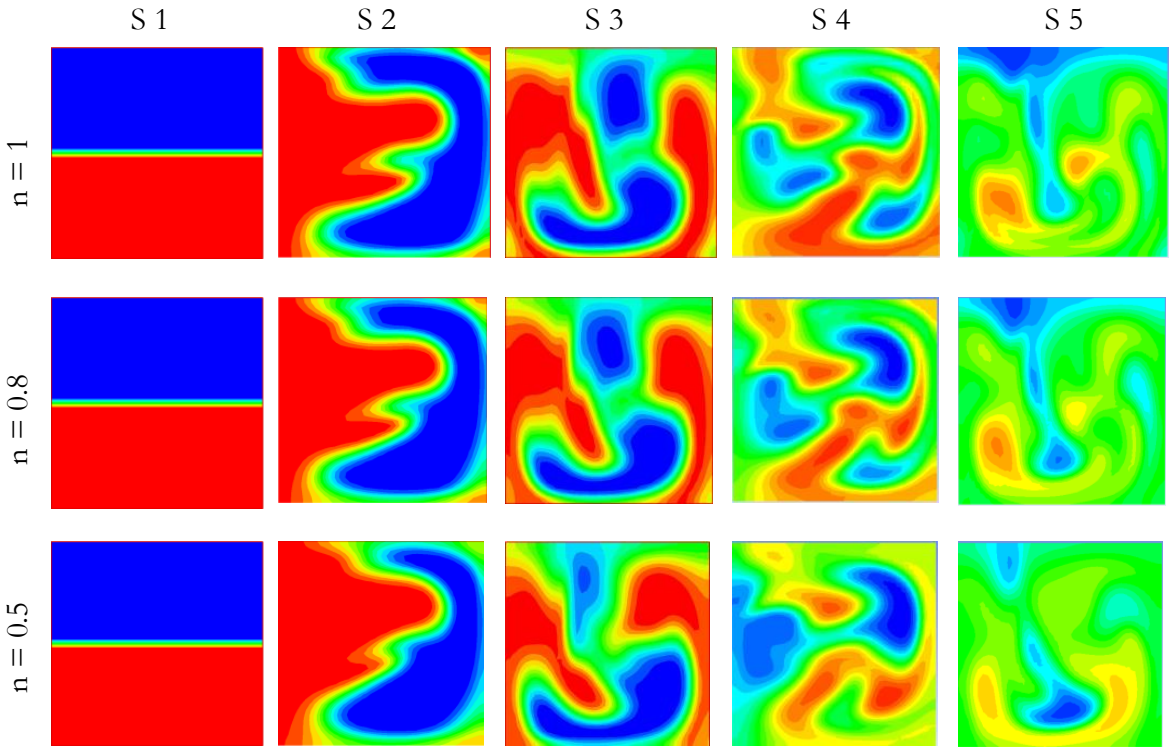

Figure 3.33: Temperature contours in the C-shaped channel for different power-law index (n = 0.5- 1) with horizontal injection (Re_g = 50) at five cross sections: S1: inlet section, S2: middle of the first period, S3: outlet of the first period, S4: middle of the second period and S5: outlet of the second period.

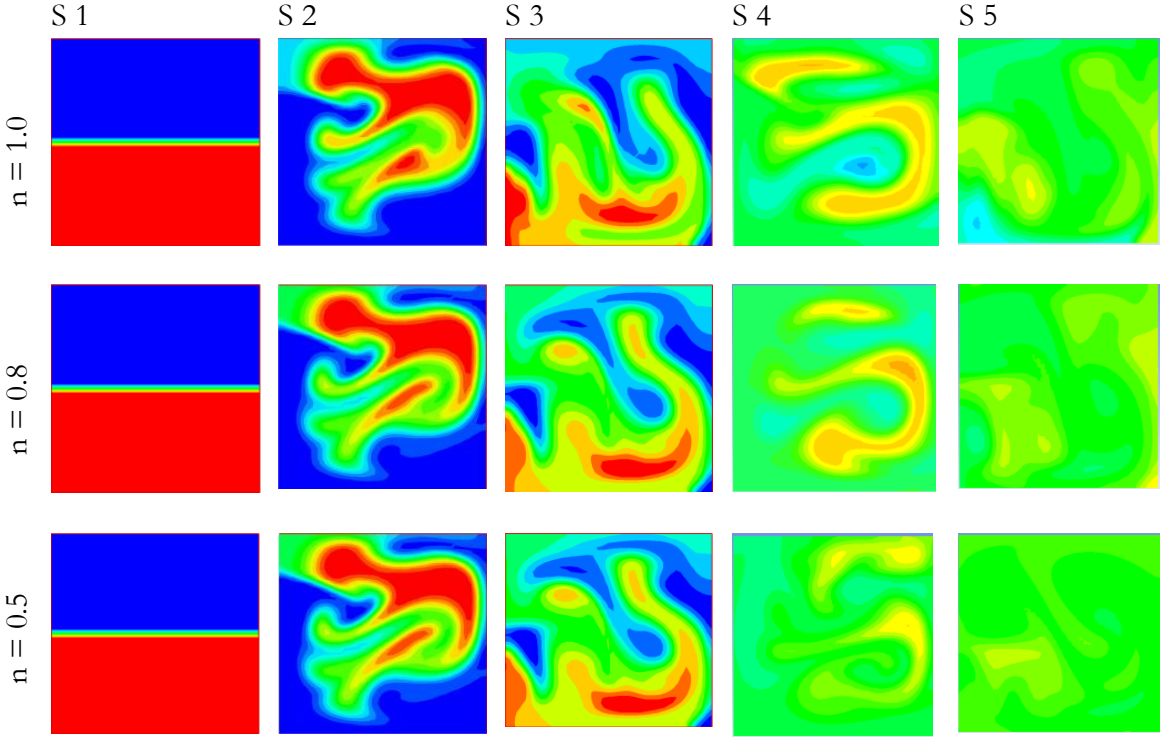

Figure 3.34: Temperature contours for different power-law index (n = 0.5, 0.8 and 1) with horizontal injection (Re_g = 150) at five sections: S1: inlet section, S2: middle of the first period, S3: outlet of the first period, S4: middle of the second period and S5: outlet of the second period.

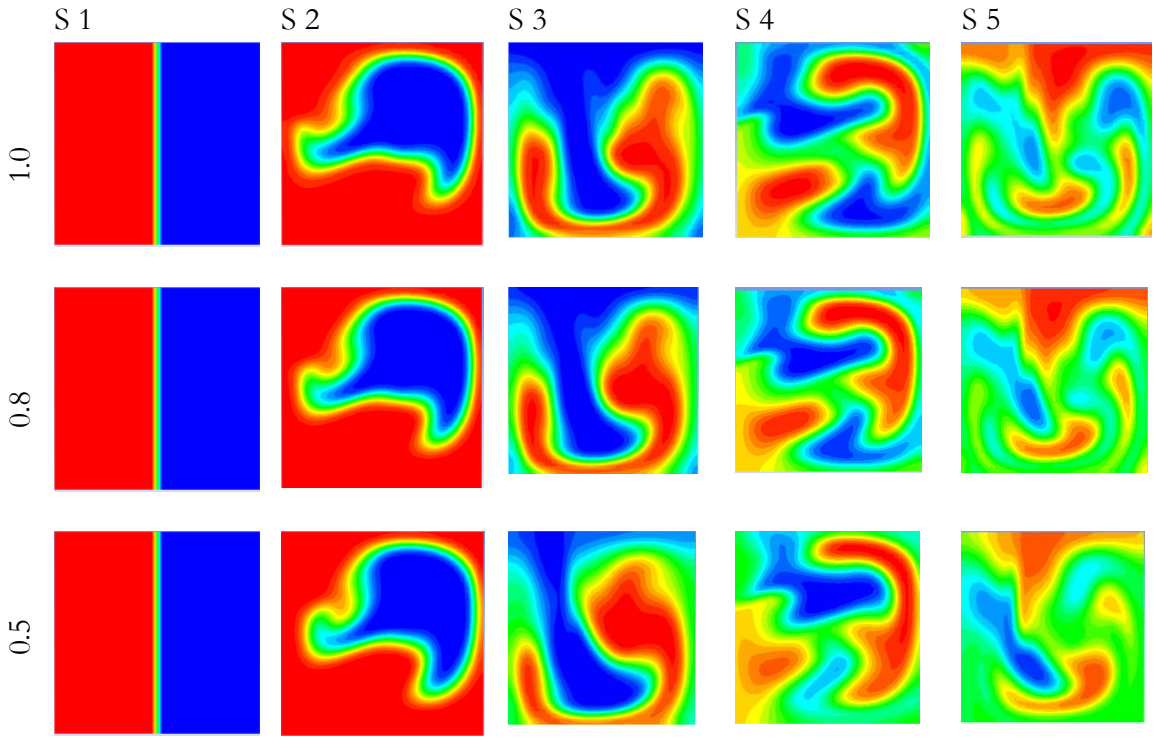

Figure 3.35: Temperature contours for different power-law index (n = 0.5, 0.8 and 1) with vertical injection (Re_g = 50) at five sections: S1: inlet section, S2: middle of the first period, S3: outlet of the first period, S4: middle of the second period and S5: outlet of the second period.

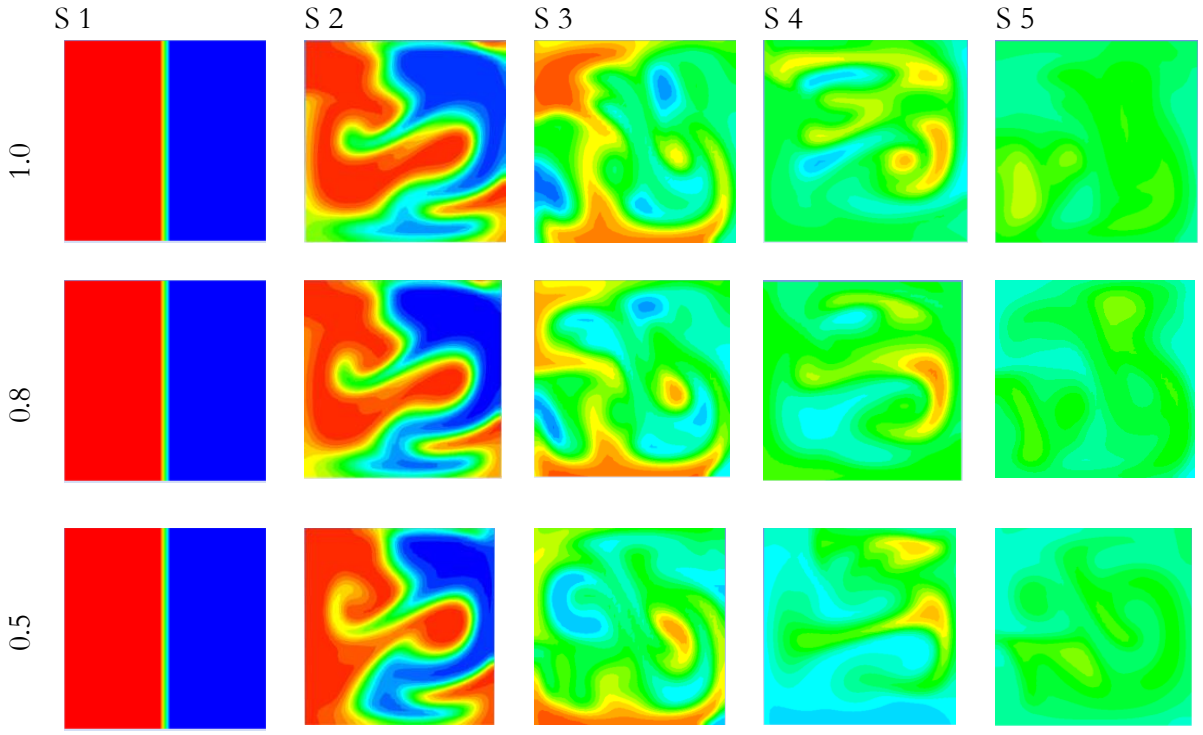

Figure 3.36: Temperature contours for different power-law index (n = 0.5, 0.8 and 1) with vertical injection (Re = 150) at five sections: S1: inlet section, S2: middle of the first period, S3: outlet of the first period, S4: middle of the second period and S5: outlet of the second period.

3.7.2 Mixing degree

3. 7.2.aThe evolutions of the Mixing degree with the non-dimensional residence

Figures 3.37 and 3.38 show the evolutions of mixing degree, M_d, with the non-dimensional residence time for initial horizontal and vertical injections, for generalized Reynolds numbers 50 and 150 and for power-law index n equal to 0.5 and 1 in the two geometries straight and C-shaped channels.

In the straight channel, the particle trajectories are parallels and consequently the heat transfer is done only by conduction through the interface between the two fluids. This leads to a very bad thermal mixing quality for all cases taken account whatever the power law index values and the generalized Reynolds number and as consequently the level mixing does not go beyond 0.2. To have a good quality mixing level it should be take a very important duration. So, the straight channel is not the appropriate channel for to use it in the thermal mixing process.

In the C-shape channel, the agitation is more vigorous due the chaotic kinematic of the trajectories and to the existence of the intense recirculation zones in the flow. This behavior contributes considerably to the enhancement of the mixing performances compared to that in the straight channel wherein the flow is regular. When the generalized Reynolds number increases, mixing is more vigorous, and the mixing degree evolves more quickly so the best quality of the thermal mixing is reached. In this type of the geometry, the mixing time does not exceed one second for the two values of the generalized numbers 50 and 150 and for the power law index n equal to 0.5 and 1. We remark that there are barely difference between the mixing levels obtained for the power law index n equal to 0.5 and 1. In addition, it is seen that the chaotic nature of the trajectories in this geometry cancels completely the effect of the mode injection on the thermal mixing of the two fluids (hot and cold).

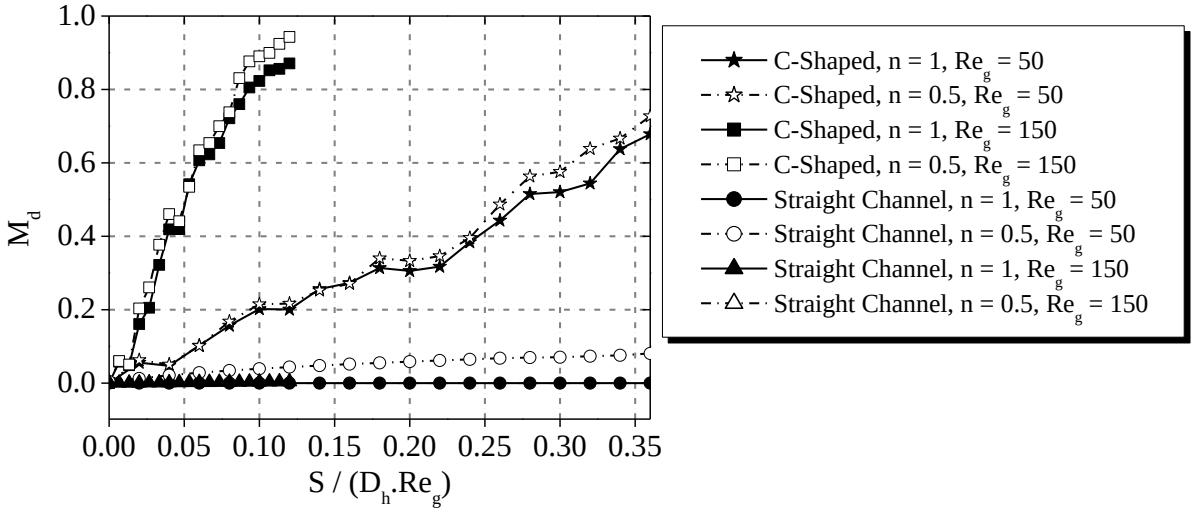

Figure 3.37: Evolution of the mixing degree VS non-dimensional residence time in the two geometries (Straight and C-shaped channels) for different power-law index and generalized Reynolds number with horizontal injection.

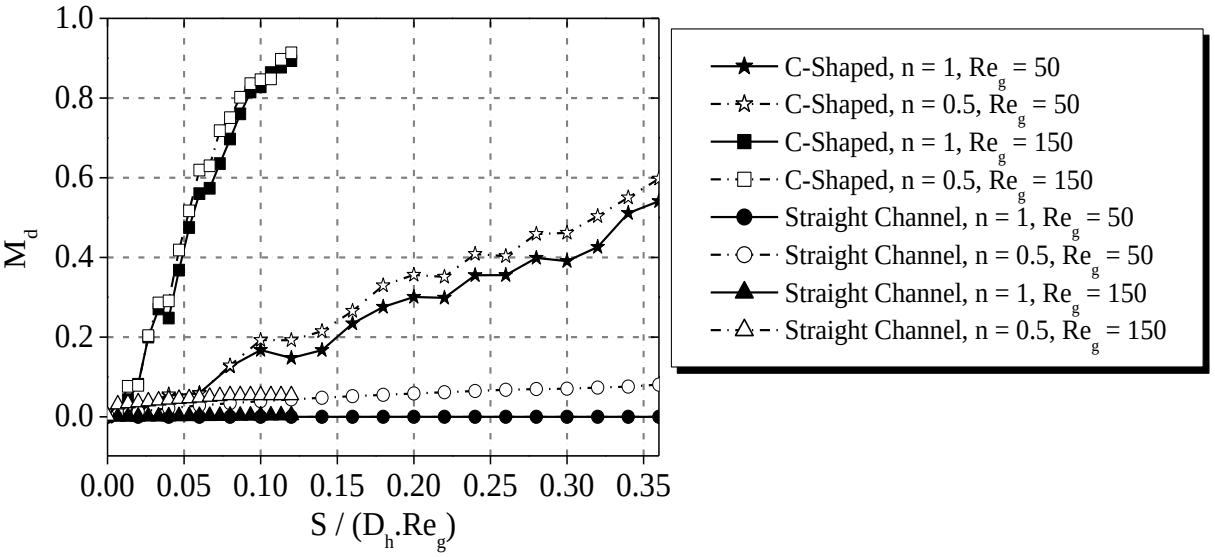

Figure 3.38: Evolution of the mixing degree VS non-dimensional residence time in the two geometries (Straight and C-shaped channels) for different power-law index and generalized Reynolds number with vertical injection.

3.7.2.b Evolutions of the Mixing degree with the generalized Reynolds number

Figures 3.39 and 3.40 show the evolutions of the mixing degree, M_d, with generalized Reynolds as function of generalized Reynolds numbers and for two power-law index values n equal to 0.5 and 1 in the two geometries straight and C-shaped channels and for initial horizontal and vertical injections as respect.

In the straight channel, the mixing degree is very weak both in horizontal or vertical injections and for the two powers law index values n in the generalized Reynolds number range. Because the heat transfer is done only by conduction the mixing decreases as function of generalized number. Despite the slight superiority of the M_d for the value of n equal to 0.5, we can see that the effect of the power law index on the mixing is almost negligible.

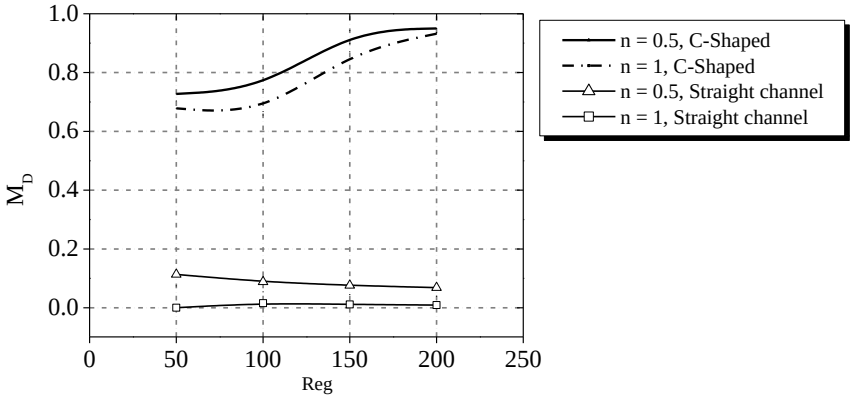

Figure 3.39: Evolutions of the mixing degree as function of generalized Reynolds number for two power-law index values n (0.5 and 1) and for horizontal injection at the outlet cross section of the 2nd period.

In the case of the C-shaped geometry, the flow is chaotic which leads to a great agitation. This behavior improves considerably the thermal mixing as function of generalized Reynolds number. For generalized Reynolds number equal to 200, the mixing degree is close to 1 and the quality mixing is perfect. The degree of mixing has an insignificant difference as a function of the power law index considered so, the power law index n has the same effect on the M_D as described above.

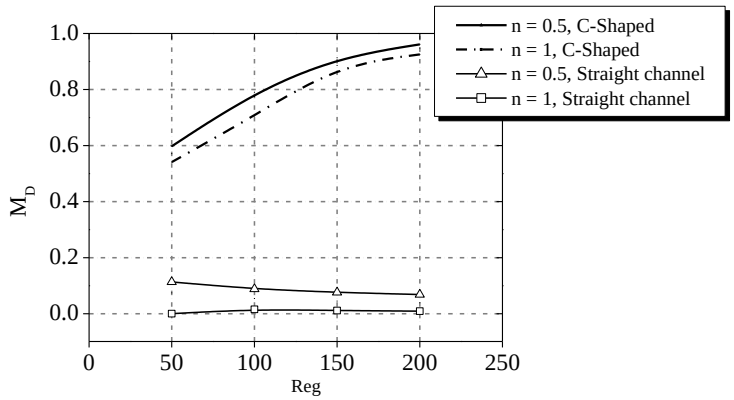

Figure 3.40: Evolutions of the mixing degree as function of generalized Reynolds number for two power-law index values n (0.5 and 1) and for vertical injection at the outlet cross section of the 2nd period.

3.7.3 Temperature distribution

The temperature distribution is influenced by the velocity field that prevails in the two geometries, straight and chaotic channels. For this aim, we present in figures 3.41 and 3.42 the probability density function at the outlet cross section of the first three periods in two considered geometries (Straight and C-shaped channels), for two values of power law index (0.5 and 1), for generalized Reynolds number equal to 100 and for two mode injections, horizontal and vertical, respectively. In the straight channel, the thermal mixing occurs only by conduction such as declared above either in horizontal or vertical injections. This mode of heat transfer is very slow in order to realize an acceptable thermal mixing level. The preview of the temperature distributions in this channel shows that the temperature field remains as it is released since the inlet section. Also, we can see that the power law index has not an effect on the mixing process and the temperature cartography is unchangeable in the three periods. The initial temperature values, 300K and 330K, have the greater percentage with a barely difference between the three periods. This indicates that the use of the straight channel in the mixing process of the fluids is not the suitable choice.

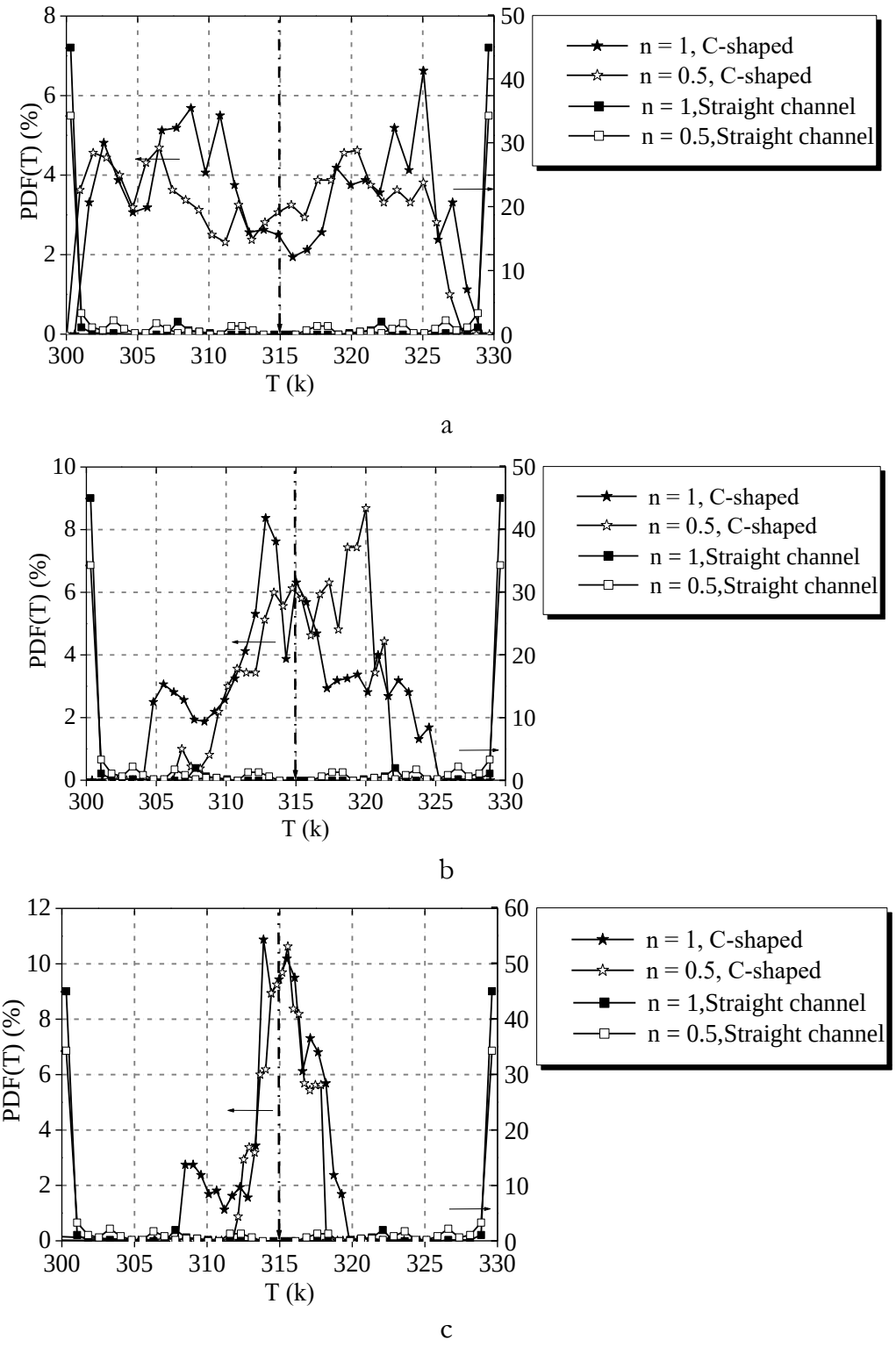

Figure 3.41: Temperature distribution at the outlet cross section in the C-shaped and straight channels for horizontal injection and for Re_g = 100, **(a)** first period **(b)** second period **(c)** third period.

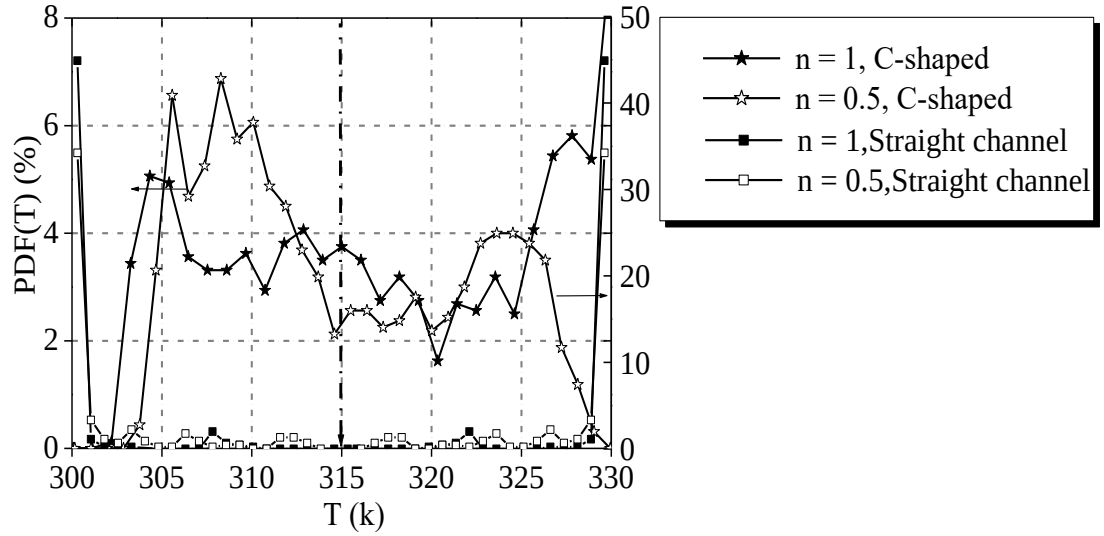

a

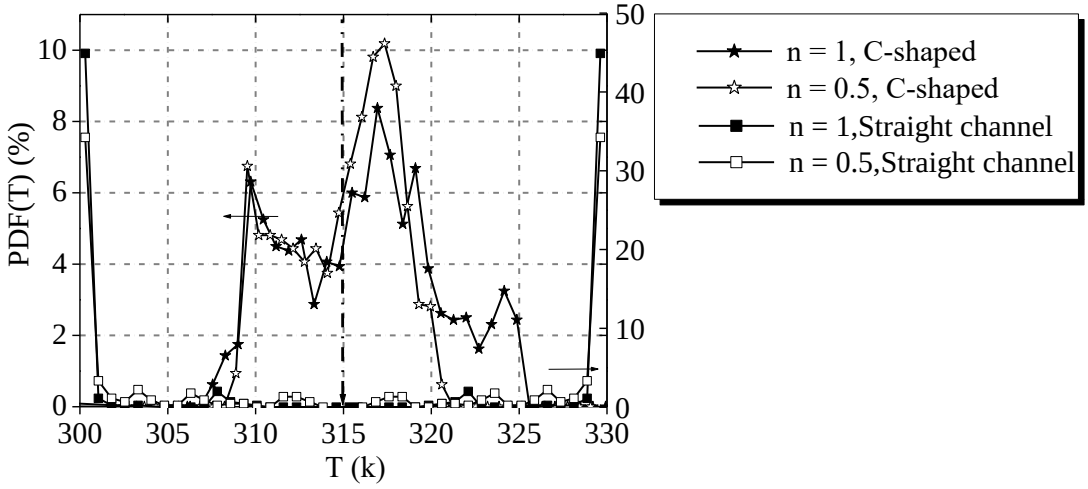

b

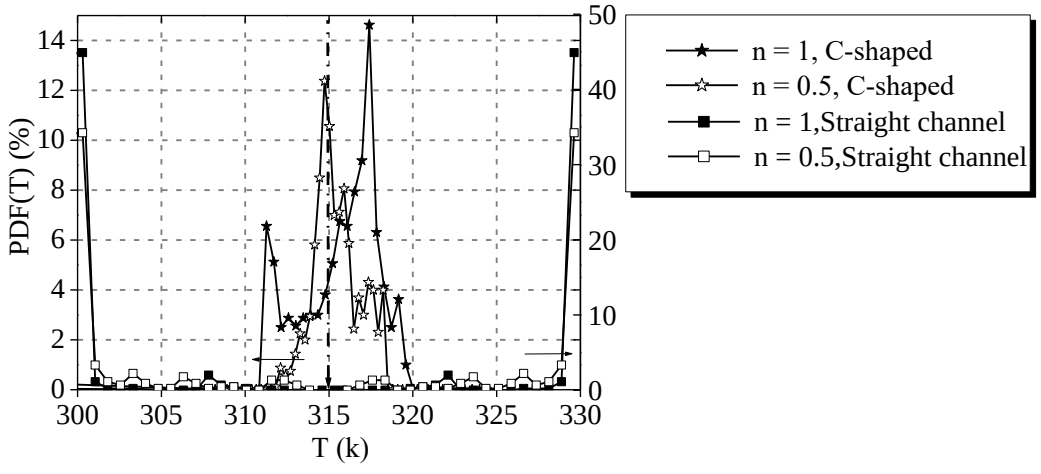

c

Figure 3.42: Temperature distribution at the outlet cross section in the C-shaped and straight channels for vertical injection and for Re_g = 100, **(a)** first period **(b)** second period **(c)** third period.

Regarding the chaotic geometry, the temperature distribution is completely different compared to that obtained by the Straight channel. At the outlet cross section of the first period, the temperature distribution begins to disperse and the temperature values are distributed over all the values included between 300K and 330K. As the fluid passes through the geometry, the fluids are well mixed and tend to be homogenized under the effect of the chaotic behavior of the flow within this geometry. So, the temperature distribution at the outlet cross section of the third period is concentrated in a narrow range of the order of 2K where the peak of this distribution is corresponding to the desired mixing temperature, 315K regardless the power law index values 0.5 or 1.

3.5 Conclusions

In this chapter, we characterized the hydrodynamic, heat transfer and thermal mixing (temperature homogenization) in two geometries, straight and chaotic channels, for generalized Reynolds number ranging from 50 to 200, for power law index values 0.3to 1. This paper outlines the evolutions of the Nusselt number and the Poiseuille number with generalized Reynolds number and with the power law index ranging from 0.5 to 1.It was observed that the local friction factor and Nusselt number starches and folded as the axial distance increases. The chaotic configuration displays a heat transfer enhancement in terms of the mean Nusselt number compared to the straight channel, however the pressure drop in this geometry increases (high Poiseuille number) for all examined Reynolds number. The mixing quality is highlighted by two criteria as the mixing degree M_d and the probability density function Pdf. These criteria confirmed that the capacities of the chaotic geometry in terms of the temperature homogenization of two pseudo plastic fluids (hot and cold) in the flow is more better compared to that prevails in the straight channel. The evaluate of the mixing degree M_d outlines that the perfect mixing is reached rapidly in the chaotic geometry where the mixing time of the homogenization don't exceed 2seconds in the worst cases but in the straight channel, the mixing time is very important and it exceeds several tens of minutes. In addition, it is proven by the Pdf function that the temperature field is well and rapidly homogenized in the chaotic geometry contrary to the straight channel where the temperature field very dispersed and it remains such that it is released at the inlet section.

CHAPTER 4

Entropy Generation Due to the Heat Transfer and Fluid FlowIn theDucts

4.1 Introduction

In this chapter, we characterize the geometries in terms of entropy generation witch due to the heat transfer and fluid friction as function of generalized Reynolds number and power-law index under the effects of different wall heat fluxes.

4.2 Quantities used for the characterization

Based on the temperature and velocity distribution of the flow field, the local entropy generation due to heat transfer irreversibility (S_T''') and thefluid friction irreversibility(S_P''') are given for three dimensional flow as follows [88] [89]:

$$S_T''' = \frac{\lambda}{T^2}\left[\left(\frac{\partial T}{\partial x}\right)^2 + \left(\frac{\partial T}{\partial y}\right)^2 + \left(\frac{\partial T}{\partial z}\right)^2\right] \tag{4.1}$$

$$S_P''' = \frac{\mu_{app}}{T}\left[2\left(\left(\frac{\partial u}{\partial x}\right)^2 + \left(\frac{\partial v}{\partial y}\right)^2 + \left(\frac{\partial w}{\partial z}\right)^2\right) + \left(\frac{\partial u}{\partial y} + \frac{\partial v}{\partial x}\right)^2 + \left(\frac{\partial u}{\partial z} + \frac{\partial w}{\partial x}\right)^2 + \left(\frac{\partial v}{\partial z} + \frac{\partial w}{\partial y}\right)^2\right] \tag{4.2}$$

The total volumetric entropy generation in the flow field can be obtained by :

$$S_{gen}''' = S_T''' + S_P''' \tag{4.3}$$

The mean entropy generation rates due to the heat transfer, $S_{mean,T}'''$, $S_{mean,P}'''$ due to fluid flow and $S_{gen,mean}'''$the whole entropy generation field are defined by:

$$S_{mean,T}''' = \frac{1}{V}\int S_T''' dV \tag{4.4}$$

$$S_{mean,P}''' = \frac{1}{V}\int S_P''' dV \tag{4.5}$$

$$S_{gen,mean}''' = \frac{1}{V}\int S_{gen}''' dV \tag{4.6}$$

Where V is the total volume of the fluid.

The non-dimensional entropy generation numbers are defined as follows [89]:

$$N_S = \frac{S_{gen,mean}'''}{\dot{Q}/T_i} \tag{4.7}$$

Where$\dot{Q}$ is the total heat transfer rate.

In addition, the Bejan number is defined as the ratio of the heat transfer entropy generation to the global entropy generation, [88]:

$$\mathrm{Be} = \frac{S_T'''}{S_{gen}'''} \tag{4.8}$$

Be=0 and Be=1 are two limiting cases representing the irreversibility is dominated by fluid friction and heat transfer, respectively.
Mean Bejan number, $\mathrm{Be_{mean}}$, is defined as follows:

$$\mathrm{Be_{mean}} = \frac{\mathrm{S'''_{mean,T}}}{S'''_{gen,mean}} \tag{4.9}$$

4.3 Effects of generalized Reynolds number on entropy generation

4.3.1 Entropy generation due to heat transfer

Figure 4.1 presents the local distributions of the entropy generation due to heat transfer (S'''_T) for the straight and C-shaped channels for wall heat flux q" = 5000 w/m^{2}with different values of power-law index and generalized Reynolds number. We remark that the entropy generation due to heat transfer is located near the corners while in the rest of the cross section is zeros. This is explained by that the temperature is not homogenized over the cross section. This behavior depends to the velocity field where this later is laminar and regular.
In C-shaped channel, the both cases of Newtonian fluid (n = 1) and non-Newtonian fluid(n = 0.6 and 0.8) the entropy generation due to heat transfer is very low over the cross section regardless the generalized Reynolds number and the power law index which verify that the C-shaped channel can effectively enhance the heat transfer performance for both Newtonian and non-Newtonian fluids.
Figure 4.2 shows the evolutions of the entropy generation rate due to heat transfer with various values of generalized Reynolds numbers and for different power law index values in both straight and C-shaped ducts. The heat entropy generation in the C-shaped channel is less than in that calculated in the straight channel. The heat entropy generation decreases with the increase of the generalized Reynolds number. This explains that the amelioration of the heat transfer in ducts decreases the creation of the entropy. Also, we found that the heat entropy generation decreases with the increase of the power law index n which explain that the increase of the viscosity decreases the creation of the entropy. These results verify again that the chaotic flow can effectively enhance the heat transfer performance by increasing in generalized Reynolds number and increasing in power-law index.

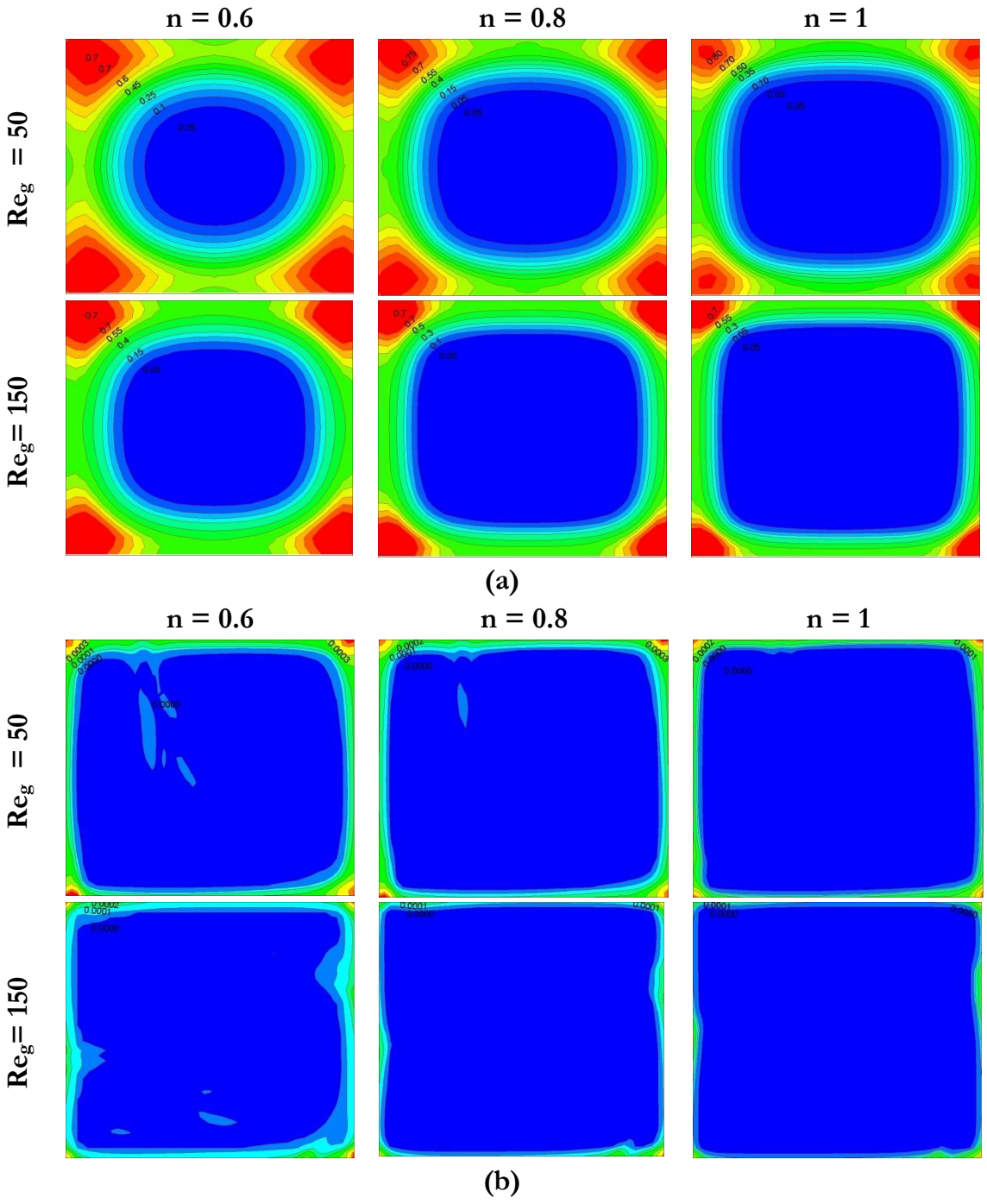

Figure 4.1: Contours of local entropy generation due to heat transfer at the outlet cross section of: (a) straight channel and (b) C-shaped channel for different power-law index and various generalized Reynolds number at constant wall heat flux (q" = 5000 w/m^2).

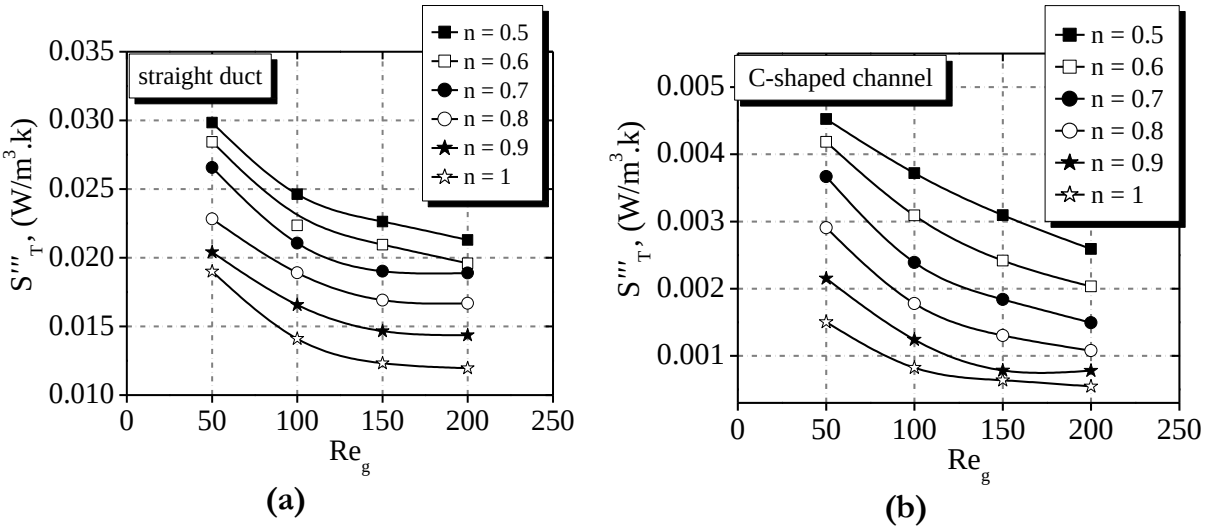

Figure 4.2: Evolutions of the entropy generation rate due to heat transfer for (a): straight duct and (b): C-shaped channel, with various values of generalized Reynolds number.

4.3.2 Entropy generation due to fluid friction

Figure 4.3 presents the local distributions of entropy generation due to fluid friction for various values of generalized Reynolds numbers and for different values of power law index in both straight and C-shaped channels. We see that the entropy generation duo to the friction increase as the power law index increases, which is attributed to the more serious fluid friction and the accompanied frictional irreversibility induced by the larger Reynolds number.

Figure 4.4 illustrates the effect of generalized Reynolds number on the entropy generation rate due to fluid friction in both straight C-shaped channels, with various values of power law index. As the power law index n increases, the irreversibility of the fluid friction increases obviously. The reason behind this trend is the fact that the velocity gradients inside the flow increase. Also we see that the difference between the results of the straight duct and the C-shaped channel are relatively minor.

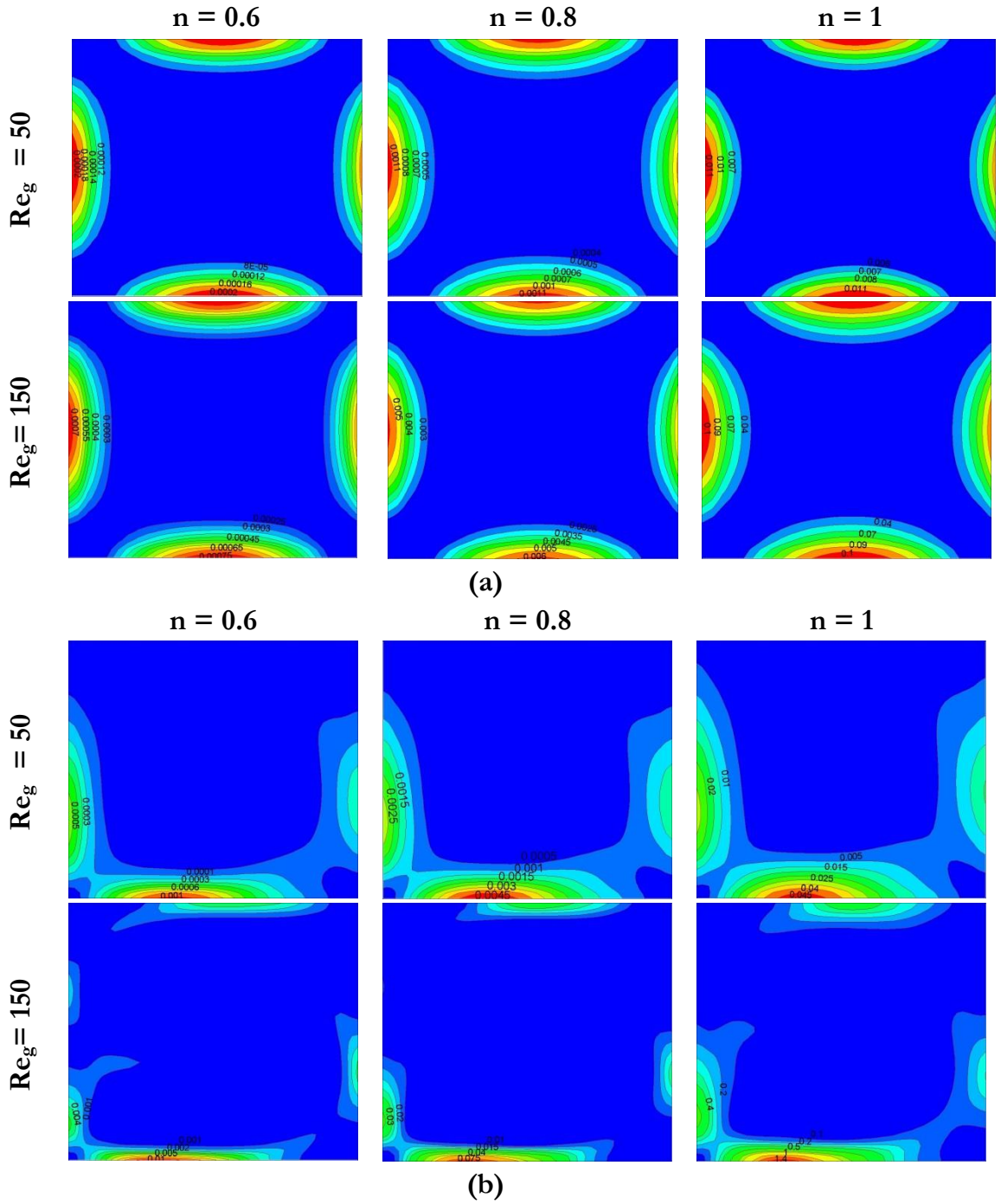

Figure 4.3: Contours of local entropy generation due to fluid friction on outlet cross section of: (a) straight channel and (b) C-shaped channel for different power-law index and various generalized Reynolds number at constant wall heat flux (q" = 5000 W/m^2).

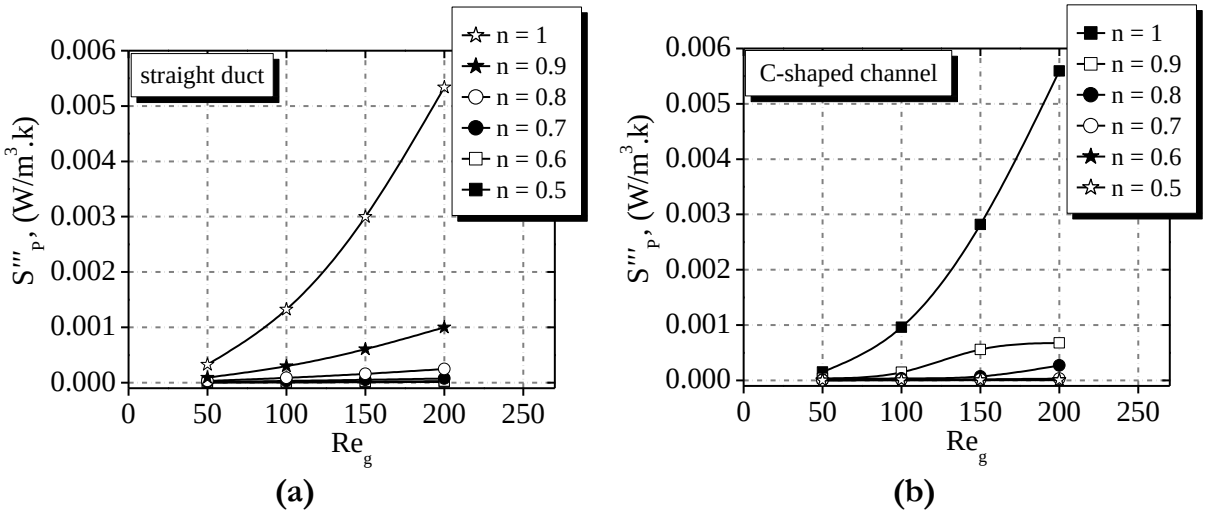

Figure 4.4: Evolutions of the entropy generation rate due to fluid friction for (a): straight duct and (b): C-shaped channel, with various values of generalized Reynolds number.

Figures 5.6 presents the evolutions of the non-dimensional entropy generation for different values of power law index (n) and for various values of generalized Reynolds number. For both straight and chaotic geometries, the non-dimensional entropy generation decreases as the generalized Reynolds number increases. Clearly, the non-dimensional entropy generation decrease with the increasing of the power law index, witch, which reveal again that the effect of the power law index on heat transfer performance is substantial.

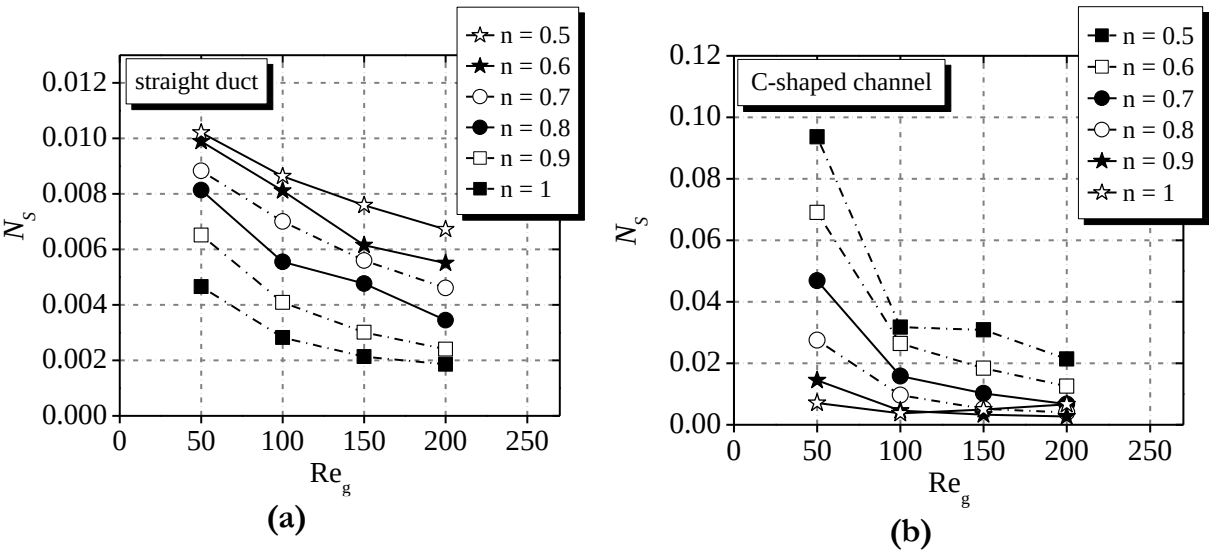

Figure 4.6: Evolutions of global non-dimensional entropy generation rate for (a): straight duct and (b): C-shaped channel, with various values of generalized Reynolds number.

4.3.4 Bejan number

Figure 4.7 presents the local distributions of Bejan number in straight and C-shaped channels with different value of power-law index and generalized Reynolds number. The maximum values of Bejan number concentrates near the heated wall, indicating entropy generation comes from the heat transfer irreversibility. Therefore, the contribution of the global entropy generation is mainly due to heat transfer irreversibility while the contribution of fluid friction irreversibility is minor.

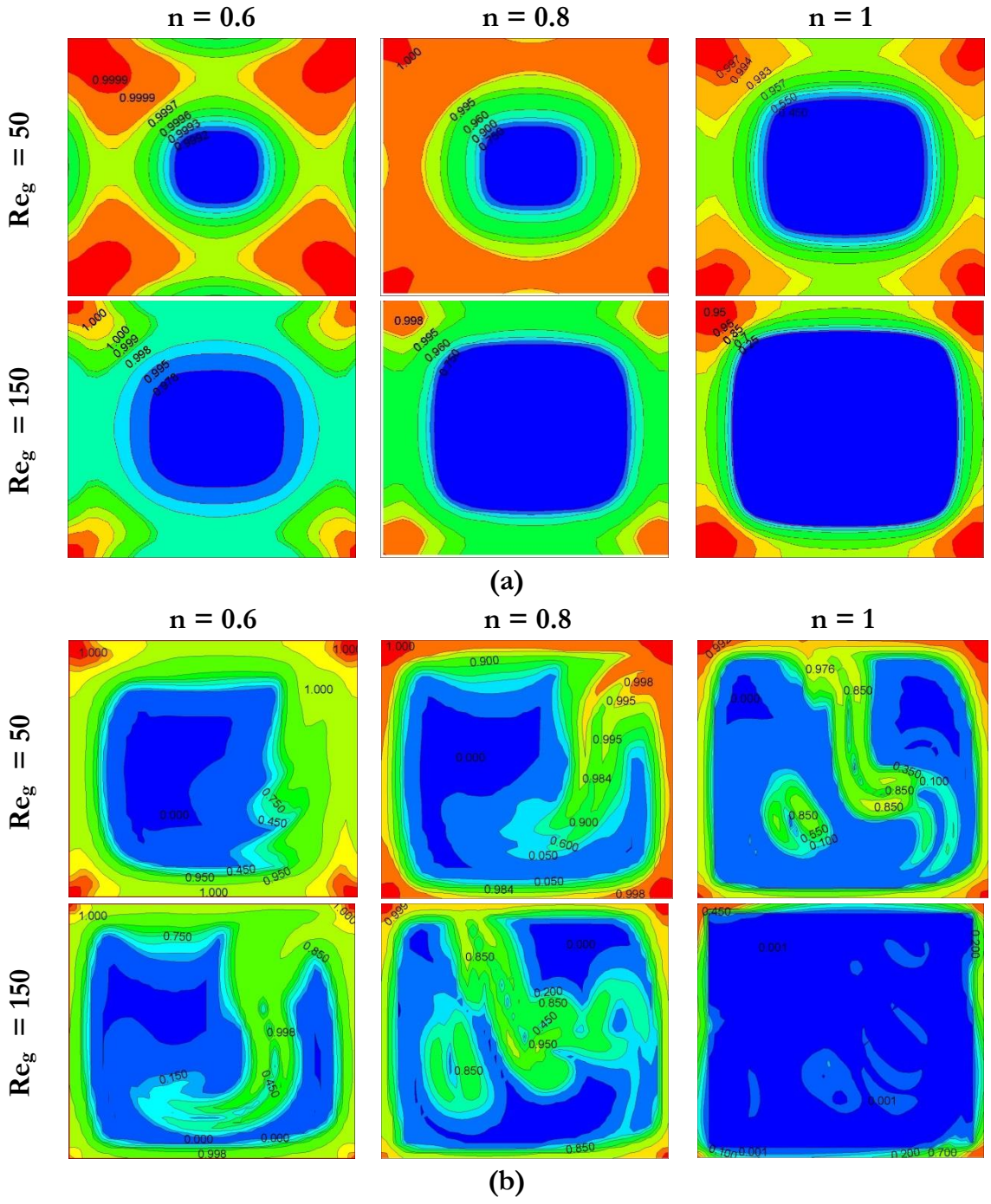

Figure 4.7: Contours of local Bejan number on outlet cross section of: (a) straight channel and (b) C-shaped channel for different power-law index and various generalized Reynolds number at constant wall heat flux (q" = 5000 w/m²).

Globally, the distribution of local Bejan number for straight duct larger than that obtained for the C-shaped channel, which indicates that the heat transfer performance is most serious in chaotic flow.

Figure 4.8 illustrates the effect of generalized Reynolds number on the global Bejan number at a given wall heat flux (q" = 5000 w/m²). For straight channel, the values of Bejan number are larger than 0.5, which is a reliable result that the entropy generation is dominated by heat transfer irreversibility. It is also noted that in C-shaped channel, the Bejan number is smaller than 0.5 for n exceeds 0.8. This is because the velocity gradients are higher than temperature gradients.

Generally, the fluid friction irreversibility is less prominent, leading to higher Bejan number in straight channel compared to the chaotic geometry.

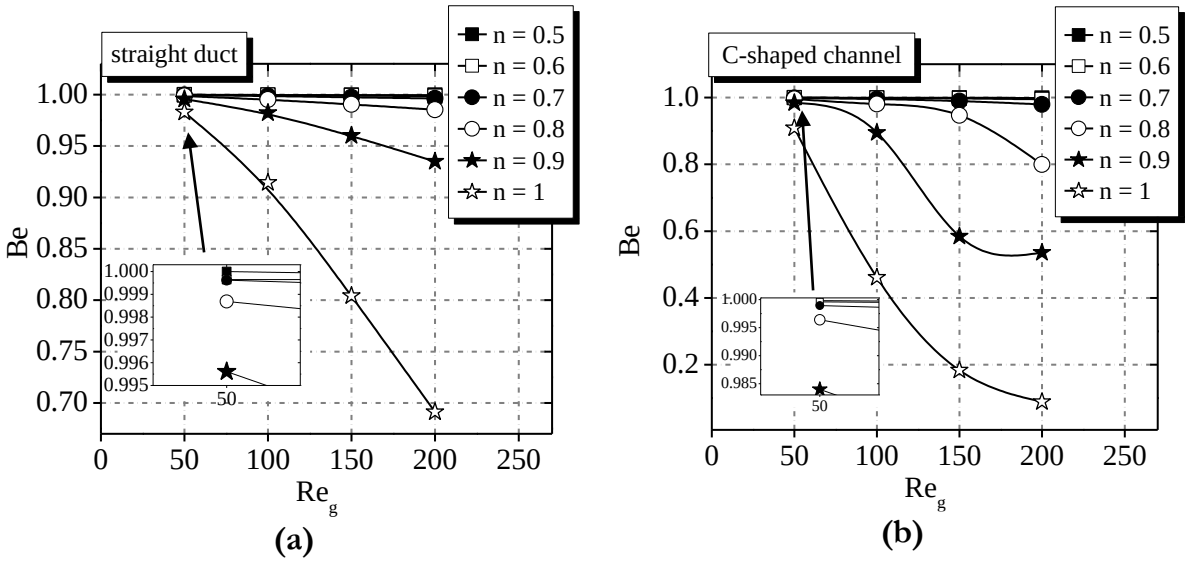

Figure 5.8: Evolutions of Bejan number for (a): straight duct and (b): C-shaped channel, with various values of generalized Reynolds number.

4.4 Effects of wall heat flux on entropy generation at given generalized Reynolds number (Re_g = 100)

4.4.1 Entropy generation due to heat transfer

Figure 4.9 displays the local distributions of the entropy generation due to heat transfer with different value of wall heat flux in straight and the C-shaped channels.

It can be observed that for straight channel, heat entropy generation concentrates at the corners, and for the C-shaped channel, the entropy generation concentrates like a thin layer near the heated wall, and gradually penetrates toward the central of the cross section. However, entropy generation due to heat transfer increases with decreasing of the power law index, because the temperature gradients are greater near the wall especially for the C-shaped channel.

Figure 5.10 shows the evolutions of the heat entropy generation in straight and C-shaped ducts, with various values of wall heat flux.

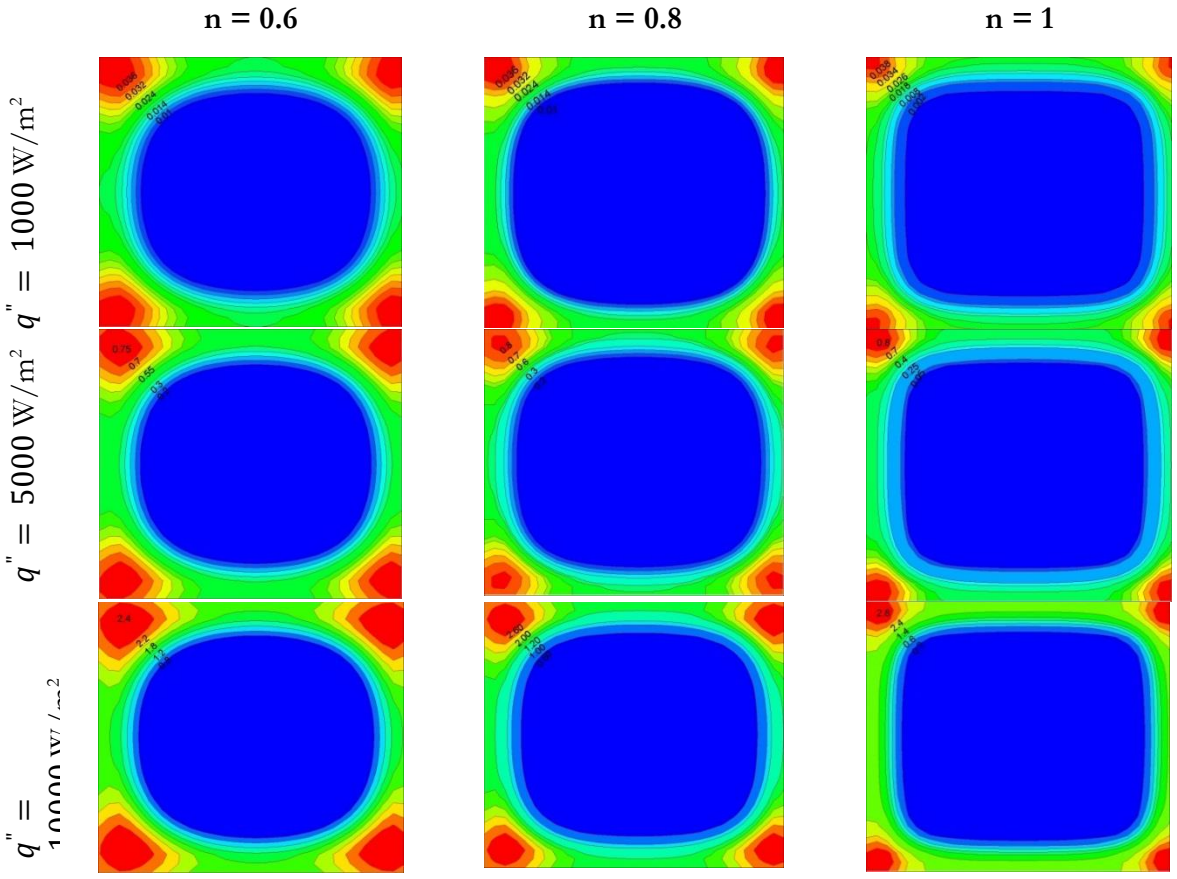

(a)

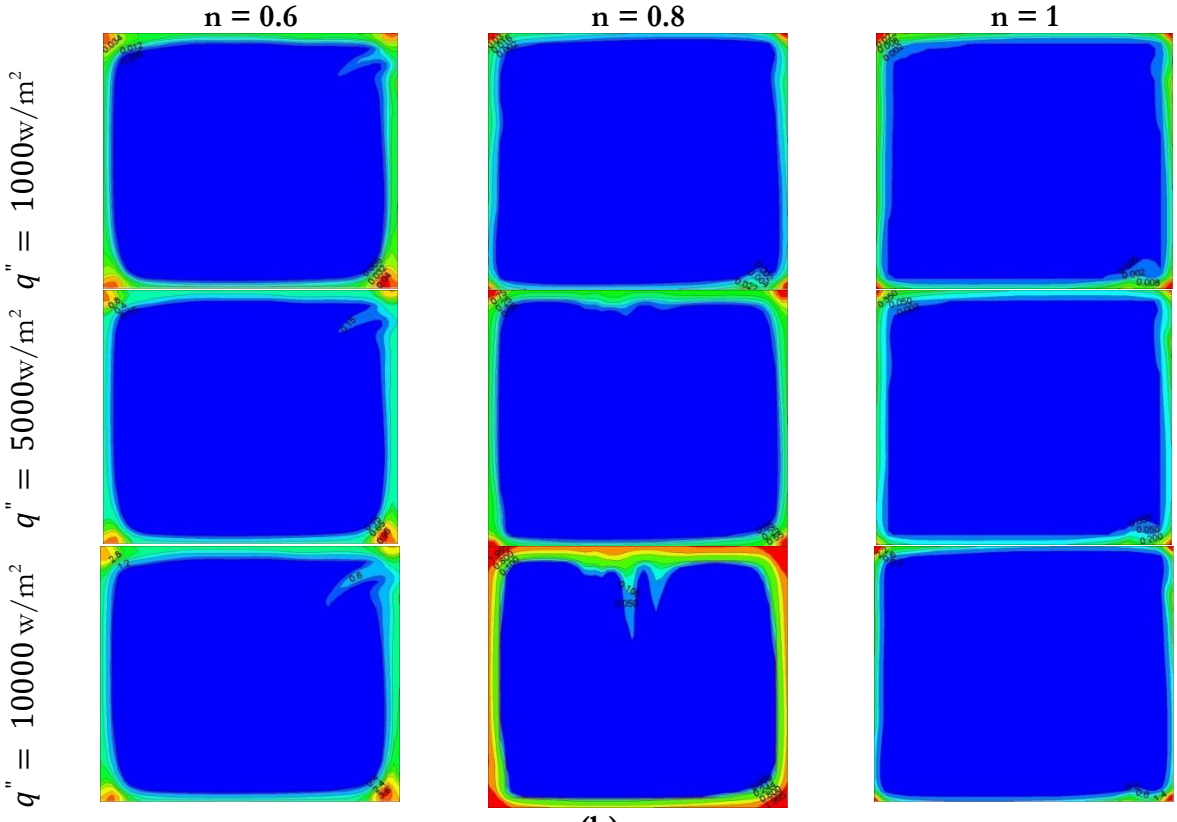

(b)

Figure 4.9: Contours of local entropy generation due to heat transfer on outlet cross section of: (a) straight channel and (b) C-shaped channel for different wall heat flux.

It can be seen, the value of heat entropy generation gradually increases as the wall heat flux increases for both geometries. The values of entropy generation due to heat transfer in C-shaped channel are generally smaller than that obtained for the straight duct, which indicates the trend that the chaotic flow created in the C-shaped channel can enhance the heat transfer and in turn to reduce heat transfer irreversibility.

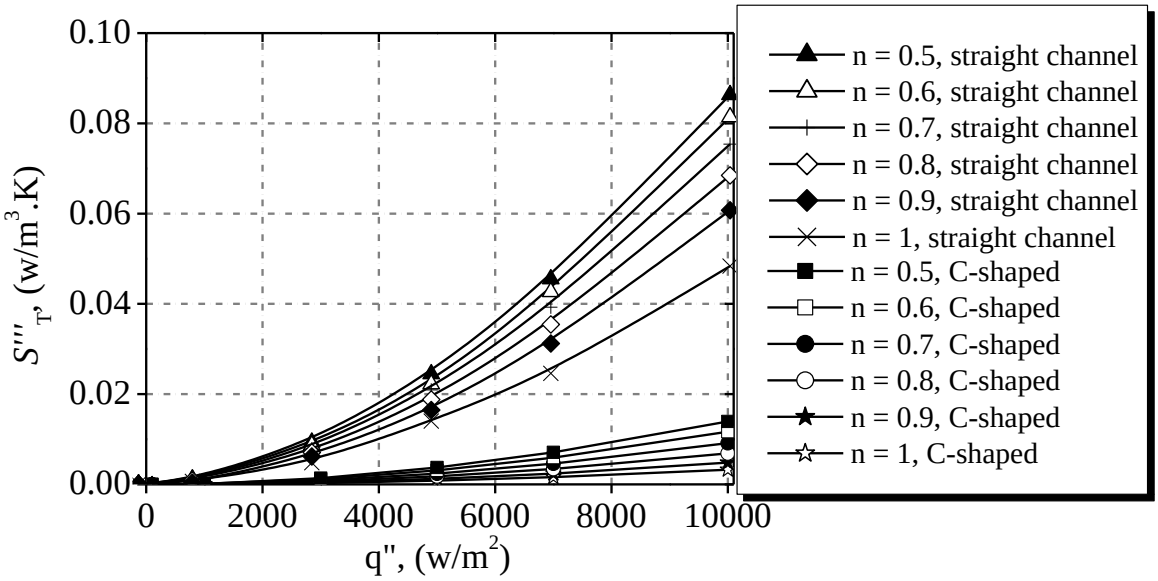

Figure 4.10: Evolutions of the heat entropy generation for (a): straight duct and (b): C-shaped channel, with various values of wall heat flux.

4.4.2 Entropy generation due to fluid friction

Figure 4.11 presents the local distributions of the entropy generation due to fluid friction in straight and C-shaped channels, with different value of wall heat flux and various power-law index. The major entropy generation due to fluid frictional irreversibility is found to concentrate at the wall of straight duct. In C-shaped channel, the values of S_P''' near the bottom wall are relatively smaller than obtained for the other sides.

Figure 4.12 shows the effect of wall heat flux on entropy generation due to fluid friction, for different values of power law index.

The maximum rates of entropy generation due to fluid friction obtained for high power-law index, and it's increases with increasing of power law index. However, the power law index induces stronger influence on the fluid friction irreversibility, which is much dependent to the velocity gradient.

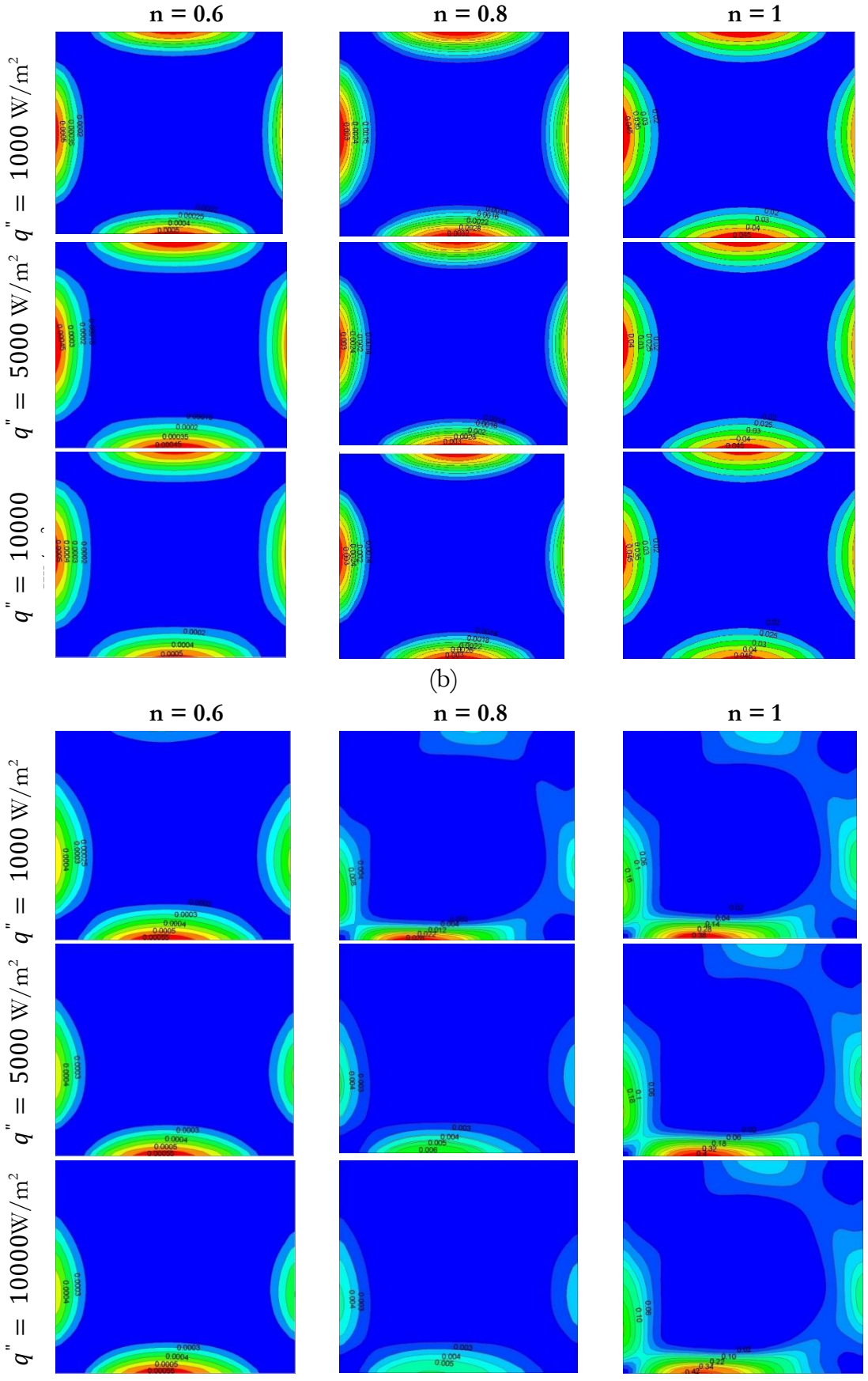

Figure 4.11: Contours of local entropy generation due to fluid friction on outlet cross-section of: (a) straight channel and (b) C-shaped channel for different wall heat flux.

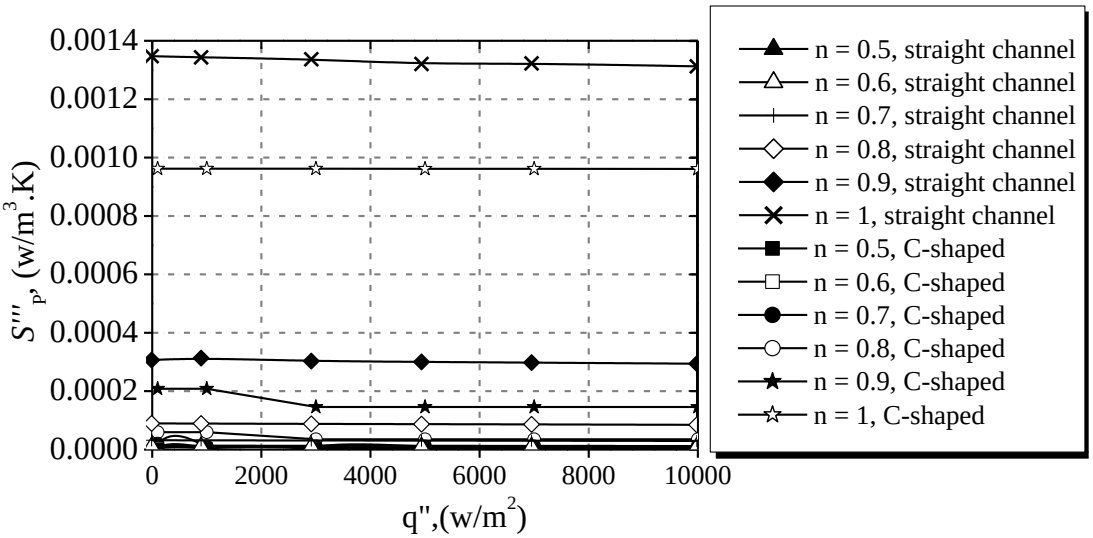

Figure 4.12: Evolutions of the entropy generation rate due to fluid friction for (a): straight duct and (b): C-shaped channel, with various values of wall heat flux.

4.4.3 Global entropy generation

Figure 4.13 shows the global non-dimensional entropy generation $N_S$with different power law index and various values wall heat flux. For high wall heat flux, more than 80% decreases in the global entropy generation rate from straight duct to C-shaped channel. Moreover, global entropy generation decrease with increasing of power law index because the entropy generation due fluid friction has dominated.

Since the heat entropy generation is higher and the entropy generation due to the fluid friction is smaller, the larger non-dimensional entropy generation rates are observed, when the wall heat flux increases for both straight and C-shaped channel. Hence, it explains that the heat transfer performance increase when the power law index rises.

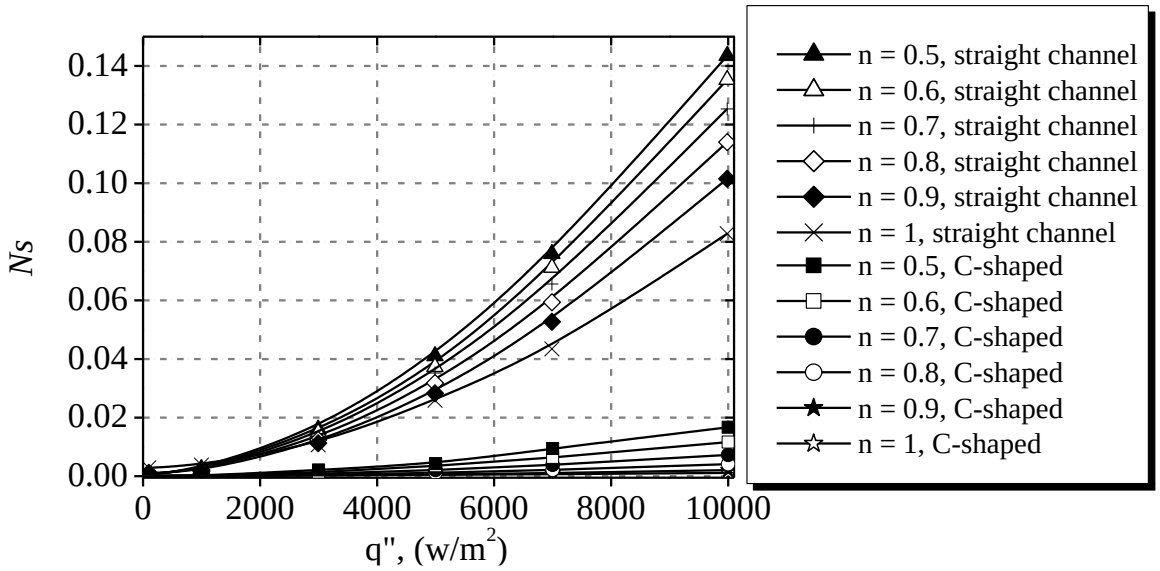

Figure 4.13: Evolutions of the global non-dimensional entropy generation rate due to heat transfer for (a): straight duct and (b): C-shaped channel, with various values of generalized Reynolds number.

4.4.4 Bejan number

Figure 4.14 presents the evolutions of the Bejan number for various values of wall heat flux in straight and the C-shaped channels.
Both straight and C-shaped channels indicate that the Bejan number increases as the wall heat flux augments. No remarkable change on Bejan number for high wall heat flux, that's mean the entropy generation due to heat transfer, has dominated for all cases of power-law index. Consequently, in order to minimize the heat entropy generation, higher power law index with lower external heat flux should be considered.

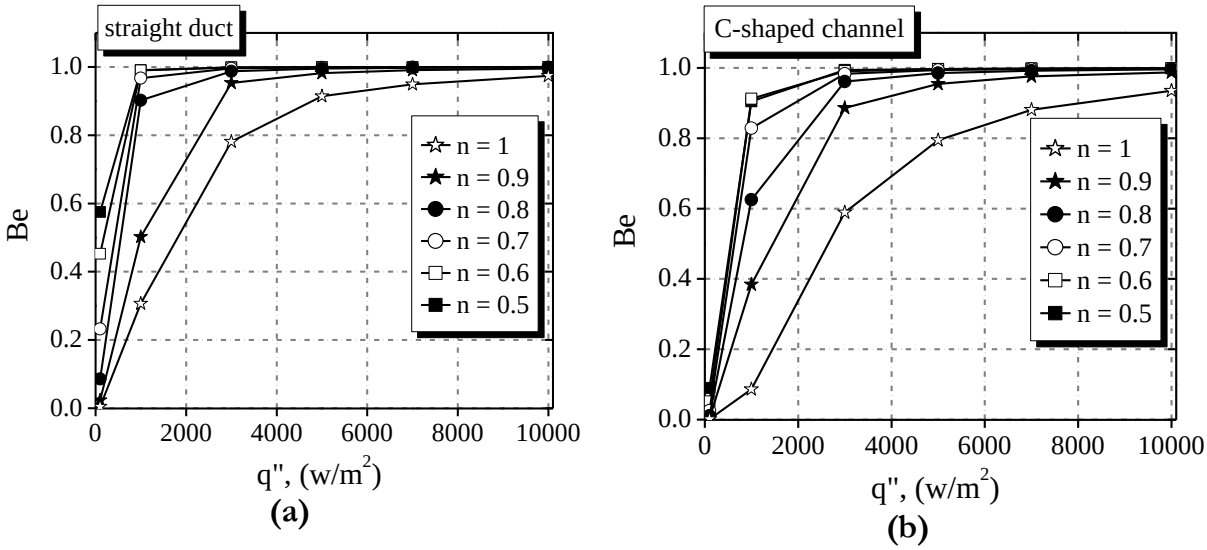

Figure 4.14: Evolutions of the Bejan number for (a): straight duct and (b): C-shaped channel, with various values of wall heat flux.

4.5 Conclusion

In this chapter, numerical study of entropy generation to Newtonian and non-Newtonian fluids flow flowing in straight and chaotic ducts is investigated. This work has been performed for the important parameters in the following ranges: generalized Reynolds number (Re_g = 50 to 200), flow behavior index (n = 0.5 to 1) and wall heat flux (q" = 5000 w/m² to 10000 w/m²). As generalized Reynolds number increases, the entropy generation due to heat transfer decreases, which reveal that the effect of the generalized Reynolds number on heat transfer performance is substantial. These results verify that the C-shaped channel can enhance the heat transfer performance for different values of power law index. Global entropy generation rate in straight duct larger than that obtained for the C-shaped channel, which leads to enhance the heat transfer performances. The increase in the value of generalized Reynolds number causes Bejan number to declines and its increase significantly, as wall heat flux augments which demonstrates a jump in the irreversibility due to heat transfer. For all cases of power-law index, the chaotic flow can effectively enhance the heat transfer performance more than that obtained for the straight duct.

General Conclusion and Perspectives

In this work, numerical simulations were performed using CFD code in order to study the flow characteristics of non-Newtonian power-law fluid in two geometries, C-shaped and straight channels.

First, the kinematic behavior of the fluid flowwas characterized in terms of the vorticity rate, Deformation rate andRotation rate. As known, the enhancement of these parameters in the fluid flow maximizes the mixing performances of the fluid.The results illustrate that the increase of both generalized Reynolds number and power law index increase the considered parameters.

Then, hydrodynamic and thermal performances are characterized by the calculation of the Poiseuille(Po) number and the Nusselt number (Nu). The chaotic configuration displays a heat transfer enhancement in terms of the mean Nusselt number compared to the straight channel, however the pressure drop in this geometry increases (high Poiseuille number) for all examined generalized Reynolds number. Although, the ratio of the Nusselt number to the Poiseuille number (Nu_{mean}/Po_{mean}) is higher in the C-shaped geometry, showing that the compromise between the heat transfer enhancement-diminution of pressure losses is obtained for the C-shaped geometry.

After that, thermal mixing was characterized inboth straight and C-shaped channels by calculate the degree of mixing (D_m) of two fluid with different inlet temperatures and for various values of generalized Reynolds numbers (Re_g = 50-200). Results have shown that the C-shaped geometry has an important efficiencyin term of the mixing than the straight channel due to the existence of the chaotic zones.

Also, we characterized these geometries in terms of thermodynamic performances. We estimate the generated entropy dues to heat and friction irreversibilities. Results showed that the created entropy generations due to the pressure losses are very low and have the same values in both straight and C-shaped channels. However, the created entropy generations due to the heat transfer are negligible in the C-shaped channel compared to that found in the straight channel. This explains that the homogenization of temperature field in C-shaped channel contributes to the diminution of the entropy.
As conclusion, this work confirms that the chaotic geometry presents a highly efficient of thermal mixing system and better performances in thermodynamics, for both Newtonian and non-Newtonian fluids.

As related to the present work, the following suggestions are recommended for future developments:

- Study the problem experimentally.
- Take in consideration various type of fluids (Bingham, dilatant fluids…etc)

References

[1] H. Aref,(1984), "Stirring by chaotic advection", *Journal of Fluid Mechanics, 143- 121.*

[2] H.L. Robin, M. A. Stremler, K. V. Sharp, M. G. Olsen, J. G. Santiago, J. Ronald, A.H. Aref, and D. J. Beebe Member, IEEE,(2000),"Passive Mixing in a Three-Dimensional Ser for horizontal heat ductserpentine Microchannel", *journal of micro electro mechanical systems, 9, 2.*

[3] D. J. Beebe, R. J.Adrian, M. G. Olsen, M. A.Stremler, H. Aref and B. Jo,(2001),"Passive Mixing in Micro-Channels: Fabrication and Flow Experiments", *Mécanique et Industries, 2, 343–348.*

[4] Y. Z Liu, B. J Kim, and H. J Sung, (2004),"Two-Fluid Mixing in a Microchannel", Int. J. Heat and Fluid Flow, 25, 986–995.

[5] Y. Lasbet, B.Auvity, C.Castelain andH.Peerhossaini, (2006),"A chaotic heat-exchanger for PEMFC cooling applications", *Journal of Power Sources, 156, 114–118.*

[6] Y. Lasbet, B. Auvity, C.CastelainandH.Peerhossaini, (2007), "Thermal and Hydrodynamic Performances of ChaoticMini-Channel: Application to the Fuel Cell Cooling", *Heat Transfer Engineering, 28, 8–9, 795–803.*

[7] Y. Lasbet, L. Aidaoui andK.Loubar,(2016) "Effects of the Geometry Scale on the Behaviour of the Local Physical Process of the Velocity Field in the laminar flow",*International journal of heat and technology, 34, March.*

[8] C.Castelain, Y. Lasbet, B.Auvity and H.Peerhossaini,*(2016),* "Experimental study of the thermal performance of chaotic geometries for their use in PEM fuel cells", *International Journal of Thermal Sciences, 101, 181–192.*

[9] J. A. Wheeler and E. H. Wissler,(1966),"The Friction Factor-Reynolds Number Relation for a Steady Flow of Pseudoplastic Fluids through Rectangular Ducts", *Aiche Journal. 11, 07-216.*

[10] B. Gervang and P.S. Larsen, (1991), "Secondary flows in straight ducts of rectangular cross section", *Journal of Non-Newtonian Fluid Mechanics, 39, 217-237.*

[11] S. Park, T. F. Irvine and J.M. Capobianchi, (1994),"Experimental and Numerical Study of Friction Factor for a Modified Power Law Fluid in a Rectangular Duct", *Experimental Thermal and Fluid Science, 9,61-68.*

[12] M. Capobianchi, (2008), "Pressure drop predictions for laminar flows of extended modified power law fluids in rectangular ducts", *International Journal of Heat and Mass Transfer, 51, 1393–1401.*

[13] P. Tazraei, and A. Riasi,(2013), "Numerical Study of Fast Transient Shearthinning Flows Considering Time ConstantVariations of the Carreau Model", *International Journal of Mining, Metallurgy & Mechanical Engineering, 1, 2320–4060.*

[14] A.Riaz, R. Ellahi and S. Nadeem, (2014), "Peristaltic transport of a Carreau fluid in a compliant rectangular duct",*Alexandria Engineering Journal.*

[15] M. Devakar , K. Ramesh, S. Chouhan and A.Raje, (2016), "Fully developed flow of non-Newtonian fluids in a straight uniform square duct through porous medium", *Journal of the Association of Arab Universities for Basic and Applied Science.*

[16] H. Fellouah, C. Castelain, A. Ould El Moctar and H. Peerhossaini, (2006),"A criterion for detection of the onset of Dean instabilityin Newtonian fluids",*European Journal of Mechanics B/Fluids 25, 505–531.*

[17] L. Kuo-Wei andY. Jing-Tang,(2007),"Chaotic mixing of fluids in a planar serpentine channel", *International Journal of Heat and Mass Transfer 50, 1269–1277.*

[18] K. Tae Gon, M. A. Hulsen, P. D. Anderson Jaap M.J. den Toonder and Han E.H. Meijer,(2007) ,"Chaotic advection using passive and externally actuated particles in a serpentine channel flow",*Chemical Engineering Science 62, 6677 – 6686*

[19] G.S. Paulo, C.M. Oishi, M.F. Tomé, M.A. Alves and F.T. Pinho, (2014), "Numerical solution of the FENE-CR model in complex flows", *Journal of Non-Newtonian Fluid Mechanics 204, 50–61.*

[20] Saatdjian, A.J.S. Rodrigo, J.P.B.Mota, (2012), "A studyofmixingbychaoticadvectionintwothree-dimensionalopenflows"*E.Chemical Engineering Science, 81, 179–190.*

[21] S. Nita, J. Bae and A P. Sasmito,(2014),"Numerical investigation of mixing performance in microchannel T-junction with wavy structure",*Computers & Fluids 96 10–19.*

[22] A. Shobha,(1994),"Numerical simulation of dispersion in the flow of power law fluids in curved tubes", *ADDI. Math. Modellina, 18.*

[23] V. Subhashini and K.D.P. Niga,(2008),"Experimental investigation of void fraction and flow patterns in coiled flow inverter", *Chemical Engineering and Processing 47, 1281–129.*

[24] T.A. Pimenta and J.B.L.M. Campos, (2012), "Friction losses of Newtonian and non-Newtonian fluids flowing in laminar regime in a helical coil", *Experimental Thermal and Fluid Science, 36, 194–204.*

[25] C. Castelain and P. Legentilhomme, (2006),"Residence time distribution of a purely viscous non-Newtonian fluid in helically coiled or spatially chaotic flows", *Chemical Engineering Journal, 120, 181–191.*

[26] B. Mohammed, H. Lionel, G.MompeanandL. Thais, (2009), "Numerical study of Dean vortices in developing Newtonian and viscoelastic flows through a curved duct of square cross-section"*C. R. Mecanique 337, 40–47.*

[27] H. Fellouah, C. Castelain, A. Ould-El-Moctar and H. Peerhossaini,*(2010),* "The Dean instability in power-law and Bingham fluids in a curved rectangular duct", *Journal of Non-Newtonian Fluid Mechanics. 165, 163–173.*

[28] N. Ali, M. Sajid, Z. Abbas and T. Javed, (2010),"Non-Newtonian fluid flow induced by peristaltic waves in a curved channel", *European Journal of Mechanics B/Fluids 29, 387-394.*

[29] H. Hossein and H.R. Mohammad,(2011),"Numerical Simulation of Non-Newtonian Pseudo-Plastic Fluid in a Micro-Channel Using the Lattice Boltzmann Method",*World Journal of Mechanics, 1, 231-242.*

[30] O. Mitsuhiro, T. Nakamura, Y. Yoshida and Y.Matsukuma,(2011), "Lattice

Boltzmann simulations of viscoplastic fluid flows through complex flow channels", *Journal of Non-Newtonian Fluid Mech, 166, 404–412.*

[31] T.C. Papanastasiou, (1987), 'Flows of materials with yield", *Journal of Rheology. 31, 385–404.*

[32] C. Ching-Chang, C. Chieh-Li andC. Cha'o-Kuang, (2012),"Electrokinetically-driven non-Newtonian fluid flow in rough microchannel with complex-wavy surface", *Journal of Non-Newtonian Fluid Mechanics 173–174, 13–20.*

[33] A. Arshad andK. Kwang-Yong, (2014), "Flow and mixing analysis of non-NewtonianFluids in straight and serpentine microchannels",*Chemical Engineering Science S0009-2509(14), 00231-0.*

[34] K. Vinit, Amit Dhiman andB. László, (2014),"Laminar flow of non-Newtonian shear-thinning fluids in a T-channel",*Computers &Fluids S0045-7930(14)00460-5.*

[35] R. K. Shah and A. L. London, (1978), "Laminar flow forced convection in ducts",*Ada. Heat Transfer.*

[36] R. K. Shah and M. S. Bhatti, (1987), "Laminar convective heat transfer in ducts. I n "Handbook ofSingle Phase Convective Heat Transfer", *Wiley, 3-1 (Interscience), New York.*

[37] M. S. Bhatti and R. K. Shah, (1987), "Turbulent and transition flow convective heat transfer in ducts."Handbook of Single Phase Convective Heat Transfer", *4-1. Wiley (Interscience), New York.*

[38] S. Shin, Young Cho, William K. Gringrichp and WelShyy, (1993), "Numerical study of laminar heat transfer withtemperature dependent fluid viscosity in a 2:lrectangular duct", *International Journal of Heat Mass Transfer 36, 18, 43654373.*

[39] A. Barletta, (1998), "Laminar mixed convection with viscous dissipation in a vertical channel", *International Journal of Heat and Mass Transfer 30, 0887, 2490-2402.*

[40] A. Barletta, (2001) "analysis of flow reversel for laminar mixed convection in a vertical rectangular duct with one or more isothermal walls", *International journal of heat mass transfer 44, 3481-3497.*

[41] A. Barletta, (2002) "Fully developed mixed convection and flow reversal in a vertical rectangular duct with uniform wall heat flux", *International journal of heat mass transfer 45, 641-654.*

[42] A. Barletta, (1999),"On the choice of the reference temperature for fully-developed mixed convection in a vertical channel", *International Journal of Heat and Mass Transfer 42, 3169-3181.*

[43] Y. S. Muzychka and M. M. Yovanovich, (2004), "Laminar Forced Convection Heat Transfer in the Combined Entry Region of Non-Circular Ducts", *Transactions of the ASME Vol. 126.*

[44] M.M.Shahmardan, M.Norouzi ,M.H.Kayhani and A.A.Delouei (2012), "An exact analytical solution for convective heat transfer in rectangular ducts", *Univ-Sci A (ApplPhys and Eng), 13, 768-78.*

[45] L.A. Sphaier and A. Barletta, (2014),"Unstable mixed convection in a

heatedhorizontal porous channel", *International Journal of Thermal Sciences 78, 77-89.*

[46] S. Seppo, (1995),"Finite-element analysis of fully developed laminar flow of power-law non-Newtonian fluid in a rectangular duct", *International Communicationsin heat mass transfer, 22, 4, 549-557.*

[47] S. Ray and D. Misra,(2010), "Laminar fully developed flow through square and equilateral triangular ducts with rounded corners subjected to H1 and H2 boundary conditions", *International Journal of Thermal Sciences, 49, 1763-1775.*

[48] P. James. Hartnett and M.Kostic, (1989), "Heat Transfer toNewtonian and Non-Newtonian Fluidsin Rectangular Ducts", *Advances in heattransfer, 19.*

[49] M.E. Sayed-Ahmed,(2000),"Laminar heat transfer for thermally developing flow of a Herschel–Bulkley fluid in a square duct", *International Communication Heat Transfer, 27, 7, 1013–1024.*

[50] M.E. Sayed-Ahmed andKarem M. Kishk, (2008),"Heat transfer for Herschel–Bulkley fluids in the entrance region of a rectangular duct", *International Communications in Heat and Mass Transfer, 35, 1007–1016.*

[51] H.Zhenbin, F. Xiaoming, Z. Zhengguo and G. Xuenon, (2016),"Numerical investigation on performance comparison of non-Newtonian fluid flow in vertical heat exchangers combined helical baffle with elliptic and circular tubes", *Applied Thermal Engineering,100, 84–97.*

[52] R. Gharraei, A. Vejdani, S. Baheri and A.A. D. Davani , (2016),"Numerical investigation on the fluid flow and heat transfer of non-Newtonian multiple impinging jets", *International Journal of Thermal Sciences, 104, 257-265.*

[53] Vimal Kumar and K.D.P. Nigam,(2007), "Laminar convective heat transfer in chaotic configuration", *International Journal of Heat and Mass Transfer, 50, 2469–2479.*

[54] S. Jung-Yang, H. Chih-Hsiang and C. Shih-Hao,(2012),"Heat transfer characteristics of a helical heat exchanger", *Applied Thermal Engineering; 39, 114–20.*

[55] C.Habchi, J.L. Harion, S.Russeil, D.Bougeard, F.Hachem andA.Elmarakbi, (2013),"Chaotic mixing by longitudinal vorticity,*Chemical Engineering Science, S0009-2509(13)00651-9.*

[56] Z.Zhanying, F. F. David andB. S. Haynes, (2013), "Chaotic advection in steady laminar heat transfer simulations: Periodic zigzag channels with square cross-sections",*International Journal of Heat and Mass Transfer 57, 274–284.*

[57] A. Tohidi , S.M. Hosseinalipour, M. Shokrpour and A.S. Mujumdar, (2015),"Heat transfer enhancement utilizing chaotic advection in coiled tube heat exchangers" *Applied Thermal Engineering, 5, 185-195.*

[58] S. Tian andM.Barigou, (2016),"Using chaotic advection to enhance the continuous heat-hold-cool sterilisation process", *Innovative Food Science and Emerging Technologies 34, 352–366.*

[59] M.Eesa, and M. Barigou, (2008),"CFD analysis of viscous non-Newtonian flow under the influence of a superimposed rotational vibration",*Computers and Fluids, 37, 24–34.*

[60] Lester, D.R., M. Rudman and G. Metcalfe, (2009), "Low Reynolds number scalar transport enhancement in viscous and non-Newtonian fluids", *International Journal of Heat and Mass Transfer, 52, 655-664.*

[61] E. O. Kamal, and Y.L.Guer, (2010), "Thermal chaotic mixing of power-law fluids in a mixer Withalternately rotating walls", *Journal of Non-Newtonian Fluid Mechanics, , 165, 641-651.*

[62] L,Ping , D. Zhang andX. Gongnan,(2016),"Flow structure and heat transfer of non-Newtonian fluids in microchannel heat sinks with dimples and protrusions", *Applied Thermal Engineering, 94, 50–58.*

[63] M. A.Waleed, D. W. Richard, J.C.D David andJ.P. Robert, (2016),"Experimental investigation of the impact of elastic turbulence on heat transfer in a serpentine channel", *Journal of Non-Newtonian Fluid Mechanics, 231, 68–78.*

[64] A. Bejan, (1982), "Entropy Generation Through Heat and Fluid Flow", *Wiley,New York.*

[65] B.S. Yilbas, S.Z. Shuja and M.O. Budair, (1999), "Second law analysis of a swirling flow in a circular duct with restriction", *International Journal of Heat and Mass Transfer, 42, 4027-404.*

[66] V.Zimparov, (2000), "Extended performance evaluationcriteriaforenhancedheat transfer surfaces: heattransferthroughductswithconstantwalltemperature. *International Journal of Heat Mass Transfer, 43, 3137–55.*

[67] H. Abbassi, M. Magherbi and A.B. Brahim, (2003), "Entropy generation in Poiseuille–Benard channel flow", *International Journal of Thermal Science, 42, 1081–8.*

[68] M. Nourollahi, M. Farhadi and K. Sedighi, (2010), "Numerical study of mixed convection andentropy generation in the Poiseulle–Benard channel in different angles"*International Journal of Thermal Science,* 14, 329–40.

[69] C.K. Chen, H.Y. Lai and C.C. Liu, (2011),"Numerical analysis of entropy generation in mixedconvection flow with viscous dissipation effects in vertical channel, *International Communication of Heat Mass Transfer, 38, 285–290.*

[70] C.K.Chen ,B.S. Chen andC.C. Liu, (2014),"Heat transfer and entropy generation in fully-developed mixed convection nanofluid flow in vertical channel", *International Journal of Heat and Mass Transfer, 79, 750–758.*

[71] G. Yang and J.Y. Wu, (2015),"Entropy generation in a rectangular channel of buoyancy opposed mixed convection", *International Journal of Heat and Mass Transfer, 86, 809–819.*

[72] C.K. Chen, B.S. Chen, C.C. Liu, (2015), "Entropy generation in mixed convection magneto hydrodynamicnanofluid flow in vertical channel", *International Journal of Heat and Mass Transfer, 91, 1026–1033.*

[73] S. Mahmud and R.A. Fraser, (2002), "Inherent irreversibility of channel and pipe flows for non-Newtonian fluids", *International Communications in Heat and Mass Transfer, 29, 577–587.*

[74] N. Luna, F. Mendez and C. Trevino, (2002), "Conjugated heat transfer in circular ducts with apower law laminar convection fluid flow", *International Journal of Heat*

Mass Transfer, 45, 655-66.

[75] B. S. Yilbas and M. Pakdemirli, (2005), "Entropy Generation Due to the Flowof a Non-Newtonian Fluid withVariable Viscosity in a Circular Pipe", *Heat Transfer Engineering, 26, 80–86.*

[76] S. Mahmud and R.A. Fraser, (2006), "Second law analysis of forced convection in a circular duct for non-Newtonian fluids", *Energy, 31, 2226–2244.*

[77] A. Sunarso, T. Yamamoto and N. Mori, (2007), "Numerical analysis of wall slip effects onflow of Newtonian and non-Newtonian fluids in macro and micro contractionchannels", *ASME Journal of Fluid Eng, 129, 23–30.*

[78] M. Barkhordari andS.Gh. Etemad, (2007), "Numerical study of slip flow heat transfer ofnon-Newtonian fluids in circular microchannels",*International journal of Heat Fluid Flow, 28, 1027–1033.*

[79] S. Saouli and S. Aiboud-Saouli, (2007), "Entropy generation in channel flow for non-Newtonian fluids with viscous dissipation effect", *Research journal of Applied Science, 2, 8, 900, 907.*

[80] Y.M. Hung, (2008), "Viscous dissipation effect on entropy generation for non-Newtonian fluids in microchannels", *International Communications in Heat and Mass Transfer, 35, 1125–1129.*

[81] H.Ragueb and K. Mansouri, (2013), "A numerical study of viscous dissipation effect on non-Newtonian fluid flow inside elliptical duct", *Energy Convers Manag 2013, 68, 124-32.*

[82] C.H. Chen, Y.L. Hwang and S.J. Hwang, (2013), "Non-Newtonian fluid flow and heat transferin microchannels", *Appl. Mech. Mater, 462, 275–277.*

[83] A. Vishal, (2014), "Slip law effects on heat transfer and entropy generation of pressure driven flow of a power law fluid in a microchannel under uniform heat flux boundary condition", *Energy, 76, 716-732.*

[84] A.Z. Sahin, (1998), "Irreversibilities in various duct geometries with constant wall heat flux and laminar flow", *Energy, 23, 6, 465–473.*

[85] A.Z. Sahin, (1996), "Thermodynamics of laminar viscous flow through a duct subjected to constant heat flux", *Energy, 21, 12, 1179–1187.*

[86] M. Shohel and A.K.M. Sadrul Islam, (2003) "Laminar free convection and entropy generation inside an inclined wavy enclosure", *International Journal of Thermal Sciences, 42, 1003–1012.*

[87] T.H. Ko and K. Ting, (2006), "Entropy generation and optimal analysis for laminar forced convection in curved rectangular ducts: a numerical study", *International Journal of Thermal Sciences, 45, 2, 138–150.*

[88] T.H. Ko and K. Ting, (2006) "Optimal Reynolds number for the fully developed laminar forced convection in a helical coiled tube", *Energy, 31, 12, 1806–1816.*

[89] T.H. Ko, (2006), "Numerical analysis of entropy generation and optimal Reynolds numberfor developing laminar forced convection in double-sine ducts with various aspectratios", *International Journal of Mass and Heat Transfer, 49, 3-4, 718–*

726.

[90] V.Zimparov,A.K. Silva, A. Bejan, (2006), "Thermodynamicoptimizationoftree-shaped flow geometries". *International Journal of Heat Mass Transfer, 49, 1619–30.*

[91] Y. Yonghua, F. Aiwu, L. Yuming, hiping Jin , E. Liu and F. Dai, (2015), "Entropy generation analysis for laminar thermal augmentation with conical strip inserts in horizontal circular tubes", *International Journal of Thermal Sciences, 88, 201-214.*

[92] A.A. Mohammad, S. Hamid, A.B. Hasan and Mohsen Khoshzat (2015), "Investigation of entropy generation in a helically coiled tube in flow boiling condition under a constant heat flux", *international journal of refrigeration 60, 217–233*

[93] C.K. Jundika, A. P. Sasmito, T. Shamim and A. S. Mujumdar, (2016),"Numerical investigation of heat transfer and entropy generation of laminar flow in helical tubes with various cross sections", *Applied Thermal Engineering ,102, 849–860.*

[94] G. Jiangfeng, X. Mingtian, T. Yujia and H. Xiulan,(2012), "The effect of temperature-dependent viscosity on entropy generation in curved square microchannel", *Chemical Engineering and Processing, 52, 85– 91.*

[95] H. Hou-Cheng, L. Zheng-Hua and A. Usmani, (1999), "Finite Element Analysisof Non-Newtonian Flow", *Theory and Software, 13, 978-1-4471-1204-4.*

[96] R.B Bird, R.C. Armstrong andO. Hassager, (1987),"Dynamics of Polymeric Liquids", *1, Wiley, New York.*

[97] W. H. Suckow, E Hrycak, and R. G. Griskey, (1980), "Heat Transfer to Non-Newtonian Dilatant (Shear-Thickening) Fluids Flowing Between Parallel Plates",*AIChE, 199,76, 257.*

[98] W.Kozicki, C. H.Chou andC. Tiu, (1966),"Non-Newtonian Flow in Ducts of Arbitrary Cross-Sectional Shape", *Chem. Engrg. Sci. 21, 665.*

[99] A. B. Metzner and J. C. Reed,(1955), "Flow of Non-Newtonian Fluids - Correlation of the Laminar Transition, and Turbulent-Flow Regions", *AIChE Journal, 1, 434.*

[100] B.Galanti, J. D.Gibbonyzk, M.Heritagez, (1997), "Vorticity alignment results for the three-dimensional Euler and Navier–Stokes equations," *Nonlinearity, 10, 1675–1694.*

[101] Khakhar, D. V., Ottino, J. M., (1986), "Deformation and breakup of slender drops in linear flows," *Journal of Fluid Mech, 166, 265–285.*

[102] R. M. Cotta, (1986), "Laminar forced convection to non-Newtonian fluids in ducts with prescribed wall heat flux", *International communication, heat mass transfer, 13, 325-334.*

Abstract

In this work, a numerical study is carried out by using CFD code (Fluent) to investigate a steady laminar flow of non-Newtonian power-law fluids in two geometries: complex geometry, called C-shaped, and straight channel. The chaotic flows created in the C-shape geometry enhance considerably the performances in terms of heat transfer and pressure losses. These performances are reported for a given geometry as function of both the generalized Reynolds number ranging from Reg=50 to 200 and power-law index n varying from 0.5 to1.

In the straight channel, the flow is a fully developing and the regime is laminar and steady. The obtained Nusselt and Poiseuille values are compared to those reported in the literature. The comparison reveals a good concordance with the theoretical results where the maximum difference is less than 0.5%.

The chaotic geometry (C-shaped) accentuate highly the heat transfer rate where the mean Nusselt number, Nu, is great at least 10 times than that obtained in the straight channel for all generalized Reynolds and power-law index values. Thereby, the chaotic geometry exhibited very important pressure losses in the flow. Consequently, the mean Poiseuille number is at least two times greater than that given by the numerical results. So, the augmentation of the pressure losses rate is negligible compared to the increase of the heat transfer rate and the better compromise (improving heat transfer - diminution pressure drops) is for the C-shaped channel.

The thermal mixing between two fluids (hot and cold) in the two considered geometries is performed where the inlet cross section for each geometry is divided in two parts (horizontally and vertically).In one part, we injected the hot fluid and in the other part we injected the cold fluid. Thermal performances are characterized by the calculation of the mixing degree. The C-shaped configuration displayed thermal mixing rate enhancement of 80-90% relative to the mixing rate in the straight channel. These geometries are characterized in terms of entropy generation in the flow which dues to thermal and hydrodynamic process. For a given wall heat flux equal to 5000W.m^{-2}, the thermal dimensional entropy generation decreases with the increase of both generalized Reynolds number and flow behavior index (n). While, the dimensional entropy generation due to the friction increases with the increase of both generalized Reynolds number and flow behavior index (n).In interesting parameter used in this study is the ratio between the total dimensional entropy generation to the heat transfer rate exchanged between the wall and the fluid N_S. The N_S coefficient presents the compromise between the entropy generation and the heat transfer rate. This parameter decreases with both generalized Reynolds and flow behavior index (n) for a non-Newtonian. For n=1, the N_S presents an increasing curve with generalized Reynolds number. As consequence, in this geometry, the heat transfer rate is more important than the entropy generation rate in the case of the non-Newtonian fluid.

Keywords: Chaotic advection, Non-Newtonian fluid, Poiseuille number, Nusselt number, Mixing degree, Entropy generation.

ملخص

في هذا العمل،تمتمحاكاةرقمية للتدفق المستمر للسوائل النيوتونية والغير النيوتونية داخل شكلين مختلفين (قناة على شكل Cوقناة مستقيمة)باستخدامبرنامجCFD .الهندسة على شكل Cهي قناة مصغرة ثلاثية الأبعاد ذات مقطع عرضي مربع. التدفقات الفوضوية التي تم إنشاؤها في هذه الهندسة تعززالتدفق ونقل الحرارة إلى حد كبير حيث تمت دراستها تحت عدّة ارقام رينولدزالمعمم ومختلف قيم من معامل السوائل الغير نيوتونية.

في البداية، تمت مقارنة النتائج الاولى لخصائص التدفق والتحول الحراري داخل قناة مستقيمة تحت تأثير حرارة ثابتة، بالكاد تختلف القيمالنظريةوالرقمية المتحصل عليها كأعداد نوسلت وبوازي حيث الفرق الاقصى اقل من 5،0 %.

استخدمت دراسة عددية ثانية بنفس خصائص السوائل داخل القناة المعقدة،حيث أظهر ت النتائج ان التحول الحراريي زداد بعشر مرات داخل هذه القناة مقارنة مع القناة المستقيم لكل ارقام رينولدس المعمم و معامل سلوك السائل. وبالتالي، فإن عدد بوازوي هوعلى الأقل أكبر بمرتين من ذلك الذي قدمته النتائج العددية. لذا،فإن زيادة معدل خسائر الضغط لايكاد يذكر بالمقارنة معزيادة معدل انتقال الحرارة في قناة شكلC (تحسين نقل الحرارة- انقاص خسائر الضغط).

خلال الجزء الثانيللدراسة، تمت دراسة محاكاة الاختلاط الحراري لسائلين مختلفي درجةالحرارة داخل القناة المستقيمة و قناة شكل ، حيث تم تقييم خصائص التحول الحراري بحساب معامل الاختلاط الحراري. اظهرت النتائج ان معامل الاختلاط يزداد بتزايد رينولدس المعمم، كشفت التحقيقات الرقمية ان قناة شكل Cتعزز الخلط الحراري بنسبة 90% مقارنة بالقناة المستقيمة.

اجرت الدراسة الرقمية الأخيرة لتحديد قيمة الاونتروبي لكل من السوائل النيوتونية والغير النيوتونية داخل القناة المستقيمة و التي على شكل C . حيثت متدراسة تأثير عدد رينولدس المعمم ومعامل سلوك السائل على قيمة اونروبي الكلية الناجم عن الاحتكاك ونقل الحرارة، حيث أشارت النتائج إلى أن زيادة رينولدس المعمم ومعامل سلوك السائل يؤدي الى انخفاض في توليد قيمة اونتروبي الناجمة عن نقل الحرارة داخل السوائل الغير نيوتونية، في حين أنه يؤدي الى ازدياد قيمة اونتروبي الناجمة عن احتكاك السائل، في الاخير نجد أن معامل سلوك السائل له اثار عكسية على قيمة الانتروبي الناجمة عن الاحتكاك مقارنة بالتي تنتج عن النقل الحرارة. معامل اخرمثير للاهتمام(Ns)والذي يجمع مابين قيمة التحول الحراري وقيمة الاونتروبي .هذا المعامل ينخفض بتزايد عدد رينولدس المعمم ومعامل سلوك السائل الغير نيوتونية و يزداد مناجل السوائل النيوتونية، بالتالي، فإن معدل نقل الحرارة له أهمية أكثر من معدل توليد قيمة الاونتروبي في حالة السوائل غيرالنيوتونية.

الكلمات المفتاحية: التأفق الفوضوي،السوائل الغير نيوتونية، رقم بوازي، رقم نوسلت، معامل الاختلاط، قيمة الاونتروبي.

Résumé

Dans le présent travail, une étude numérique a été réalisée, en utilisant le code CFD, pour enquêter sur l'écoulement laminaire des fluides non-Newtonien à travers deux géométries : géométrie complexe, appelée géométrie en forme de C, et canal droit. Les flux chaotiques créés dans la géométrie en forme de C à améliorer considérablement le champ hydrodynamique, le transfert de chaleur et la performance thermodynamique. Ces performances sont rapportées pour une géométrie donnéeen fonction du nombre de Reynolds généralisée (Re_g = 50-200) et l'indice de loi de puissance(n = 0,5-1).

Dans le canal droit, l'écoulement est laminaire entièrement établi. Les valeurs de Poiseuille et Nusselt obtenus sont comparés à ceux rapportés dans la littérature. La comparaison révèle une bonne concordance avec les résultats théoriques où l'écart maximal est inférieur à 0,5 %.

La géométrie chaotique accentue fortement le transfert de chaleur où la moyenne nombre de Nusselt, Nu, est grande au moins 10 fois plus que celle obtenue dans le canal droit pour tous les nombres de Reynolds généralisés et les valeurs de l'indice de la loi de puissance. Ainsi, la géométrie chaotique montrentdes pertes de pression très importantes dans l'écoulement. Ainsi, l'augmentation du taux de pertes de charges est négligeable par rapport à l'augmentation du taux de transfert de chaleur et la meilleure solution reste le canal en forme de C, en ce qui concerne l'amélioration du transfert de chaleur et la diminution de perte de charge.

Le mélange thermique entre les deux fluides (chaud et froid) dans les deux géométries considérées a été exécuté selon deux types d'injection (horizontale et verticale). Les performances thermiques sont caractérisées par le calcul du degré du mélange. Il est observé que le mélange thermique dans la géométrie en forme de C affiche une amélioration de 80 à 90 % par rapport à celui affiché dans le canal droit. Ces géométries sont caractérisées en termes de génération d'entropie qui sont dues aux irréversibilités thermiques et hydrodynamiques.Pour un flux de chaleur imposé égale à 5000W.m^{-2}, la génération d'entropie thermique diminue avec l'augmentation du nombre de Reynolds généralisé et l'indice d'écoulement (n). Alors, que la génération d'entropie due à la friction des fluides augmente avec l'augmentation du nombre de Reynolds généralisé et l'indice d'écoulement (n). Ce qui ressort de l'étude est que le paramètre Ns utilisé est le rapport entre la génération d'entropie globale due au transfert de chaleur échangée entre le mur et le fluide.Ce paramètre Ns diminue en fonction de l'indice d'écoulement (n) et le nombre de Reynolds généralisépour lesfluides non-Newtoniens. Pour n =1, le NS présente une courbe croissante avec la généralisation de nombre de Reynolds. En conséquence, dans cette géométrie, le taux de transfert de chaleur est plus important que le taux de génération d'entropie dans le cas du fluide non newtonien.

Mots-clés : advection chaotique, fluide non-Newtonien, nombre de Poiseuille, nombre de Nusselt, degré de mélange, génération d'entropie.

IJHT INTERNATIONAL JOURNAL OF HEAT AND TECHNOLOGY

ISSN: 0392-8764
Vol. 34, No. 2, June 2016, pp.
DOI: 10.18280/ijht.340214

A publication of IIETA

IIETA International Information and Engineering Technology Association

http://www.iieta.org/Journals/IJHT

CHARACTERIZATION OF PRESSURE DROPS AND HEAT TRANSFER OF NON-NEWTONIAN POWER-LAW FLUID FLOW FLOWING IN CHAOTIC GEOMETRY

Toufik Tayeb Naas [1*], Yahia Lasbet [1], Ahmed Benzaoui [2], Khaled Loubar[3]

[1*] Laboratoire de Développement en Mécanique et Matériaux (LDMM), Université de Djelfa 17000, Algeria
[2] Laboratoire Thermodynamique et Systèmes Energétiques (LTSE), Université de Houari Boumedien, Algeria
[3] Ecole des Mines de Nantes. 44307 Nantes Cedex 3, France
Email: toufiknaas@gmail.com

ABSTRACT

In this work, a numerical study is carried out by using CFD code to investigate a steady laminar flow of non-Newtonian power-law fluids in two geometries: complex geometry, called C-shaped, and straight channel. C-shaped geometry is a three-dimensional mini-channel of square cross-section. The chaotic flows created in this geometry enhance considerably the flow and the heat transfer performances. These performances are reported for a fixed geometry over a range of generalized Reynolds number (Re_g=50-200) and power law index (n = 0.5-1). The higher heat transfer performance is provided by the C-shaped geometry and the lower pressure drops are obtained for the straight channel. However, the better compromise (improving heat transfer - diminution pressure drops) is for the C-shaped channel. This is evaluated via the calculation of the ratio between the Nusselt number and the Poiseuille number Nu/Po.

Keywords: Non-Newtonian power-law fluid; laminar flow; Poiseuille number; Nusselt number; chaotic advection

1. INTRODUCTION

Enhancement of the heat transfer of non-Newtonian fluids flowing in ducts is required in many practical engineering domains [1] [2]. To achieve this goal, researchers focused on two types of geometries, curved and chaotic channels. Since the work realized by Dean [3] and [4] where he initiated theoretical studies of viscous flow, the curved pipes are widely studied numerically and experimentally. The Dean vortexes formed in these ducts have a significant effect on the pressure loss and heat transfer of non-Newtonian fluids flow [5-8]. The second alternative method is to create chaotic trajectories [9] while keeping the laminar flow that ensures the efficient stretching and folding of material lines. This type of flows is more efficient and provides better performance in terms of heat transfer [10] [11]. Kamal et al. [10] investigate numerically the enhancement of both mixing and heat transfer in a two-rod mixer for highly viscous non-Newtonian fluids. The mixer was composed of two vertical circular rods in a cylindrical tank. Chaotic flows were obtained by imposing the temporal modulations of the rotational velocities of the walls. Three different stirring protocols were chosen: non-modulated, continuous and alternating (non-continuous). The last two protocols were able to give chaotic flow trajectories. The authors confirmed that chaotic mixing is suitable for shear thickening fluids for which it is observed a clear enhancement of the thermal mixing (heat extraction and homogenization). This is due to the increase in the apparent fluid viscosity close to the rotating walls. Lester [11] quantifies asymptotic scalar transport (temperature or concentration) by the application of a novel spectral method within both Newtonian and non-Newtonian fluids over the control parameter space of a chaotic flow, the Rotated Arc Mixer (RAM). The non-Newtonian fluid under consideration is a yield stress shear thinning fluid, which is traditional problematic traditional problematic for transport enhancement due to the existence of plug flow regions.

Our contribution in this paper is to outline and analyze the thermal and hydrodynamic behavior of power law non-Newtonian fluid in complex geometry, called in this paper C-shaped geometry, in comparison to the straight channel. The C-shaped geometry is proposed in the first time by Beeb et al [12]. By the calculation of the Poincare section, Robin et al [13] showed the existence of chaotic trajectories within this geometry. In addition, Lasbet et al [14] characterized this geometry as a new design for the PEM fuel cell cooling system where the fluid is Newtonian (water). Their heat performance is considerably improved compared to that when the flow is regular (straight channel).

Different non-dimensional parameters are used to estimate flow and heat characteristic: Poiseuille number, Nusselt mber and the ratio Nu/Re as function of generalized ynolds number for large range of the power law index (n = 5-1). The ratio Nu/Po characterizes the compromise tween the improvement of the heat transfer and the minution of pressure losses.

MODEL AND NUMERICAL SOLUTION

1 Governing equations

Figure 1 presents the basic elements of the two considered ometries called period(C-shaped and the straight channels). The channel cross-section is square (1.5 cm × 1.5 cm). ie hydraulic diameter D_h is 1.5 cm. The unfolded length of ie period C-shaped geometry is equal to 13.5 cm.

The mass conservation, Navier–Stokes and energy uations, which given by equations (1), (2) and (3) spectively, are numerically solved by using the commercial FD code Fluent©. In this study, the fluid is considered as compressible, non-Newtonian power-law while the flow gime is steady and laminar:

$$div\vec{V}=0 \tag{1}$$

here $\vec{V}$ is the velocity vector.

$$\vec{V}.\vec{\nabla}\vec{V}=-\frac{1}{\rho}\vec{\nabla}P+div\tau \tag{2}$$

Where τ (Pa) is shear stress and P is the pressure.

$$\rho c\vec{V}.\vec{\nabla}T=\lambda\Delta T \tag{3}$$

Where ρ, λ and T are the density, the conductivity and the temperature of the fluid, respectevley.

The constitutive relation between the shear stress τ (Pa) and the shear rate $\dot{\gamma}$ (s^{-1}) can be described by a simple power law expression:

$$\tau=k\dot{\gamma}^{n} \tag{4}$$

Where, k ($Pa.s^{-1}$) is power-law consistency index and n is the power-law index.

The apparent viscosity of the work fluid is given by:

$$\mu=k\dot{\gamma}^{n-1} \tag{5}$$

The applied boundary conditions are:

- at the inlet section, uniform velocity profile equal to the mean velocity.
- at solid walls, no–slip conditions and a uniform wall heat surface flux.
- at the outlet section, the pressure outlet condition is considered.

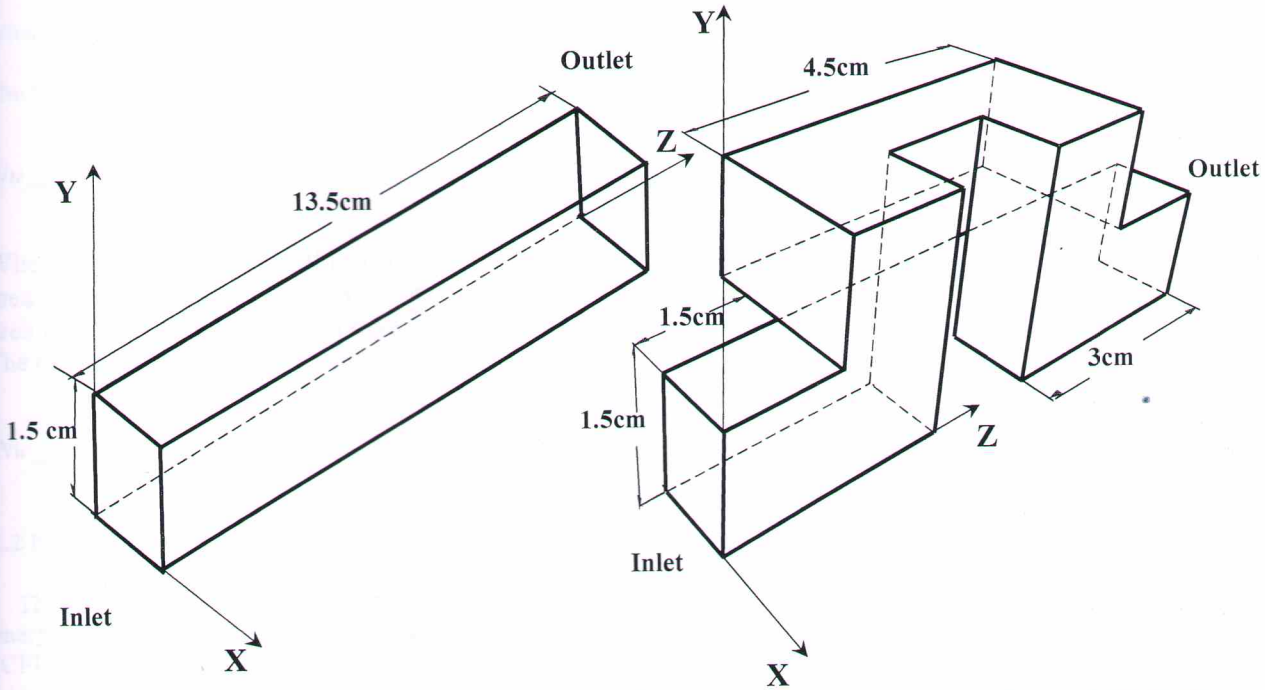

Figure 1. Schematic representation of the studied geometries: (a) straight channel, (b) C-shaped geometry.

The non-dimensional parameters that characterize the flow regime are the generalized Reynolds number (Re_g) Poiseuille number (Po) and Nusselt number (Nu). These parameters are developed as following:

Generalized Reynolds number

The generalized Reynolds number (Re_g) for power-law fluids is defined by Metzner and Reed [15]:

$$_g = \frac{\rho U_i^{2-n} D_h^n}{\left[8^{n-1} \left(b^* + \frac{a^*}{n} \right)^n k \right]} \quad (6)$$

ıere, a* and b* equal 0.2121and 0.6771 respectively, for ıare channel and U_i(m/s) is inlet velocity.

Poiseuille number (Po) :

e hydrodynamic performance of all geometries is ıracterized by the evolution along the curvilinear ›rdinate *s* of the local friction coefficient *f*, defined as:

$$= \frac{2\left(\frac{dp}{ds}\right) D_h}{\rho U_i^2} \quad (7)$$

ıere *dp/ds* is the local pressure gradient along the ·vilinear coordinate of the channel. Because this parameter ›ends on the Reynolds number, it is preferable to follow the ›lution of the local Poiseuille number:

$$_{local} = f.\mathrm{Re}_g \quad (8)$$

e mean Poiseuille number is calculated as:

$$_{mean} = \frac{1}{L} \int_0^L Po_{local} ds \quad (9)$$

here s is the axial coordinate.

Nusselt number:

e local Nusselt number defined as:

$$u_{mean} = \frac{q_w}{(T_b - T_w)} \frac{d_h}{\lambda} \quad (10)$$

here, q_w (w/m^2) is the wall heat flux, T_b (k) is the ean bulk temperature fluid over the cross-sectional ea and T_w(k) is perimeter average wall temperature. ıe mean Nusselt number is given by the following equation:

$$u_{mean} = \frac{1}{L} \int_0^L Nu_{local} ds \quad (11)$$

2 Numerical solution methodology

The conservation equations for mass, momentum and ıergy were solved by using computational fluid dynamics FD) code, Fluent®. The standard scheme is used for essure discretization, and the SIMPLE scheme is employed r pressure-velocity coupling. The momentum and energy uations are solved with second-order up-wind scheme. The ımputations were considered to be converged once all the aled residuals are less than 10^{-7} and the global imbalances, presenting overall conservation don't exceed 10^{-5}.

2.3 Grid mesh sensibility

To perform grid independence studies, four grids were used for simulations of non-Newtonian fluid flow in the C-shaped geometry considering a steady laminar flow, forced convection, at a generalized Reynolds number of 200and n = 0.5. These grids are ranging from 30 to 60 nodes in the x and y direction, and from 30 to 60in the z direction. The Nusselt number, the Poiseuille number, velocity and temperature profiles were assessed for increasing mesh densities.

Figures2 and 3 show the evolutions of static temperature and the axial velocity versus x and y coordinates for various grids at the center line of the outflow section. It can be seen that the temperature profiles in both x and y directions are superimposed for all mesh densities. This illustrates that the temperature profiles are not affected by the grid mesh. However, it can be observed that the velocity profiles are sensitive to the grid mesh except for the mesh densities (50x50x50) and (60x60x60) where no significant difference is seen. As consequence, the (50x50x50) grid is chosen as the optimal grid mesh for the computation.

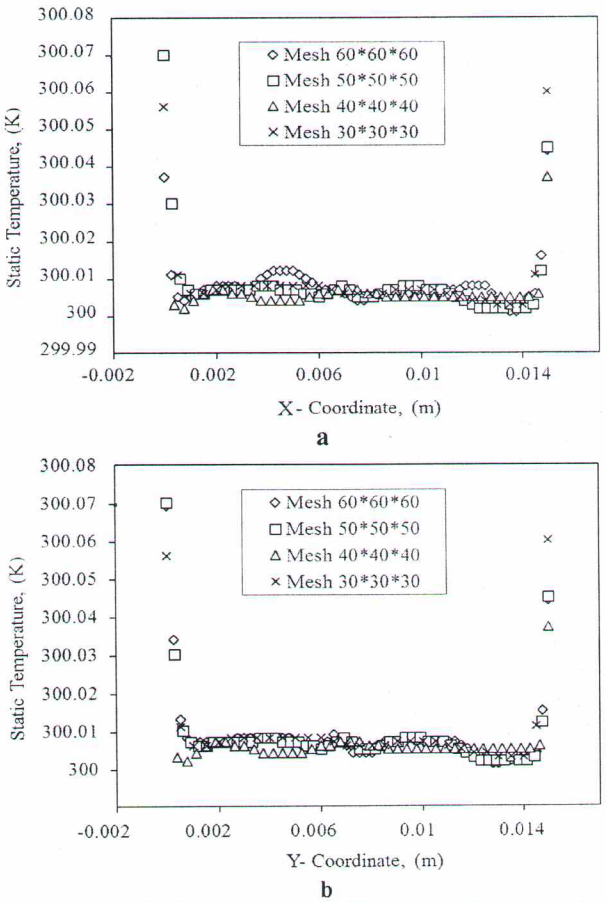

Figure 2. Temperature profiles for different mesh densities for n = 0.5 and Re_g = 200 at the outlet section of the C-shaped channel, (a) X-Coordinate (b) Y-coordinate.

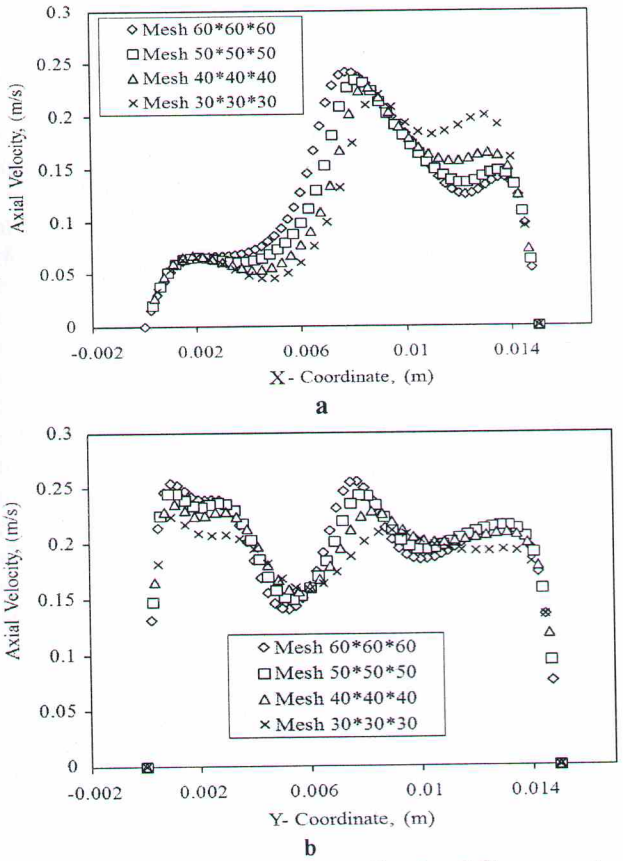

Figure 3. Axial-Velocity profiles for different mesh densities for n = 0.5 and Re_g = 200

Table 1 presents the mean values of the Poiseuille number between inlet and outlet sections of the C-shaped geometry and the values of the local Nusselt number at the outlet section for all grid densities. It shows that the differences between the two grids mesh (50x50x50) and (60x60x60) of the Poiseuille and the Nusselt numbers change by less than 0.24% and 1.4% respectively. This presents another argument to select the (50x50x50) grid mesh as the optimal mesh density for the rest of the computations.

Table 1. Mean Poiseuille number and local Nusselt number for different mesh densities for n = 0.5 and Re_g = 200 in the C-shaped channel.

Mesh	Po_{mean}	Error/ Po_{mean}	Nu_{mean}	Error/ Nu_{mean}
30x30x30	218.270	0.13%	41.741	13.56%
40*40*40	219.270	- 0.32%	45.8307	5.09%
50*50*50	219.099	- 0.24%	47.6098	1.41%
60*60*60	218.561	0.00%	48.2904	0.00%

3. VALIDATION

In this section, in order to check the reliability and the precision of the CFD computation, a comparison with other results provided in the literature is carried out. A fully developing laminar steady flow of non-Newtonian power-law fluid in straight channel with square cross section is considered.

Tables 2 and 3 present, respectively, a comparison of the values of the Poiseuille number and the Nusselt number obtained in the present study and those provided in the literature for large range of a power-law index (n = 0.3-1).The numerical values barely differ from the case of the theoretical values where the maximum difference is less than 0.5%. These values are in fair agreement and the comparison is satisfactory and reveals a very good concordance.

Table 2. Poiseuille number, Po, of fully developed laminar flow in square straight channel for different power-law index (n = 0.3-1).

n	1	0.9	0.8	0.7	0.6	0.5	0.4	0.3
Present work	56.90	47.47	39.32	33.00	27.52	22.90	18.99	15.66
Wheeler and Wissler [16]	56.92	47.53	39.67	33.07	27.54	22.89	18.97	15.65
Seppo [17]	56.90	47.52	39.65	33.06	27.53	22.88	18.96	15.64
Simsoo et al [18]	56.90	47.89	40.29	33.89	28.49	23.91	20.01	-
Kozicki et al [19]	56.91	47.88	40.26	33.82	28.37	23.75	19.82	-
Sayed-Ahmed [20]	56.90	-	-	-	-	22.88	-	-
Error (%)/ [17]	0.007	0.09	0.82	0.17	0.05	-0.06	-0.14	-0.14

Table 3. Nusselt number of fully developed laminar flow in square straight channel for different power-law index (n = 0.5-1)

n	1	0.9	0.8	0.7	0.6	0.5
Present work	3.0704	3.1140	3.1463	3.1832	3.228	3.2818
Wheeler and Wissler [16]	3.0950	3.106	3.135	3.171	3.216	3.274
Error (%)/[16]	0.2407	- 0.2580	- 0.3607	- 0.3869	- 0.3736	- 0.2386

)ISCUSSION AND RESULTS

n this section, the flow and heat transfer characteristics for ower law non Newtonian fluid are studied in detail based the numerical solution. The flow structure is the main ıtribution factor which affects the flow and heat transfer formances in the geometries. Furthermore, these formances are a complex function of generalized Reynolds nber and power law index. As known, the improvement of heat transfer performance is accompanied with an gmentation of the pressure drop penalty. According to ve, it is interesting to measure the energetic efficiency of considered geometries. This efficiency illustrates the mpromise between heat transfer and pressure losses. Three in parameters are considered in order to achieve the used goals: Poiseuille number (Po) for the flow aracteristics, Nusselt number (Nu) for the heat aracteristics and the ratio (Po/Nu) for the efficiency asurement. These parameters are evaluated for generalized number and power law index ranging from 50 to 200 and 0.5 to 1 respectively.

4.1 Flow characteristics

Figure 6 and 7 show the evolutions of the axial velocity profiles with x and y coordinates at the center line of the straight channel outlet section for power law non-Newtonian fluid for two generalized Reynolds number 50 and 150. The power-law index varies from 0.5 to 1. The profiles of the velocity are symmetric and parabolic. The maximum velocity is located in the center of the cross section and it increases considerably with the increase of the power law index. It can be seen clearly that, in the straight channel, particles Pathlines released from the inlet section are parallel resulting in no motion of the fluid particles in the transverse direction of the flow, see figures 4. In addition, figure 5 displays that there is no secondary flows appeared in the outlet cross section. So, the momentum transfer is limited only to the molecular diffusion mode for all cases of the power law index n.

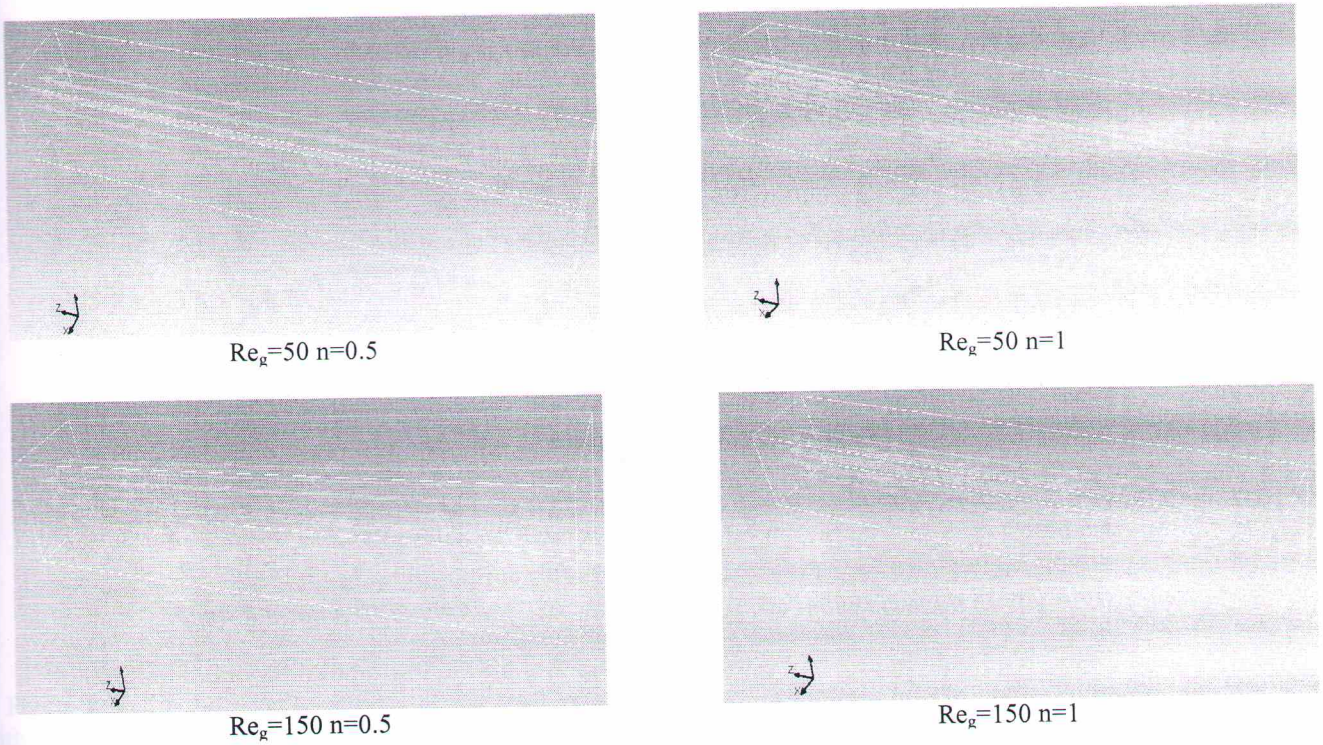

Figure 4. Particle Pathlines released from the inlet section.

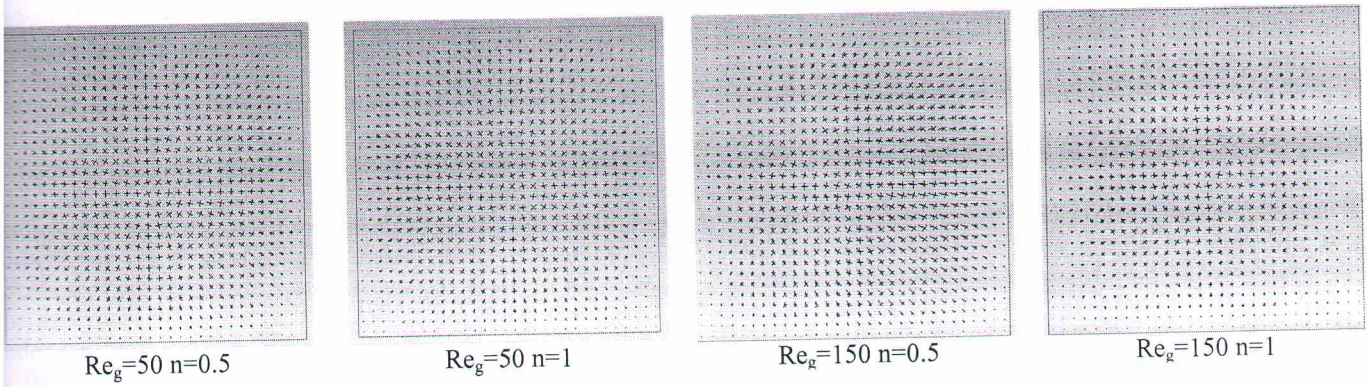

Figure 5. Velocity vectors distribution in outlet cross section.

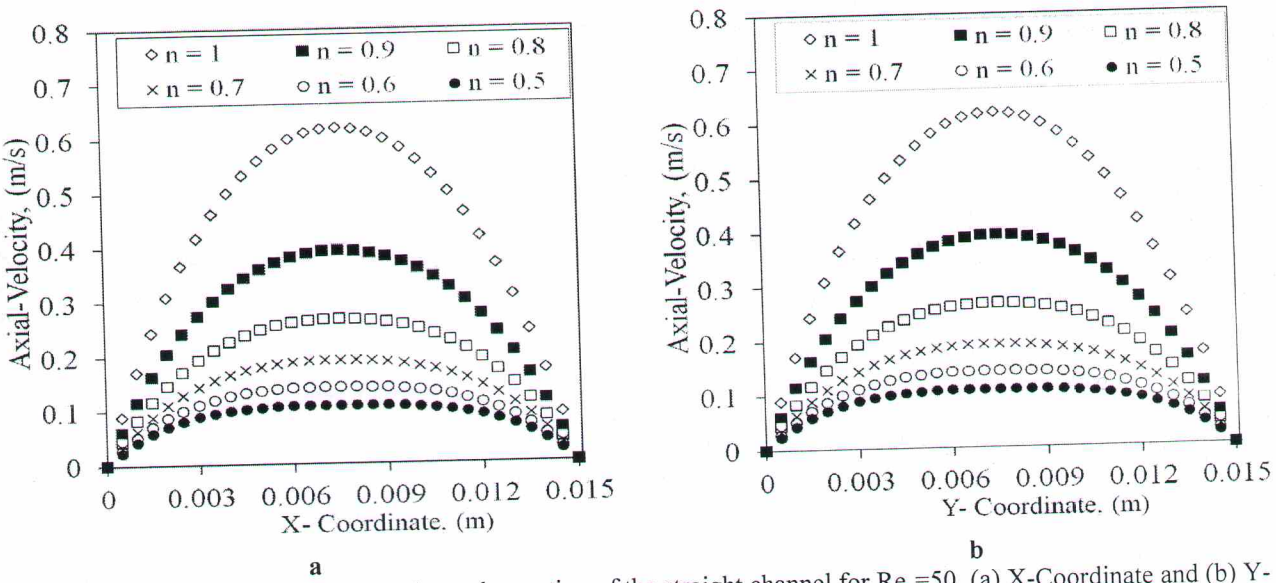

a b

Figure 6. Axial velocity profiles at the outlet section of the straight channel for Re_g=50, (a) X-Coordinate and (b) Y-Coordinate.

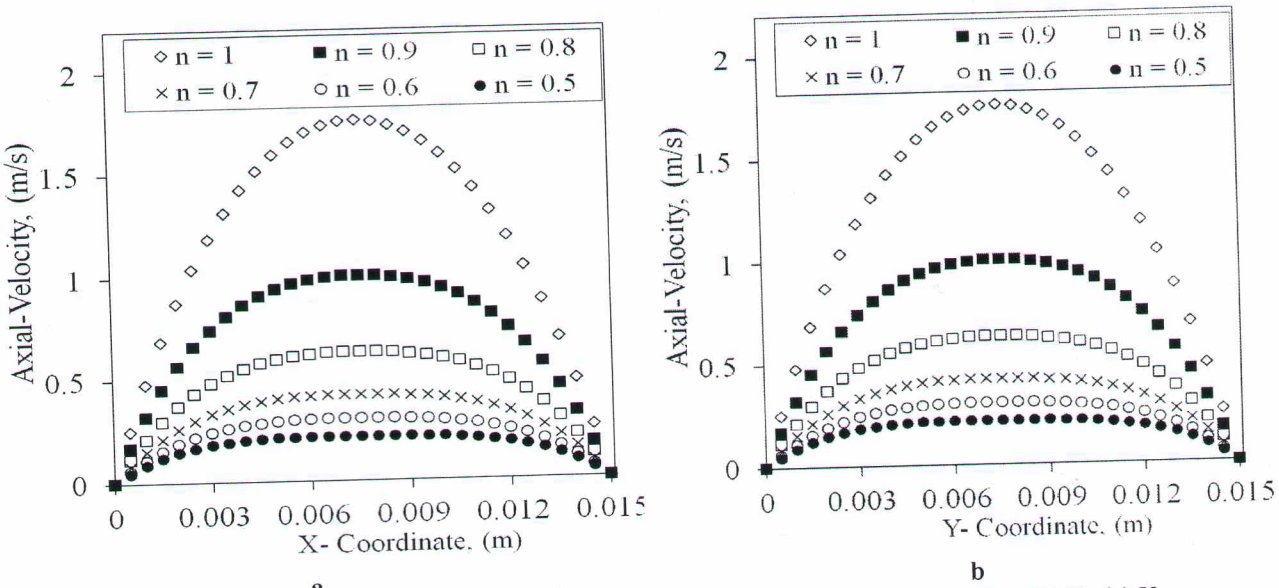

a b

Figure 7. Axial velocity profiles at the outlet section of the straight channel for Re_g = 150, (a) X-Coordinate and (b) Y-Coordinate.

Figure 8 and 9 show the evolutions of the axial velocity with x and y coordinate at the center line of the outlet section in the C-shaped geometry for power law non-Newtonian fluid for two generalized Reynolds number 50 and 150.The velocity distributions within the channel highlight the flow complexity where the symmetric nature of the velocity profile is disrupted under the effect of the secondary flows. The velocity profiles in the central core region are more lower compared to that in the straight channel. The location of the maximum velocity point in this type of geometry is of interest. One can gain the general idea about the secondary flow pattern and the intensity of secondary flow. The results show clearly that the effect of the secondary flows is to shift the location of the maximum value toward the walls. In addition, the maximum value increases as the value of the power law index increases.

Besides, the evolutions of the local and the mean Poiseuille numbers in the interest of channels are examined. This parameter depends strongly on the nature of the kinematic trajectories of fluid particles in the flow. Figure 10 presents the evolutions of the local Poiseuille number with the curvilinear coordinate for a generalized Reynolds number equal to 100 and for two values of the power law index 0.5 and 1 in three periods of the straight and C-shaped channels.

Because the flow is regular in the straight channel, the local Poiseuille number decreases rapidly at the entrance of the channel as function of the curvilinear coordinate and it tends towards an asymptotic value once the flow is established. This value increases with the power law index n. In the C-shaped geometry and from the second period, the variation of the local Poiseuille number is periodic. This is explained by the fact that the velocity field is itself periodic (figure 11). The flow is enough disrupted due to the existence of the geometrical perturbations which prevents the establishment of the boundary layer. This phenomen on increases strongly the pressure drop. Figure 12 presents the evolution of the mean Poiseuille number with generalized Reynolds number for the two considered geometries and for power law index ranging from 0.5 to 1.

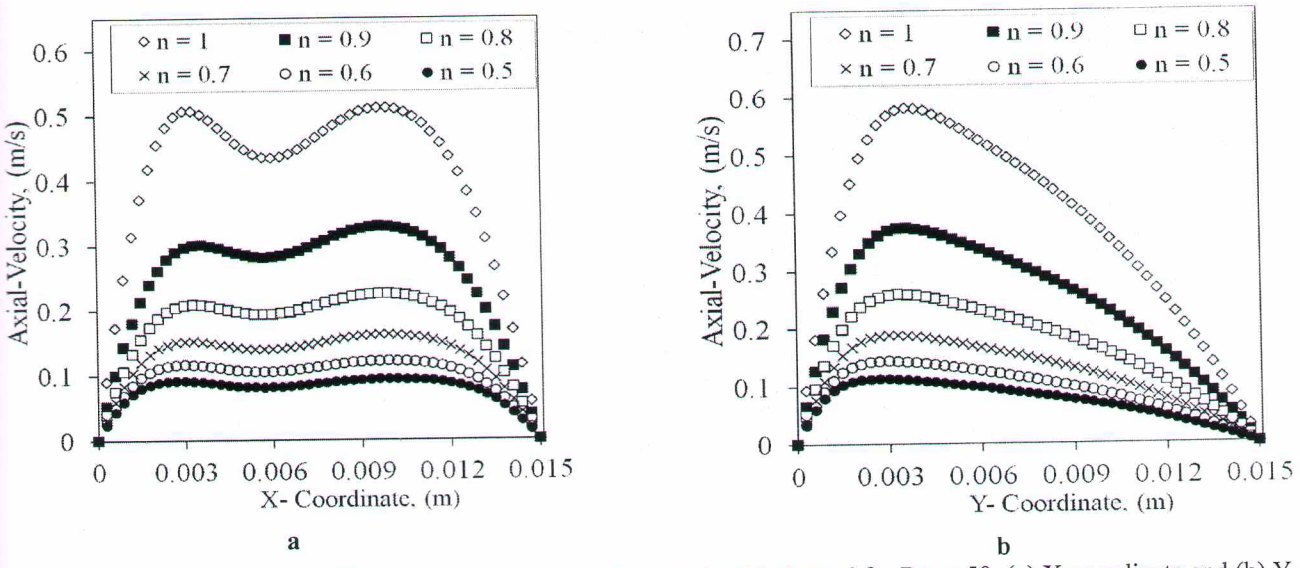

Figure 8. Axial velocity profiles at the outlet section of the C-shaped channel for $Re_g = 50$, (a) X-coordinate and (b) Y-coordinate.

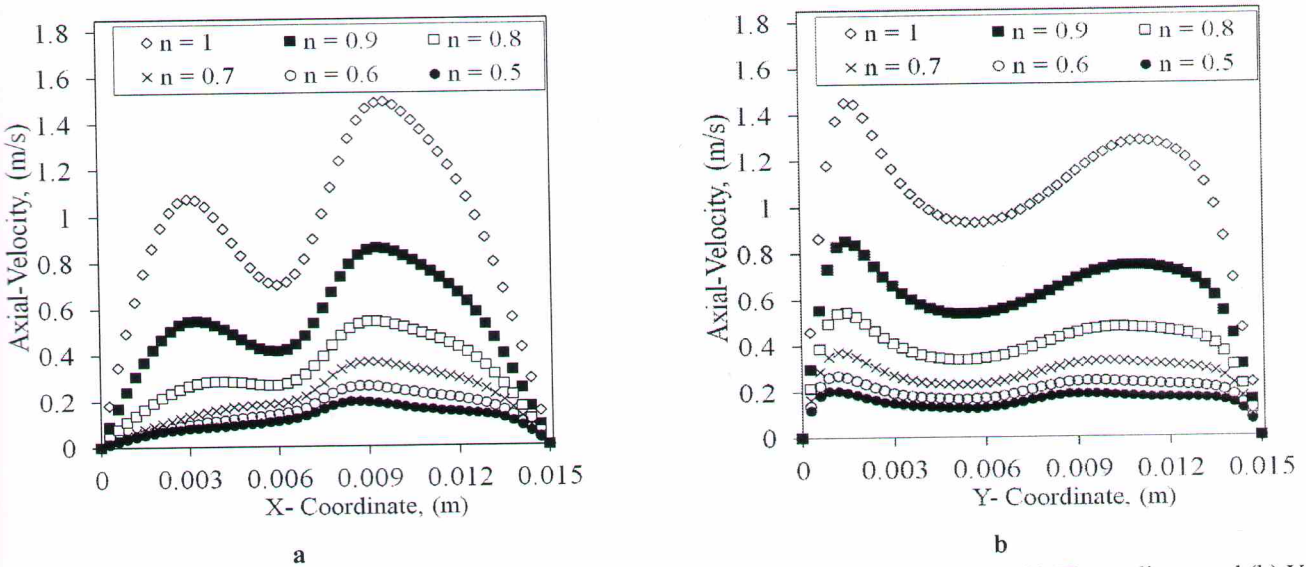

Figure 9. Axial velocity profiles at the outlet section of the C-shaped channel for $Re_g = 150$, (a) X-coordinate and (b) Y-coordinate.

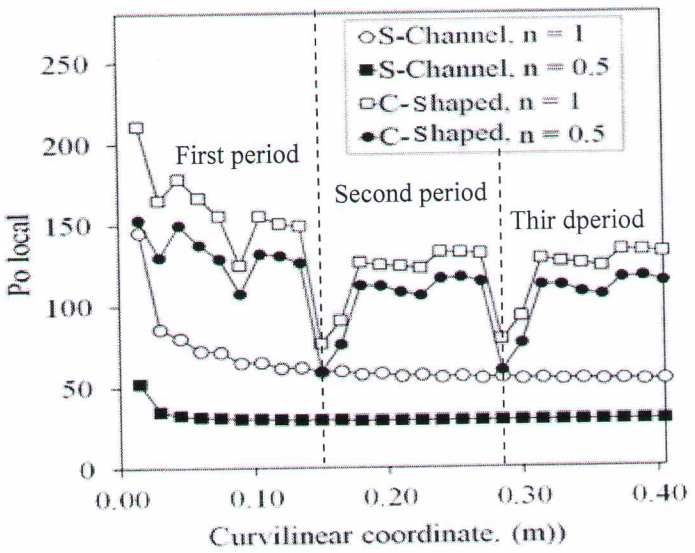

Figure 10. Evolutions of the local Poiseuille number with the curvilinear coordinate for the two geometries for a power law index of 0.5 and 1 ($Re_g = 100$).

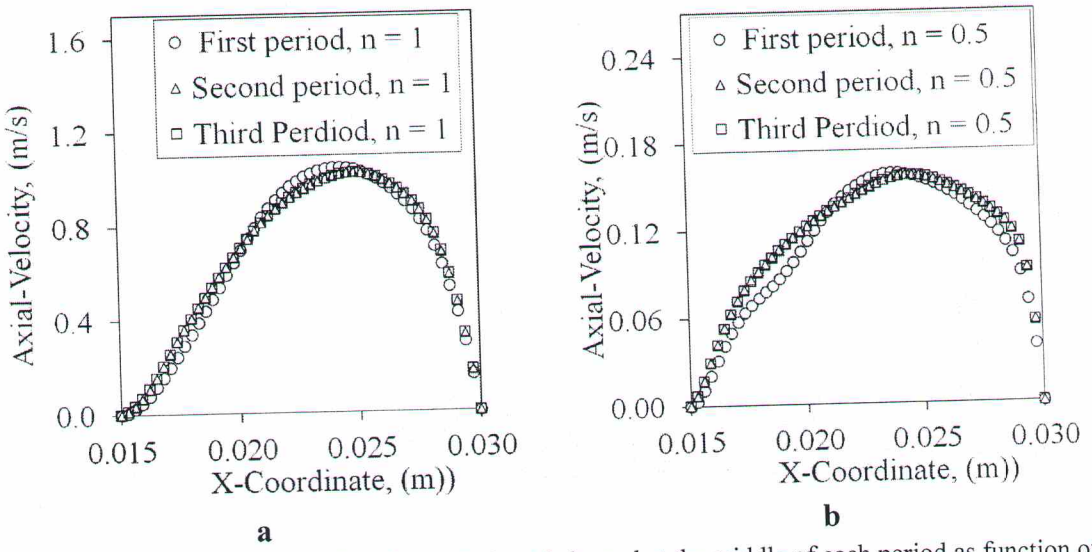

Figure.11: Axial-Velocity profiles in the C-shaped channel at the middle of each period as function of X-coordinate, (a) n = 1 , (b) n = 0.5

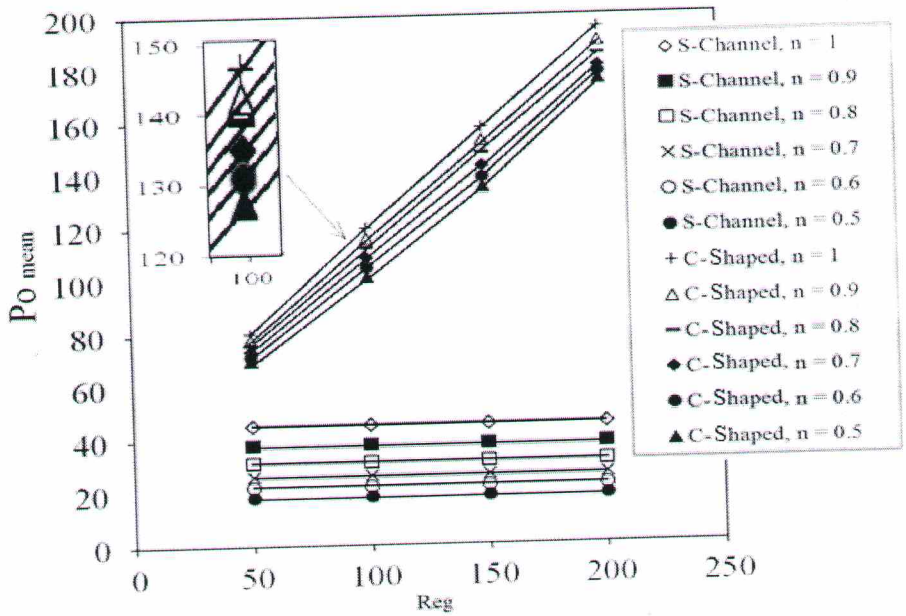

Figure12. Evolution of the mean Poiseuille number with generalized Reynolds number in straight (S-channel) and C-shaped channels.

In the straight channel and when the flow regime is tablished, the mean Poiseuille number keep a constant value hatever the generalized Reynolds number for a given value power law index n. This parameter (Po mean) increases ith the growth of the power law index. As mentioned to ove, the pressure drops are influenced by the intense condary flows and accentuated with the increase of the neralized number and the power law index. So, the mean oiseuille number is very significant in the C-shaped than that lculated in the straight channel.

.2 Heat characteristics

Figure 13 presents the evolutions of the local Nusselt umber with the curvilinear coordinate in the interest eometries for two values of the power law index 0.5 and 1 nd for a generalized number equal to 100.In the entrance ength of the straight channel, the local Nusselt number lecreases strongly to reach an asymptotic value which lepends on the power law index. However, in the C-shaped geometry, the chaotic behavior exhibits a marked influence on heat transfer distributions in the system. Due to the continuous effect of the boundary layer destruction, the local Nusselt number evolves periodically with the curvilinear coordinate which allowed us to make the computation in one period. Consequently, the thermal boundary layer in the chaotic tube became thin and the heat transfer is very sensitive to temperature changes between the wall temperature and the mean bulk temperature. The maximum variation of the local Nusselt number is very considerable and it is around 40.In order to compare the heat performances between the two geometries, the variation of the mean Nusselt number as function of generalized Reynolds number for several power law index values ranging from 0.5 to 1 is estimated (figure 14).

In the straight channel, the mean Nusselt number is independent of the generalized Reynolds number and keeps a constant value which increases with the power law index value n.

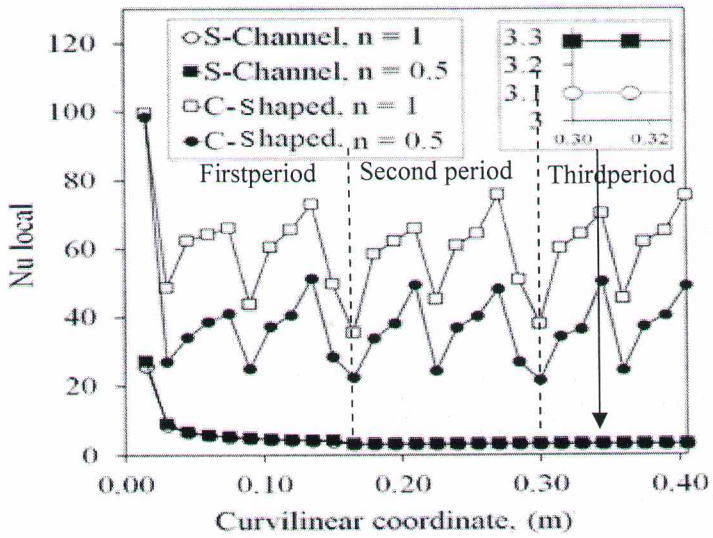

igure 13. Evolutions of the local Nusselt number with the curvilinear coordinate in the two geometries for two values of the power law index 0.5 and 1 (Re_g = 100).

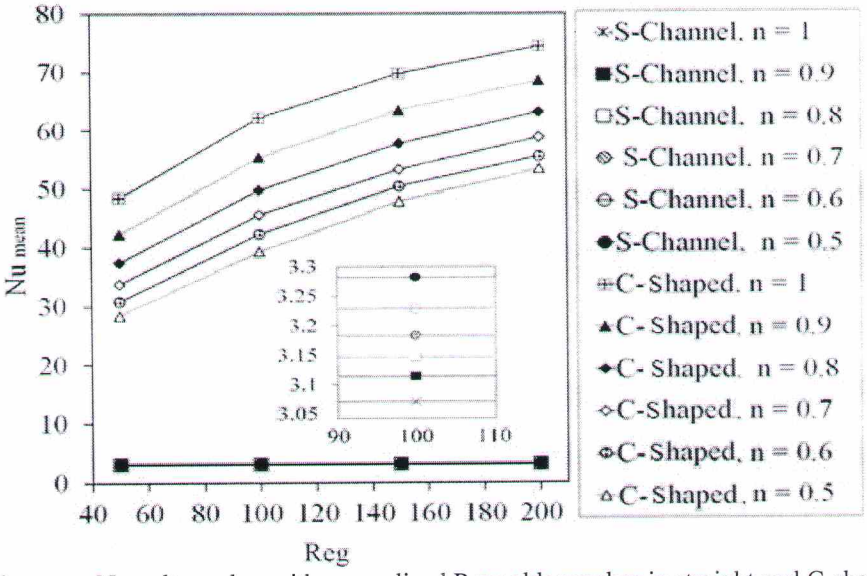

igure 14. Evolution of the mean Nusselt number with generalized Reynolds number in straight and C-shaped channels Power law index (n = 1 to 0.5).

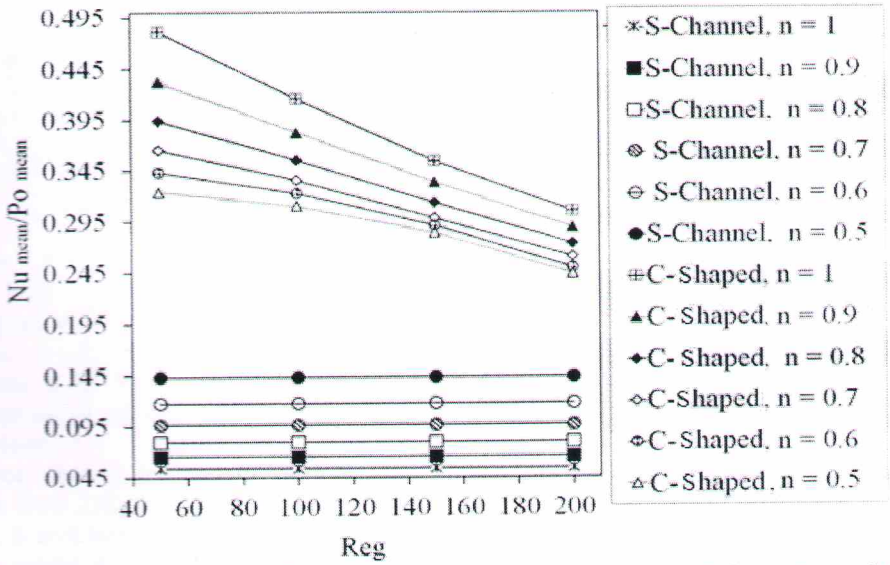

Figure.15. Evolution of the ratio of the Poiseuille number to the Nusselt number with different Power law index for straight channel and C-shaped geometry.

This is due to the effect of the chaotic kinematics of the particles. With a view to examine the increase of heat transfer rate rather than the decrease of pressure drop, we present on the figure 15 the evolutions of the ratio Nu_{mean}/Po_{mean} with the generalized Reynolds number for the power law index values. When this ratio is high, the compromise (improving heat transfer- diminution pressure losses) is the best. In the straight channel, this parameter has a constant value for a given power law index and is lower when n = 1.

However, in the C-shaped geometry, the ratio Nu/Po becomes higher with the increase of the power law index but it decreases with the generalized Reynolds number. As conclusion, the compromise (improving heat transfer-diminution pressure losses) provided by the C-shaped is very significant in comparison with that calculated in the straight channel.

5. Conclusions

In this work, numerical simulations were performed by using CFD code in order to study flow characteristics of the non-Newtonian power law fluid in two geometries, C-shaped and straight channels, in terms of heat transfer and fluid flow. This paper outlines the evolutions of the Nusselt number and the Poiseuille number with generalized Reynolds number and with the power law index ranging from 0.5 to 1.It was observed that the local friction factor and Nusselt number straches and folded as the axial distance increases. The chaotic configuration displays a heat transfer enhancement in terms of the mean Nusselt number compared to the straight channel, however the pressure drop in this geometry increases (high Poiseuille number) for all examined Reynolds number. Despite this, the ratio of the Nusselt number to the Poiseuille number is higher in the C-shaped geometry, showing that the heat transfer enhancement is important than the pressure loss increase. The study of thermal mixing in the C-shaped geometry of the Non-Newtonian fluids is in progress.

REFERENCES

[1] Nazmeev, Y.G., "Intensification of convective heat exchange by ribbon swirlers in the flow of an omalously viscous liquid sinpipes", *J. Eng Phys.*, vol. 37, pp. 910-913, 1979. DOI: 10.1007/BF00861442.

[2] A.G.Patil, "Laminar flow heat transfer and pressure drop characteristics of power-law fluids inside tubes with varying width twisted tape inserts", *J. Heat Transfer.*, vol. 122, pp. 143-149, 2000. DOI: 10.1115/1.521448.

[3] Dean, W.R., "Note on the notion of fluid in a curved pipe", *Phil. Mag*,. vol.7, no. 4, pp. 208-223, 1927. DOI: 10.1080/14786440708564324.

[4] Dean, W.R., "The stream-line motion of fluid in a curved pipe", *Philos. Mag.*, vol. 7, no. 5, pp. 673-695, 1928. DOI: 10.1080/14786440408564513.

[5] Zabielski, L and Mestel A. J., "Unsteady blood flow in a helically symmetrical pipe", *J. of Fluid Mech.*, Vol. 370, pp. 321-345, 1998. DOI: 10.1017/S0022112098001992.

[6] Ali, S.S, Kayvan, S and Mehrdad, R., "On the use of lattice Boltzmann model for simulating dean flow of non-Newtonian fluids in curved square ducts", *Com Nonlinear Sci Numer Simulat.*, vol. 17, pp. 4250-4260, 2012. DOI: 10.1016/j.cnsns.2012.03.026.

[7] Pimenta, T.A. and Campos. J.B.L.M., "Heat transfer coefficients from Newtonian and non-Newtonian fluids flowing in laminar regime in a helical coil", *Int J. Heat and Mass Trans.*, vol. 58, pp. 676–690, 2013. DOI: 10.1016/j.ijheatmasstransfer.2012.10.078.

[8] Norouzi, M., Davoodi M and Anwar Bég O., "An analytical solution for convective heat transfer of viscoelastic flows in rotating curved pipes", *Int J. Ther Sci.*, vol. 90, pp. 90-111, 2015. DOI: 10.1016/j.ijthermalsci.2014.11.025.

[9] Aref, H., "Stirring by chaotic advection", J. *Fluid Mech.*, vol. 143, pp. 1-21, 1984. DOI: http://dx.doi.org/10.1017/S0022112084001233.

[10] Kamal, E. O and Guer Y.L, "Thermal chaotic mixing of power-law fluids in a mixer with alternately rotating walls", *J. Non-Newt Fluid Mech.*, vol. 165, pp. 641-651, 2010. DOI: 10.1016/j.jnnfm.2010.03.004.

[11] Lester, D.R., Rudman M and Metcalfe G., "Low Reynolds number scalar transport enhancement in viscous and non-Newtonian fluids", *Int J. Heat and Mass Tran.*, vol. 52, pp. 655-664, 2009. DOI: 10.1016/j.ijheatmasstransfer.2008.06.039.

[12] Beebe, D. J., Adrian, R. J., Olsen, M. G., Stremler, M. A., Aref, H., and Jo, B., "Passive Mixing in Micro-Channels: Fabrication and Flow Experiments", *J. Mécanique et Industries.*, vol. 2, pp. 343-348, 2001. DOI: S 1057-7157(00)04860-5.

[13] Liu, R. H, Stremler, M. A, Sharp, K. V, Olsen, M. G, Santiago, J. G, Adrian, R. J, Aref, H. and Beebe, D. J., "Passive Mixing in a Three-Dimensional Serpentine Microchannel", *J. Microelectromech Sys.*, vol. 9, pp. 190-197, 2000. DOI: 10.1109/84.846699 .

[14] Yahia, L., Bruno, A., Cathy, C. and Hassan, P., "Thermal and Hydrodynamic Performances of Chaotic Mini-Channel: Application to the Fuel Cell Cooling", *J. Heat Tran Eng.*, vol. 28, no. 8, pp. 795-803, 2007. DOI: 10.1080/01457630701328908.

[15] Metzner, A. B. and Reed, J. C., "Flow of Non-Newtonian Fluids Correlation of the Laminar Transition, and Turbulent-Flow Regions", *AIChE J.*, no. 1, vol. 434, 1955. DOI: 10.1002/aic.690010409.

[16] Wheeler, J. A and Wissler, E. H., "The Friction Factor-Reynolds Number Relation for a Steady Flow of Pseudoplastic Fluids through Rectangular Ducts", *Aiche J*,. vol. 11, pp. 07-216, 1966. DOI: 10.1002/aic.690110208.

[17] Seppo, S., "Finite-element analysis of fully developed laminar flow of power-law non-Newtonian fluid in a rectangular duct", *int. corant heat mass transfer.*, vol. 22, no. 4, pp, 549-557, 1995. DOI: 10.1016/0735-1933(95)00040-6.

[18] Simsoo, P., Irvine, T. F. and Capobianchi, Jr.M., "Experimental and Numerical Study of Friction Factor for a Modified Power Law Fluid in a Rectangular Duct", *J. Exp Ther and Fluid* Sci., vol.9, pp. 61-68, 1994. DOI: 10.1016/0894-1777(94)90009-4.

[19] Kozieki, W., Chou, C. H., Tiu, C., "Non-Newtonian Flow in Ducts of Arbitrary Cross-Sectional Shape", *J. Che. Engrg Sci.*, vol. 665, no. 21, 1966. DOI: 10.1016/0009-2509(66)80016-7.

[20] Sayed-Ahmed, M.E., "Laminar heat transfer for thermally developing flow of a Herschel–Bulkley fluid in a square duct", *Int. Comm. Heat Transfer.*, vol. 27, no. 7, pp. 1013-1024, 2000. DOI: 10.1016/S0735-1933(00)00181-0.